Application of Effective Medium Modeling to Plasmonic Nanosphere Waveguides

by

Paul Hale

A Thesis Presented in Partial Fulfillment
of the Requirements for the Degree
Master of Science

Approved April 2013 by the
Graduate Supervisory Committee:

Rodolfo Diaz, Chair
Stephen Goodnick
James Aberle
Joseph Palais

ARIZONA STATE UNIVERSITY

May 2013

ABSTRACT

A proposed visible spectrum nanoscale imaging method requires material with permittivity values much larger than those available in real world materials to shrink the visible wavelength to attain the desired resolution. It has been proposed that the extraordinarily slow propagation experienced by light guided along plasmon resonant structures is a viable approach to obtaining these short wavelengths. To assess the feasibility of such a system, an effective medium model of a chain of Noble metal plasmonic nanospheres is developed, leading to a straightforward calculation of the waveguiding properties.

Evaluation of other models for such structures that have appeared in the literature, including an eigenvalue problem nearest neighbor approximation, a multi-neighbor approximation with retardation, and a method-of-moments method for a finite chain, show conflicting expectations of such a structure. In particular, recent publications suggest the possibility of regions of invalidity for eigenvalue problem solutions that are considered far below the onset of guidance, and for solutions that assume the loss is low enough to justify perturbation approximations. Even the published method-of-moments approach suffers from an unjustified assumption in the original interpretation, leading to overly optimistic estimations of the attenuation of the plasmon guided wave.

In this work it is shown that the method of moments approach solution was dominated by the radiation from the source dipole, and not the waveguiding behavior claimed. If this dipolar radiation is removed the remaining fields ought to contain the desired guided wave information. Using a Prony's-method-based algorithm the

dispersion properties of the chain of spheres are assessed at two frequencies, and shown to be dramatically different from the optimistic expectations in much of the literature.

A reliable alternative to these models is to replace the chain of spheres with an effective medium model, thus mapping the chain problem into the well-known problem of the dielectric rod. The solution of the Green function problem for excitation of the symmetric longitudinal mode (TM01) is performed by numerical integration. Using this method the frequency ranges over which the rod guides and the associated attenuation are clearly seen. The effective medium model readily allows for variation of the sphere size and separation, and can be taken to the limit where instead of a chain of spheres we have a solid Noble metal rod. This latter case turns out to be the optimal for minimizing the attenuation of the guided wave.

Future work is proposed to simulate the chain of photonic nanospheres and the nanowire using finite-difference time-domain to verify observed guided behavior in the Green's function method devised in this thesis and to simulate the proposed nanosensing devices.

ACKNOWLEDGMENTS

This work was only possible due to the efforts and assistance of my professors, and through the generous funding of the National Science Foundation through their Graduate Research Fellowship program.

TABLE OF CONTENTS

Page

LIST OF FIGURES

Figure Page

Figure Page

Figure Page

Chapter 1

INTRODUCTION

Nanoscale imaging and detection methods are becoming ever more important as industry and research focus attention to the use, application, and characteristics of nanoscale devices and structures.

Semiconductor and medical research areas are particularly hindered by the limitations of current nanoscale imaging and detection capabilities, which fail to offer the combination of high resolution (small scale), low cost, and high speed. Efforts in these areas could be significantly assisted by an imaging and detection method which combines all three of these capabilities.

Current nanoscale imaging and detection is performed by scanning probe instruments, which utilize a near-field detection system. Differing methods detect differing fields; such as Atomic Force Microscopy detecting electrostatic force, Magnetic Force Microscopy detecting a magnetic force, Scanning Tunneling Microscopy detecting current from quantum tunneling, or Near-field Optical Microscopy detecting an evanescent electromagnetic field. All of these methods function under the same principle, which is to employ a probe to detect a given field, and scan it closely over an object to detect its features.

A very high resolution may be achieved using such methods, on the order of 0.1 nm in the lateral direction and 0.01 nm in depth for the most sensitive method (STM) [1].

However, even at lower resolutions, the linear scanning speed of such devices are on the order of 1 mm/s [2]. Assuming step sizes between scanned lines are on the order of 10 nm, scanning time would be on the order of days for a square centimeter of material. While near field microscopy is well suited for atomic level imaging, it is much too slow for macro level imaging with atomic level detail.

Conversely, current optical imaging methods are relatively inexpensive and fast for small scale imaging and defect detection, however the resolution is limited by the diffraction limit of light, which is on the order of the wavelength of the light used [3]. As the sizes of small scale structures and devices continues to shrink beyond the wavelength of visible light, this limit is proving problematic, and the well developed methods of defect detection are becoming unable to resolve features of objects under test.

To leverage existing optical methods, it is desirable to break past the diffraction limit. Past and present work to achieve this has been devised at ASU, including Wave Interrogated Near Field Array (WINFA) methods [4]. WINFA allows defects smaller than the diffraction limit of the probing light to be detected by observing the changes the small defect has on the scattering properties of a larger nearby antenna.

Another method suggested at ASU, which has been a central theme in multiple proposals yet still largely undeveloped, is an Optical Real-Time Imaging Of Nanostructures (ORION) system. In general, an ORION system would apply a coherent evanescent wave imaging method, which depends on the contraction of wavelength in a

high dielectric constant material and radar-like evaluation of scattering to produce an image.

The originally proposed coherent evanescent wave imaging system consists of: (a) a coherent light source, (b) transducer that converts coherent light source into an evanescent wave, (c) an engineering detector surface that supports slow surface waves (20 to 100 times slower than the free-space speed of light), (d) an interaction region spanning thousands of square wavelengths, (e) a positioning mechanism to bring the sensor surface proximate to the nanostructure to be imaged, and (f) a transducer boundary to out-couple the scattered wave into a coherent signal for the imaging by a detector array (g). [5]

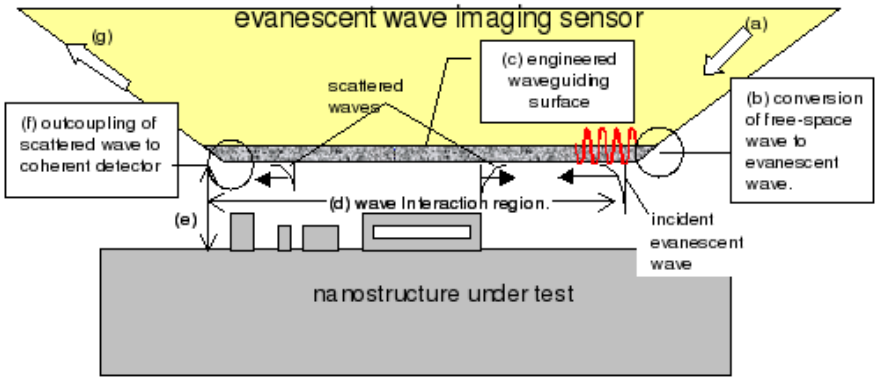

Fig. 1-1 Coherent Wave Imaging Sensor [5]

This originally proposed system calls for a generic "engineered waveguiding *surface*", which would support plane wave propagation. Wave propagation would be slowed to shrink the wavelength to nanometric scale.

At radio frequencies this may be easily achieved by using a waveguiding surface made from translucent material with appropriately high enough dielectric constant to slow the wave sufficiently for the desired behavior. However, there exists no real world homogeneous translucent low loss material of sufficiently large dielectric constant for the same purpose at optical frequencies.

Overcoming this lack of appropriate material for the desired behavior at the frequencies of interest might be achieved by engineering a waveguiding structure which behaves like a homogeneous structure of desired permittivity. There are a variety of methods and models for creating an effective permittivity in a medium. Alternatively there have been reported waveguiding structures that slow down the wave enough to attain the desired wavelength shortening effect. Invariably, these proposed structures exploit the surface plasmon resonance in noble metal materials, and particularly in arrays of nanoparticles.

Given that the latter structures guide slow waves the same way that very large index of refraction medium would, it should be possible to construct a formal effective medium model connection between the heterogeneous waveguiding structure and a homogeneous equivalent. However, verification of the characteristics of the expected behavior of such structures as described in the literature must be made.

Given the novelty of the imaging approach, the overall utility, and potential vast application in industry, ASU was granted a patent to the general ORION approach [6]. ORION was also the subject of a proposal to the NSF for the establishment of a nano-

engineering research center comprising four interconnected multi-disciplinary core activities, collaboration by six universities, two national labs, a dozen professors with complimentary skill sets, and a proportional number of graduate students and researchers to complete the project. Despite encouraging reviews of the proposal, due to some of the more radical components of the proposal, the initiative was deemed too high risk by the NSF to fund.

To reduce the perceived risk and enable further research into the ORION approach, a study into a part of the initiative has been undertaken, namely, the design of a waveguiding surface. In performing this study the question is asked, are current models of these plasmon nanosphere waveguides found in the literature valid? If so, is the resultant structure equivalent to other classical homogeneous structures with better known electromagnetic wave behavior properties?

After evaluating the properties and validity of some of the models found in the literature, an application of effective medium theory used in conjunction with a Green function numerical method is proposed as an alternative method to model these waveguides.

Finally, the results are summarized and future work laid out based on the discoveries contained.

Chapter 2

PLASMONIC WAVEGUIDING STRUCTURES

2.1 Original Proposal and Suggested Proof of Concept

The original ORION proposal called for an evanescent imaging sensor, as described in Figure 1-1 of the introduction. The original simplified sensor called for a waveguiding homogeneous low loss dielectric slab. The unavailability of appropriate low loss very high permittivity material at optical frequencies motivated an initial design of a waveguiding surface based on colloidal gold nanoparticles. Such surfaces had been constructed by the Colloidal Chemistry group of the University of Vigo under the direction of Professor Luis Liz-Marzan. The goal was to slow the guided wave by a factors of 50 to 500 to obtain wavelengths of the order of single nanometers [7].

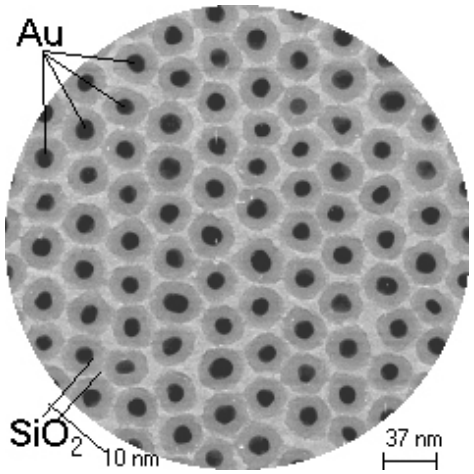

Fig. 2-1 Proposed Waveguiding Material Comprised of Colloidal Spheres [7]

The effective permittivity of such a medium composed of spheres has been successfully modeled using effective medium theory over the frequencies of interest. Effective medium theory is valid in the quasi-static limit, that is to say that the unit cell of the effective material is small compared to wavelength. Work on tailoring the surface plasmon resonance of colloidal spheres [8] has shown that at optical frequencies such an assumption is satisfied for such objects by noting their single resonance and a 3dB extinction cross section bandwidth consistent with excitation of only the surface plasmon dipole mode. Figure 2-2 for colloidal spheres with gold cores, and Figure 2-3 show the resonance peak sharpening as expected when the radius of the Drude metal core shrinks. Figure 2-3 also shows that the frequency of resonance may be shifted by increasing the thickness of the glass coating of the colloidal spheres (because this reduces the coupling between the metal cores), which thus allows for resonance to be dialed in at a desired frequency.

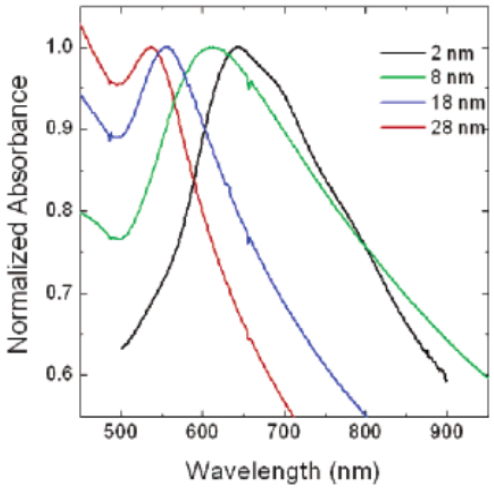

Fig. 2-2 Normalized UV-visible spectra of Drude metal (gold) Spheres Coated with Five Monolayers of Nanoparticles, with Silica Shell Thickness Indicated in Graph [8]

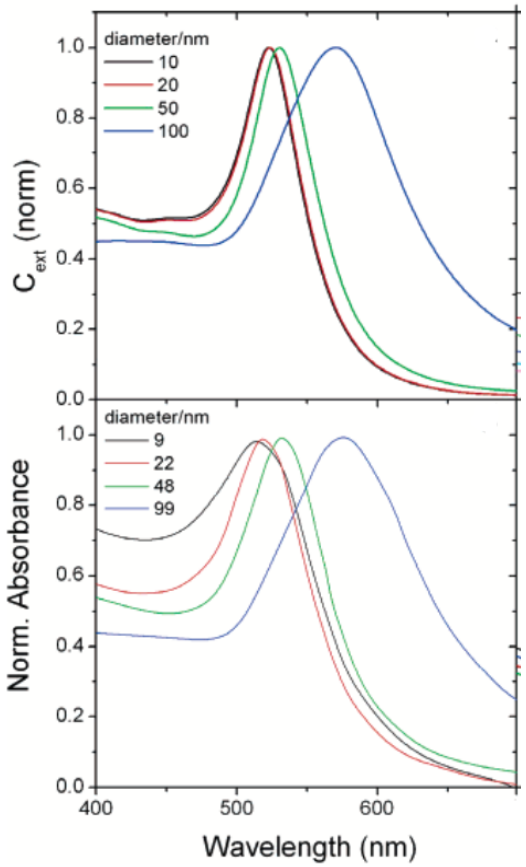

Fig. 2-3 Calculated Extinction Cross Section (top) of Drude Metal Spheres, with Varying Diameters, and Measured Absorbance (bottom) [8]

While consideration of a surface comprised of these spheres is appropriate for the original ORION imaging device, a proof of concept by reduction of complexity was suggested by Professor E. Dan Hirleman of Purdue University, in which only a rod of this material would be considered, instead of an entire plane of material used as a waveguide for the imaging device. The cylindrical rod would guide waves and be scanned across a surface, enabling the same capability, with a simpler model of reduced complexity.

If this reduction of complexity and proof of concept is to be pursued, the question becomes, what is this rod made of? Three options are most evident, as shown in figures 2-4, 2-5, and 2-6. One, a single chain of spheres periodically placed, behaving in a similar manner to a homogeneous dielectric rod. Two, an actual nano-wire of conducting material. Or three, a rod made of a larger bulk collection of the colloidal spheres.

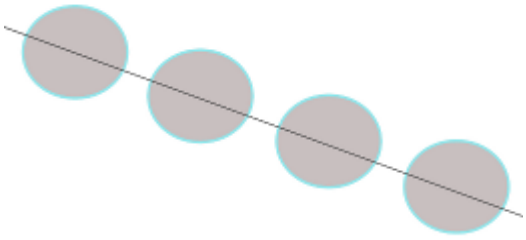

Fig. 2-4 First Suggested Option for Waveguiding Structure, Chain of Spheres

Fig. 2-5 Second Suggested Option for Waveguiding Structure, Nanowire

Fig. 2-6 Third Suggested Option for Waveguiding Structure, Cylinder of Effective Media Constructed from Colloidal Spheres

Suitability of such structures must by determined by defining figures of merit. The first obvious figure of merit, is that the structure must guide a wave. Second, it should be “low” loss. The latter is obviously a relative consideration depending on the required length of the device. However, it is reasonable to expect that a device will require a minimum length to obtain a clear separation between the excitation region where the wave is fed, the interaction region where the wave interacts with the surface to be imaged, and the collection region where the signal is received to measure S21.

Third, the propagating wave must suffer minimal dispersion. Again, this is a relative consideration, depending on the shortness of the pulse required for desired imaging modality (e.g. radar versus tomography). The fact that narrow bandwidths are generally sufficient at optical frequencies for most applications, suggests that this would not be a problem except for the most extreme occurrences of dispersion. However, any time we propose to use a resonant phenomenon (like the plasmon resonance) as the anchor of an instrument, dispersion problems cannot be ignored.

The above considerations combine into a fourth figure of merit, that the waves guided by the structure need to be able to achieve the desired resolution. This may be achieved in a few ways. First, if the wave is slowed sufficiently, the wavelength in the direction of propagation may be small enough to interact with objects of the dimension of interest. Second, if the phase of the wave can be accurately measured, then changes in the phase due to small objects may be used for imaging, even if the wavelength of the illuminating light is too long to be scattered by the small objects. Finally, concentration

of the electromagnetic fields in the direction transverse to the direction of propagation may be utilized to obtain “cross range” resolution.

This thesis will mainly focus on the first type of structure, the chain of spheres structure of Figure 2-4; and examine whether the models found in the literature for such structures are valid. Given the pitfalls and uncertainty in those previous methods, a Green function numerical solution to the problem is proposed here. Using established effective medium model methods, the problem is reduced to the problem of a dispersive dielectric rod. This approach unambiguously identifies the frequencies of guidance and the dispersive properties of the waveguide over those frequencies. The same method is applied to the second structure (Figure 2-5), the silver nanowire, and the results evaluated and compared to the chain of spheres.

2.2 Synopsis of Waveguiding Chain Results as Presented In Literature

Within the literature, there have been many groups modeling the waveguiding properties of periodically spaced plasmonic spheres, with varying predictions and results. Some groups only consider longitudinal modes, while others consider both longitudinal and transverse. Some consider silver, others gold, and even those considering the same material use a different model for the material. For instance Quinten et al [10] considered silver nanoparticles with silver material data that had three times as much loss as the measured values by Johnson and Christy [30]. While the measured data by Johnson and

Christy has the imaginary component of the permittivity on the order of one tenth those measured by Palik [26]. Given a group chooses a material, say silver, and picks a set of measured material parameters, whether it be measured data by Johnson and Christy, Palik, or other; they typically neglect to incorporate the effects of the small size of the particle and its diminished mean free path [31]. This means the silver data used for the model implies less loss than should be expected. Even when using the same material parameters data, the model used to fit to the data often differs as well. For instance Weber and Ford [13] use a Drude model for silver with $\epsilon_\infty = 1$, while Udagedara et al also used a Drude model, but assumed a more accurate $\epsilon_\infty = 5$.

Maeir et al [11] calculated longitudinal mode energy decay lengths of $\alpha_L = 1.386 \times 10^7 m^{-1}$ ($30 dB/500 nm$) and group velocity $v_{gL} = 1.6 \times 10^7 m/s$ for gold nanospheres, but in the same paper came to a finite-difference time-domain simulation conclusion of $\alpha_L = 4.95 \times 10^6 m^{-1}$ ($10.7 dB/500 nm$). It is questionable if the manner in which they simulated the system resulted in an accurate measurement of the attenuation of *only* the guided wave. Chau et al [43] use a "method" of stimulating a chain of nanoparticles with a plane wave traveling in the direction of the axis of the chain, then assumed any field along this axis past the third sphere must be from a guided wave because the other spheres in the chain are in the "shadow" of the first few spheres, completely ignoring diffraction and surface waves on the first and subsequent spheres. Weber and Ford also appear to neglect taking into account the non-guided field, resulting in a calculated attenuation of the order of $3.13 dB/500\text{nm}$.

Beyond the different assumptions of materials, and well established physical behavior, different groups have used different mathematical approaches to solving the problem, leading to differences in results. Many groups [10-12] use an eigenvalue problem approach, while others a method-of-moments like approach [13], and even others exotic approaches such as application of polylogarithms to avoid complex poles during integration [14].

All claim very good representation of physical phenomena, even though the dispersion diagram between the models can vary greatly, and results even varying within a single paper depending on whether performing an analytic derivation or measuring results from finite-difference time-domain simulation.

For the desired application for a nanophotonic imaging device, the attenuation of waves guided by the structure is needed to evaluate whether it is sufficiently low loss; and the propagation constant to determine if the wavelength is sufficiently small in the z direction for scattering with the objects of interest, and to determine how sensitive the structure is to dispersion.

The main question is, do these models agree? And if so, when and how; and if not, why? To decide, three of the models will be evaluated from two of the groups. A model which applies a nearest neighbor approximation, a second which applies a multi-neighbor approximation including retardation, and a third which applies a method-of-moments solution. Beyond whether the models agree, it must be determined if they are

even modeling a *guided* wave, and if the models are being applied in a region of validity for an eigenvalue solution.

2.3 Nearest Neighbor Approximation

The nearest neighbor approximation is an application of Förster Theory [16] and is based on the idea of near-field energy transfer between nearest neighbor particles. This method may be applied to model a string of identical equidistant particles in a host medium.

To apply the approximation, one must first express the fields of each particle. This is achieved by considering the multipole expansion of the electric field of a particle given its charge distribution, and by noting that at the frequencies and distances of interest (visible light and distances on the order of 1 nm), and that the total charge of the particles of interest are 0, that the most significant term of the expansion is the dipole term [15].

With an expression for the field of a given particle, one may temporarily restrict their view of the chain of particles to two neighboring particles. The first particle will be considered to be energized and labeled the "donor" particle, while the second particle will be the next in the chain to receive the energy of the a traveling wave and labeled the "acceptor" [16].

Given the dipole representation of each particle is Hertzian, a simple equation of motion for the charge of each particle may be obtained, where the "restoring force" on any given induced dipole is composed of the electric fields of its two nearest neighbors [12]. This equation of motion may be solved by a propagating wave solution, which leads to a dispersion relation.

If the material that the particles are composed of has a negative permittivity in the visible range (such as silver or gold), the spherical shape of the particle will lead to a surface plasmon resonance in which the surface plasmon resonance is the dominant term. The dispersion relation may be simplified with an approximation which leads to a simple expression for the group velocity of the propagating wave.

The electric field of a dipole is $E_{dip} = -\frac{\gamma_i p}{4\pi\epsilon r^3}$ where $\gamma_{transverse} = \gamma_t = 1$ for transverse polarization, $\gamma_{longitudinal} = \gamma_L = -2$ for longitudinal, *p* is the dipole moment. Consider a chain of spheres represented by dipoles. The total electric field at a dipole *m* may be determined by superposition of the fields created by each dipole in the chain.

To justify the nearest neighbor approximation, note that the energy transfer rate from donor to acceptor is a function of the square of the electric field, that is to say it is function of d^{-6} [12]. Let the energy at the *m*th dipole be given by En_m and consider an infinite chain, and given the energy level of each dipole is the same, observe the ratio of the energy transfer from the nearest neighbors versus the rest of all the dipoles:

$$\frac{2\sum_{m=2}^{\infty} En_m}{2\,En_1} = \frac{\sum_{m=2}^{\infty} (m\cdot d)^{-6}}{d^{-6}} = \sum_{m=2}^{\infty} (m)^{-6}$$

which is a Riemann Zeta function. Since 6>1 the function is convergent and solvable numerically. Using MathCAD 14 to numerically solve gives $\sum_{m=2}^{\infty} (m)^{-6} = 0.017$. The nearest neighbor effect is almost 50 times stronger than the sum of all the other terms. So given the energy level of each dipole is of the same order, the nearest neighbor approximation is valid. If the energy levels are not of the same order (which can be expected if a wave is traveling down the chain), then the nearest neighbor approximation may need to be refined, and is likely missing relevant interactions between particles farther down the chain than the simple nearest neighbor model would suggest. We will not consider this at the moment.

The *m*th dipole produces the following field at the location of the *m*+1 and *m*-1 dipoles:

$$E_{i,m} = -\frac{\gamma_i\, p_{i,m}(t)}{4\pi\epsilon\, d^3}$$

The equation of motion for the dipole moment of the Hertzian dipole on a given particle is derived as follows: Assuming no radiation and perfect conductors there would be no damping and we would have:

$$m\cdot\frac{d^2x}{dt^2} = -k\cdot x$$

Where now *k* is the spring constant that models the restoring force responsible for the

plasmon resonance of the particle (this is the force that tends to bring the charges in the resonating dipole back together again). In reality we are not using a lossless perfect conductor, so the equation of motion must account for damping of the motion:

$$m\frac{d^2x}{dt^2}+m\Gamma_I\frac{dx}{dt}+k\,x=0$$

Our particles have charge, and are undergoing acceleration (moving back and forth between the poles). Charge undergoing acceleration radiates, hence our equation should have a radiation driving function:

$$m\frac{d^2x}{dt^2}+m\Gamma_I\frac{dx}{dt}+k\,x=F$$

This radiation damping by an accelerated charge is assumed to be governed by the Lamor formula [17]:

$$En_{rad}\propto\frac{2e^2a^2T}{3c^2}$$

Where En_{rad} is the energy radiated, e is the charge of the particle being accelerated (in our case we would replace e with q), a is the magnitude of the acceleration, and T the period of acceleration.

The Larmor power formula may be used to determine the power radiated by such an accelerated particle:

$$P(t)=\frac{2}{3}\frac{e^2}{c^3}(\ddot{x})^2$$

Which gives radiation reaction force on the charge of the dipole as:

$$F_{rad} = \frac{2}{3}\frac{e^2}{c^3}\ddot{x}$$

This can be seen by noting that a particle of mass *m* and charge *e* acted on by external force **F** moves according to Newton's equation of motion, $\boldsymbol{F}_{ext} = m\dot{\boldsymbol{v}}$. Since the particle is accelerated, it emits radiation at a rate given by the Larmor power formula, $P(t) = \frac{2}{3}\frac{e^2}{c^3}(\dot{\boldsymbol{v}})^2$. To account for radiative energy loss and the effect this loss will have on the mechanical motion of the particle, modify Newton's equation by adding a radiative reaction force $\boldsymbol{F}_{rad}$, $m\dot{\boldsymbol{v}} = \boldsymbol{F}_{ext} + \boldsymbol{F}_{rad}$. To determine $\boldsymbol{F}_{rad}$, demand that the work done by this force on the particle in a given time interval $t_1 < t < t_2$ be equal to the negative of the energy radiated in that time span:

$$\int_{t_1}^{t_2} \boldsymbol{F}_{rad}\cdot\boldsymbol{v}\,dt = -\int_{t_1}^{t_2} \frac{2}{3}\frac{e^2}{c^3}\dot{\boldsymbol{v}}\cdot\dot{\boldsymbol{v}}\,dt$$

Integration by parts of the right side:

$$\int_{t_1}^{t_2} \boldsymbol{F}_{rad}\cdot\boldsymbol{v}\,dt = -\frac{2}{3}\frac{e^2}{c^3}\dot{\boldsymbol{v}}\cdot\boldsymbol{v}\Big|_{t_1}^{t_2} + \frac{2}{3}\frac{e^2}{c^3}\int_{t_1}^{t_2}\ddot{\boldsymbol{v}}\cdot\boldsymbol{v}\,dt$$

The motion is periodic, so with judicious choice of t_1 and t_2 $\dot{\boldsymbol{v}}\cdot\boldsymbol{v} = 0$ and $\int_{t_1}^{t_2} \boldsymbol{F}_{rad}\cdot\boldsymbol{v}\,dt = \frac{2}{3}\frac{e^2}{c^3}\int_{t_1}^{t_2}\ddot{\boldsymbol{v}}\cdot\boldsymbol{v}\,dt$ so:

$$\boldsymbol{F}_{rad} = \frac{2}{3}\frac{e^2}{c^3}\ddot{\boldsymbol{v}} \quad [17]$$

Define the characteristic time as $\tau = \frac{2}{3}\frac{e^2}{m c^3}$, the relaxation frequency due to radiation into the far field as $\Gamma_R = \omega_0^2 \tau$ then $F_{rad} = \frac{2}{3}\frac{e^2}{c^3}\dddot{x} = m\tau\ddot{x} = m\frac{\Gamma_R}{\omega_0^2}\ddot{x}$ and the equation of motion for the charge of the dipole including damping from finite conductivity and radiation reaction is:

$$m\frac{d^2x}{dt^2} + m\Gamma_I\frac{dx}{dt} + kx = m\frac{\Gamma_R}{\omega_0^2}\frac{d^3x}{dx^3}$$

Then accounting for the force placed on the *m*th dipole from its nearest neighbors we have:

$$m\frac{d^2x}{dt^2} + m\Gamma_I\frac{dx}{dt} + kx = m\frac{\Gamma_R}{\omega_0^2}\frac{d^3x}{dx^3} - q\cdot\frac{\gamma_i p_{m-1}}{4\pi\epsilon d^3} - q\cdot\frac{\gamma_i p_{m+1}}{4\pi\epsilon d^3}$$

We're interested in the effect on the *m*th dipole moment which is defined by $q\cdot x$ so multiplying and dividing the left side by *q* gives:

$$m\cdot\frac{d^2x}{dt^2} = \frac{m}{q}\cdot\frac{d^2q\cdot x}{dt^2}$$

And back substitution and simplification:

$$\frac{d^2q\cdot x}{dt^2} = -\frac{k}{m}\cdot q\cdot x - q\cdot\frac{q}{m}\cdot\frac{\gamma_i p_{m-1}}{4\pi\epsilon d^3} - q\cdot\frac{q}{m}\cdot\frac{\gamma_i p_{m+1}}{4\pi\epsilon d^3}$$

$$\frac{d^2q\cdot x}{dt^2} + \Gamma_I\frac{dq\cdot x}{dt} + \frac{k}{m}q\cdot x = \frac{\Gamma_R}{\omega_0^2}\frac{d^3q\cdot x}{dx^3} - \frac{q^2}{m}\cdot\frac{\gamma_i p_{m-1}}{4\pi\epsilon d^3} - \frac{q^2}{m}\cdot\frac{\gamma_i p_{m+1}}{4\pi\epsilon d^3}$$

Recognizing that $q\cdot x = p_m$ and $\frac{q}{m} = \frac{e\cdot N_e}{m_e\cdot N_e} = \frac{e}{m_e}$ then:

$$\ddot{p}_{i,m} = -\frac{k}{m}\cdot p_{i,m} - \Gamma_I \dot{p}_{i,m} + \frac{\Gamma_R}{\omega_0^2}\dddot{p}_{i,m} - \gamma_i \cdot \frac{qe}{4\pi m_e \epsilon d^3}\cdot\left(p_{m-1} + p_{m+1}\right)$$

$$= -\omega_0^2 \cdot p_{i,m} - \Gamma_I \dot{p}_{i,m} + \frac{\Gamma_R}{\omega_0^2}\dddot{p}_{i,m} - \gamma_i \cdot \omega_1^2 \cdot \left(p_{m-1} + p_{m+1}\right)$$

Where ω_0 is the circular resonance frequency of the dipole, and ω_1 is the circular resonance frequency between nearest neighbor dipoles. The total field at the *m*th dipole is given by the superposition of all the fields at the location of the *m*th dipole. Restricting our view to the nearest neighbor's, then the approximate field is given by:

$$E_m = -\frac{\gamma_i p_{i,m}(t)}{4\pi\epsilon d^3}$$

Given the motion of the charge is sinusoidal, then $p_{i,m}(t)$ has a propagating wave solution:

$$p_{i,m} = P_{i,0} e^{-\alpha m d + j(\omega t \pm \beta m d)}$$

Where $P_{i,0}$ is the maximum of the dipole moment for the $m = 0$ dipole in the *i* direction. $(\omega t - \beta m d)$ is appropriate when the phase and group velocity are parallel, and $(\omega + \beta m d)$ when anti-parallel. The damping of the plasmon wave per is given by α, while the angular frequency and wave vector of the plasmon wave are given by ω and β.

Back substitution gives:

$$\ddot{p}_{i,m} = \left(P_i e^{-\alpha m d + j(\omega t \pm \beta m d)}\right)$$

$$= -\omega_0^2 P_{i,0} e^{-\alpha m d + j(\omega t \pm \beta m d)} - \Gamma_I \left(P_{i,0} e^{-\alpha m \dot{d} + j(\omega t \pm \beta m d)} \right) + \frac{\Gamma_R}{\omega_0^2} \left(P_{i,0} e^{-\alpha m \dddot{d} + j(\omega t \pm \beta m d)} \right)$$
$$- \gamma_i \omega_1^2 \left[P_{i,0} e^{-\alpha (m+1) d + j(\omega t \pm \beta (m+1) d)} + P_{i,0} e^{-\alpha (m-1) d + j(\omega t \pm \beta (m-1) d)} \right]$$

$$= -\omega_0^2 P_{i,0} e^{-\alpha m d + j(\omega t \pm \beta m d)} - j\omega \Gamma_I P_{i,0} e^{-\alpha m d + j(\omega t \pm \beta m d)} - j\omega^3 \frac{\Gamma_R}{\omega_0^2} P_{i,0} e^{-\alpha m d + j(\omega t \pm \beta m d)}$$
$$- \gamma_i \omega_1^2 \left[P_{i,0} e^{-\alpha (m+1) d + j(\omega t \pm \beta (m+1) d)} + P_{i,0} e^{-\alpha (m-1) d + j(\omega t \pm \beta (m-1) d)} \right]$$

separation of real and imaginary parts gives:

$$\omega^2 = \omega_0^2 + 2\gamma_i \omega_1^2 \cos(\beta d) \cosh(\alpha d) \quad \text{(dispersion relation)}$$

$$0 = \omega \Gamma_I + \frac{\omega^3 \Gamma_R}{\omega_0^2} + 2\gamma_i \omega_1^2 \sin(\beta d) \sinh(\alpha d)$$

We essentially may have two cases. The first, small damping, allows for a simple approximation (i.e. $\alpha d \ll 1$); and the second, large damping, which does not permit such a simplification. We will assume small damping, and verify our assumption was correct. Note that given spacing d may be on the order of tens to hundreds of nanometers, α might be quite large by traditional standards, and yet still fall under the regime of "small damping". For small damping we have dispersion relation:

$$\omega^2 = \omega_0^2 + 2\gamma_i \omega_1^2 \cos(\beta d)$$

Which gives dispersion diagram:

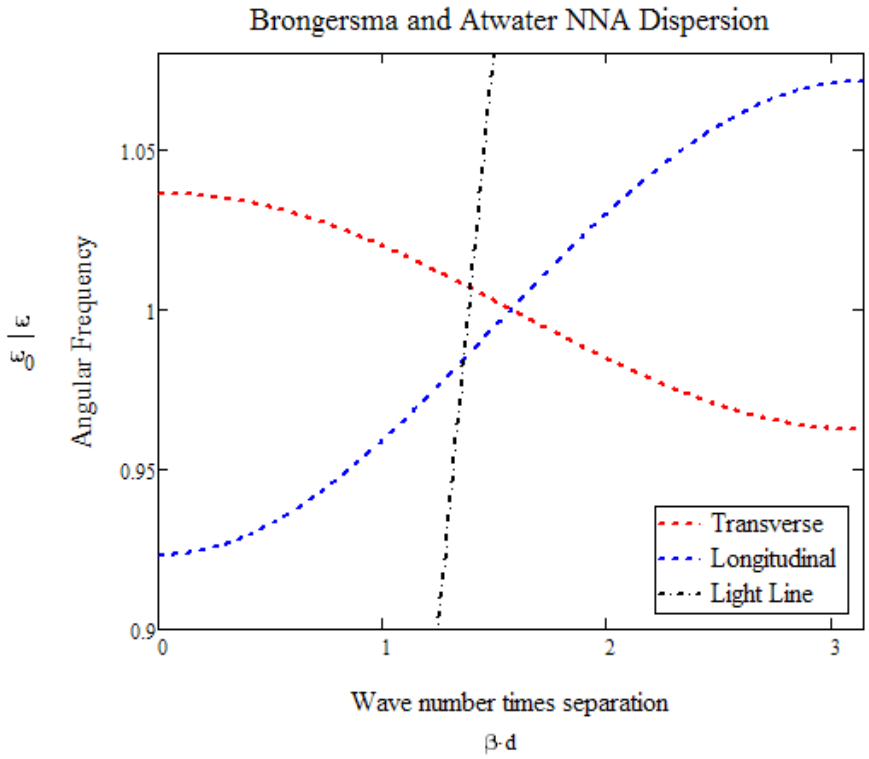

Fig. 2-7 Brongersma and Atwater Dispersion Diagram for Nearest Neighbor Model

This was achieved by assuming that for surface-plasmon resonance in the visible spectrum, $\omega_0 \approx 5\times10^{15} s^{-1}$ [12]. For a given nanoparticle, the magnitude of the oscillating charge q is given by $q = e\rho_{el}V$, where e is the charge of an electron, ρ_{el} is the charge concentration, and V is the volume of the given particle. Given the nanoparticles are silver then $\rho_{el} = 5.85\times10^{22} cm^{-3}$ [12][37].

Given the particle radius is assumed to be $r = 25\,nm$, suspended in vacuum (refractive index $n = 1$), and spaced a distance $d = 75\,nm$ apart; charge $q = 6.1\times10^{-13}\,C$ [12], effective electron mass of an electron in silver at optical frequencies $m_e = 8.7\times10^{-31}\,kg$ then:

$$\omega_1 = \sqrt{\frac{q\,e}{4\pi\,m_e\epsilon_0 n^2 d^3}} = \sqrt{\frac{e^2\rho_{el}r^3}{3\,m_e\epsilon_0 n^2 d^3}} = 1.4\times10^{15}\,s^{-1}$$

The group velocity:

$$v_g = \frac{d\,\omega}{d\beta} = \frac{\frac{d\,\omega^2}{d\beta}}{\frac{d\,\omega^2}{d\,\omega}}$$

And for small damping: $\frac{d\,\omega}{d\beta} = \frac{\frac{d}{d\beta}\left(\omega_0^2 + 2\,\gamma_i\,\omega_1^2\cos(\beta\,d)\right)}{\frac{d(\omega^2)}{d\,\omega}} = \frac{d\,\gamma_i\,\omega_1^2\sin(\beta\,d)}{\omega}$.

Also note, since $\frac{d\,\omega^2}{d\beta}$ is the slope of the dispersion diagram of Fig. 2-7, according to this model it appears that the longitudinal modes propagate faster than transverse modes. Within the bounds of this model this understanding will be accepted, but improved models will contradict this. So within the bounds of this model, transverse modes are better at slowing the wave, as may be desired in some applications, but the question remains as to which modes undergo the greatest attenuation; as a slow mode that attenuates too quickly would be useless. The slope also implies the transverse modes are backwards traveling waves.

Again, considering the regime of small damping $\alpha d \ll 1$, we can simplify:

$$0 = \omega\Gamma_I + \frac{\omega^3\Gamma_R}{\omega_0^2} + 2\gamma_i\omega_1^2\sin(\beta d)\sinh(\alpha d) \Rightarrow 0 = \omega\Gamma_I + \frac{\omega^3\Gamma_R}{\omega_0^2} - 2v_g\frac{\omega}{d}\sinh(\alpha d)$$

$$\approx \omega\Gamma_I + \frac{\omega^3\Gamma_R}{\omega_0^2} - 2v_g\frac{\omega}{d}\alpha d \Rightarrow \alpha = \frac{\Gamma_I + \frac{\omega^2}{\omega_0^2}\Gamma_R}{2v_g}$$

Γ_R is already known, Γ_I must be determined. There are two possible approaches. First, as was done in the literature that defined this model, an application of Matthiessen's rule can be made, as well as various semiconductor theory parameters cited, and without much proof, given various assumptions about mean free path etc., the approximation $\Gamma_I = 7.9\times10^{13}s^{-1}$ is stated. For Γ_R , $\Gamma_R = \omega_0^2\tau$ where $\tau = \frac{2e^2}{3m_ec^3} = 6.26\times10^{-24}s^{-1}$ which gives $\Gamma_R = 1.6\times10^8 s^{-1}$. Since $\frac{\Gamma_I}{\Gamma_R} \propto 10^5$ Γ_R may be neglected. Hence $\alpha = 7.9\times10^{13}\frac{s^{-1}}{2v_g}$. At resonance, $v_{g,L} = 5.8\times10^7 m/s$ and $v_{g,T} = 2.9\times10^7 m/s$ for the given distance and radius parameters. This means for a longitudinal wave $\alpha = \frac{7.9\times10^{13}s^{-1}}{2\cdot5.8\times10^7 m/s} = 6.8\times10^5 m^{-1}$, or $\alpha = 3dB/500nm$. Recall this was assuming small damping, so to verify that we truly are in the small damping regime, $\alpha d = 6.8\times10^5\cdot75\times10^{-9} = 5.1\times10^{-2}$,which reasonably satisfies $\alpha d \ll 1$ and confirms that small damping is a fair assumption. Finally, attenuation for the transverse mode is twice that for the longitudinal mode, $\alpha_T = 3\text{dB}/250nm$.

So for the application of imaging, attenuation may be a serious concern if the distance in which the wave must be guided is significant. While we want smaller velocity to shrink the wavelength, we also desire a lager velocity since, at least according to this model, the attenuation is proportional to the inverse of velocity.

These results were arrived at using a bit of a blind assumption for Γ_I . The second, and more preferred method of calculating Γ_I , is to diverge from what was used in the literature, and use a Drude model for silver (see Appendix A and B), and recognize that Γ_I is nothing more than the fitting parameter γ of a Drude model. Assuming a particle radius of 25 nm, then a Drude model we fit for Γ_1 (i.e. γ in the typical Drude notation) is $\Gamma_1 = 4.9942\times10^{13} s^{-1}$. We still have the same calculation for the parameter $\Gamma_R = \omega_0^2 \tau$, which gives $\Gamma_R = 1.6\times10^{8} s^{-1}$. So again we have case $\frac{\Gamma_I}{\Gamma_R} \propto 10^5$ and Γ_R may be neglected. Finally:

$$\alpha = \frac{4.99\times10^{13} s^{-1}}{2 v_g}$$

$$v_{g,T} = \frac{d\,\gamma_i \omega_1^2 \sin(\beta d)}{\omega} = \frac{d\,\omega_1^2 \sin(\beta d)}{\omega}$$

$$v_{g,L} = 2 v_{g,T}$$

As already determined, $\omega_1 = 1.4\times10^{15} s^{-1}$. At resonance, $\omega = \omega_0$ so $\omega^2 = \omega_0^2 + 2\gamma_i \omega_1^2 \cos(\beta d) \Rightarrow \omega_0^2 = \omega_0^2 + 2\gamma_i \omega_1^2 \cos(\beta d) \Rightarrow \cos(\beta d) = 0$ so $\beta d = \frac{\pi}{2}$ and at resonance $\sin(\beta d) = 1$ and at resonance:

$$v_{g,T} = \frac{d\,\gamma_i\,\omega_1^2 \sin(\beta\, d)}{\omega} = \frac{d\,\omega_1^2 \sin(\beta\, d)}{\omega_0} = \frac{75\times10^{-9}\,m\cdot\left(1.4\times10^{15}\,s^{-1}\right)^2}{\omega_0} = \frac{1.470\times10^{23}}{\omega_0}\,m/s$$

The original model of Brongersma and Atwater[12] used an assumed plasmon resonance frequency for silver which was given by $\omega_0 \approx 5\times10^{15}\,s^{-1}$. Note that this is where confusion by the term *plasmon resonance* comes into play. We are interested in the circular resonance of the dipole which is the resonance of the silver *sphere*, not just the resonance of *material* the sphere is made out of. Approximate values for ω_0 work reasonably well for either a sphere or bulk material, because the resonance in either case are of the same order, but a lack of precision is presented by assuming they are in fact the same.

We, on the other hand, are using a Drude model fit to measured data and adjusted for our exact sphere dimensions, which means we *have* an exact value for the sphere resonance frequency, given our model. As determined in Appendix A, the resonance occurs at our parameter $\omega_{pole} \approx 5.192\times10^{15}$. Note this is the fit parameter ω_p offset by $\frac{1}{\sqrt{8}}$ to account for $\epsilon_\infty = 6$ of the Drude model, and the fact that resonance for a sphere occurs at $\epsilon_r = -2$ instead of $\epsilon_r = 0$, as in the case for an infinite distribution of material, as described in the appendix. So from our Drude model:

$$v_{g,T} = \frac{1.470\times10^{23}}{\omega_0}\,m/s = \frac{1.470\times10^{23}}{5.192\times10^{15}}\,m/s = 2.831\times10^{7}\,m/s$$

$$v_{g,L} = 2\,v_{g,T} = 5.663\times10^{7}\,m/s$$

This permits the attenuation to be determined from $\alpha = \frac{4.99 \times 10^{13}\, s^{-1}}{2 v_g}$ which gives:

$$\alpha_L = 4.406 \times 10^5 \quad \text{or in terms of intensity} \quad \alpha_{L\,intensity} = 2\alpha_L$$

$$\alpha_T = 8.812 \times 10^5 \quad \text{or in terms of intensity} \quad \alpha_{T\,intensity} = 2\alpha_T$$

For comparison to Brongersma and Atwater [12], in dB the attenuation per 500 nm is $\alpha_{L\,intensity} = 1.914\, dB/500\text{nm}$, and $\alpha_{T\,intensity} = 3.828\, dB/500\text{nm}$ (i.e. $\alpha_{L\,intensity} = 3\, dB/784\, nm$, whereas Brongersma and Atwater [12] give result $\alpha_{L\,Bron\,At} = 3\, dB/500\text{nm}$. So we are somewhat lower with our more precise silver model.

2.4 Multi-Neighbor Approximation with Retardation

In a similar approach to the Nearest Neighbor Approximation by Brongersma et al, as described in the previous section, a multi-neighbor approach which takes into account dipolar retardation may be utilized, as detailed by Weber and Ford [13]. In the appropriate limit it may be reduced to a nearest neighbor approximation with retardation and compared to the previous model.

The fundamental excitations that support propagation are the dipolar resonances of the particles, which are often also referred to as Mie resonances (Appendix C) or plasma resonances. As selected before, the noble metal silver will be used, with a Drude

model like the one given in (Appendix A), with the exception that $\epsilon_\infty = 1$ to match the work in the literature.

Again consider the infinite chain of equidistant identical particles, and assume the fields that define the interaction are the fields of an infinitesimal dipole. This is adequate so long as the center-to-center separation between the particles *d* is greater than three radii. Then the fields of an infinitesimal dipole (that now contains higher order dynamic terms not considered in the case given in the previous section)

$$E_r = \eta \frac{I_0 L \cos\theta}{2\pi r^2}\left[1 + \frac{1}{jkr}\right] e^{-jkr}$$

$$E_\theta = j\eta \frac{k I_0 L \sin\theta}{4\pi r}\left[1 + \frac{1}{jkr} - \frac{1}{(kr)^2}\right] e^{-jkr}$$

$$E_\varphi = 0$$

Given $j\omega p = I L$ then $\eta I L = \sqrt{\frac{\mu}{\epsilon}}\, j\omega p = \frac{jkp}{\epsilon}$ and:

$$E_r = \frac{\cos\theta}{2\pi\epsilon}\left[\frac{1}{r^3} + \frac{jk}{r^2}\right] e^{-jkr} p$$

$$E_\theta = \frac{\sin\theta}{4\pi\epsilon}\left[\frac{-k^2}{r} + \frac{jk}{r^2} + \frac{1}{(r)^3}\right] e^{-jkr} p$$

$$E_\varphi = 0$$

Then for longitudinal modes, $\theta = 0$ in the z-direction, so z-directed E:

$$E_{z\_L} = \frac{1}{2\pi\epsilon}\left[\frac{1}{r^3} + \frac{jk}{r^2}\right] e^{-jkr} p$$

And for transverse modes:

$$E_{z\_T} = \frac{1}{4\pi\epsilon}\left[\frac{-k^2}{r} + \frac{jk}{r^2} + \frac{1}{(r)^3}\right] e^{-jkr}\, p$$

Unfortunately, to follow the convention in the literature and textbooks, the symbol used for the polarizability is α, the same symbol used for the attenuation constant. In the following derivations I will be careful to indicate when we are done using the polarizability and revert back to that symbol for attenuation. Also, note that the convention in the literature is to label the wave number k for this multi-neighbor approach, and later in continuation for the finite chain approach. In this process, the wave number k is initially considered completely real, then later converted to a complex wave number through a perturbation assumption. It is important to recognize that during the analysis, a completely real k is equivalent to β of the previous section when comparisons are made, before k is converted to a complex quantity. There are concerns about the validity of the conversion presented in the literature, which will be discussed, but it is important to clarify why a change in notation for real wave number is occuring. It is to keep in line with the literature and in preparation for conversion to a complex quantity.

For a linear chain of point dipoles spaced a distance *d*, in the absence of any externally applied field, the induced dipole moment for any given dipole is its polarizability times the total field at the location of the dipole. Then the total field is the contribution from all other dipoles in the chain:

$$p_n = \alpha(\omega) \sum_{m,m\neq n} E_z(r = |n-m|d)$$

So for longitudinal modes:

$$p_n = \alpha(\omega) \sum_{m,m\neq n} \frac{1}{2\pi\epsilon}\left[\frac{1}{|n-m|^3 d^3} + \frac{jk}{|n-m|^2 d^2}\right] e^{-jk|n-m|d}\, p_m$$

and for transverse modes:

$$p_n = \alpha(\omega) \sum_{m,m\neq n} \frac{1}{4\pi\epsilon}\left[\frac{-k^2}{|n-m|d} + \frac{jk}{|n-m|^2 d^2} + \frac{1}{|n-m|^3 d^3}\right] e^{-jk|n-m|d}\, p_m$$

For a periodic structure, the supported modes are Floquet modes, hence

$p_m = p_n e^{-jk(m-n)d}$ and for longitudinal modes:

$$p_n = \alpha(\omega) \sum_{m,m\neq n} \frac{1}{2\pi\epsilon}\left[\frac{1}{|n-m|^3 d^3} + \frac{jk}{|n-m|^2 d^2}\right] e^{-jk|n-m|d}\, p_n e^{-jk(m-n)d}$$

let $L = n-m$ then:

$$1 = \alpha(\omega) \sum_{L,L\neq 0} \frac{1}{\pi\epsilon}\left[\frac{1}{|L|^3 d^3} + \frac{jk}{|L|^2 d^2}\right] e^{-jk|L|d} e^{jk(L)d}$$

$$= \alpha(\omega) \sum_{L=1}^{\infty} \frac{1}{\pi\epsilon}\left[\frac{1}{L^3 d^3} + \frac{jk}{L^2 d^2}\right] \cos(kLd)\, e^{-jkLd}$$

or:

$$1 - \alpha(\omega) \sum_{L=1}^{\infty} \frac{1}{\pi\epsilon}\left[\frac{1}{L^3 d^3} + \frac{jk}{L^2 d^2}\right] \cos(kLd)\, e^{-jkLd} = 0$$

Similarly for transverse modes:

$$p_n = \alpha(\omega) \sum_{m,m\neq n} \frac{1}{4\pi\epsilon}\left[\frac{-k^2}{|n-m|d} + \frac{jk}{|n-m|^2 d^2} + \frac{1}{|n-m|^3 d^3}\right] e^{-jk|n-m|d}\, p_n e^{-jk(m-n)d}$$

let $L = n-m$ then:

$$1 = \alpha(\omega) \sum_{L, L \neq 0} \frac{1}{4\pi\epsilon} \left[\frac{-k^2}{|L| d} + \frac{jk}{|L|^2 d^2} + \frac{1}{|L|^3 d^3} \right] e^{-jk|L|d} e^{jk(L)d} =$$

$$\alpha(\omega) \sum_{L=1}^{\infty} \frac{1}{2\pi\epsilon} \left[\frac{-k^2}{L d} + \frac{jk}{L^2 d^2} + \frac{1}{L^3 d^3} \right] \cos(k L d) e^{-jkLd}$$

$$\text{hence} \quad 1 - \alpha(\omega) \sum_{L=1}^{\infty} \frac{1}{2\pi\epsilon} \left[\frac{-k^2}{L d} + \frac{jk}{L^2 d^2} + \frac{1}{L^3 d^3} \right] \cos(k L d) e^{-jkLd} = 0$$

L is a natural number, so for clarity lets just redefine *n* such that $n = L$ then the dispersion relations are:

$$\text{Longitudinal:} \quad 1 - \alpha(\omega) \sum_{n=1}^{\infty} \frac{1}{\pi\epsilon} \left[\frac{1}{n^3 d^3} + \frac{jk}{n^2 d^2} \right] \cos(k n d) e^{-jknd} = 0$$

$$\text{Transverse:} \quad 1 - \alpha(\omega) \sum_{n=1}^{\infty} \frac{1}{2\pi\epsilon} \left[\frac{-k^2}{n d} + \frac{jk}{n^2 d^2} + \frac{1}{n^3 d^3} \right] \cos(k n d) e^{-jknd} = 0$$

For completely real *k*, these dispersion relations **<u>can be solved for complex frequencies</u>** $\omega = \omega(k)$. The modes must be decaying in time, hence for our time convention $e^{j\omega t}$, $\Im(\omega) \geq 0$, but factor $e^{-jkd} = e^{-j\omega\sqrt{\mu\epsilon}d}$ implies the sums expressed in the dispersion relations only converge for $\Im(\omega) \leq 0$. This may be addressed by casting the sums into the complex plane, evaluating them in the upper half-plane, then analytically continue them into the lower-half plane. This method is applied by other groups, namely Alu and Engheta [14].

Although this complex frequency method has been used by other authors for waveguide problems it should be used with caution. Conforti and Guasoni [40] state categorically that “In view of these aspects we can assert that above the light line, calculating the dispersion curve by fixing real wavevector leads to totally wrong results.”

This means that below the onset of guided waves the results cannot be trusted. But since we are trying to solve the problem to determine among other things the onset of guided waves, this leaves us in a precarious position if we rely on this complex frequency approach.

Conforti and Guasoni also point out that: “when a real metal is considered, the losses are so high that the effects on the dispersion curves cannot be treated by first order perturbation, as it is evident from the big influence of absorption also in the real part of propagation constant.” This brings into question any derivation that assumes from the outset low attenuation, therefore derives the propagation constant under this assumption and then attempts to force the attenuation to fit in as a perturbation.

The issues with the complex frequency approach, and with infinities in the infinite chain model, may be avoided by considering the finite chain, as done in Section 2.5. However it is important to show that the more “physically correct” model of multi-neighbor interactions reduces to the nearest neighbor interaction of Section 2.3 in the appropriate limit.

For a dielectric sphere in vacuum, the quasi-static dipole polarizability is given by $\alpha(\omega) = \frac{\epsilon(\omega)-1}{\epsilon(\omega)+2} 4\pi\epsilon_0 a^3$ (Appendix D) where a is the radius of the sphere and $\epsilon(\omega)$ is the relative permittivity of the sphere. This polarizability for the moment ignores the effect of radiation reaction. For metal spheres, and keeping in line with what is presented in the literature, use the simple Drude model for dielectric response, i.e.

$\epsilon(\omega) = 1 - \frac{{\omega_p}^2}{\omega(\omega + j\nu)}$ [18] (as noted earlier, there is a difference in ϵ_∞ from our more precise Drude model in Appendix A – we will use the literatures less precise model and update only after affirming if the method is valid), where ω_p is the plasma frequency of the metal, and ν is the electron scattering rate, a damping term corresponding to the the collision of free electrons with the crystal lattice of the metal or impurities within.

Then $\alpha(\omega) = \frac{-{\omega_p}^2}{-{\omega_p}^2 + 3\omega(\omega + j\nu)} 4\pi\epsilon_0 a^3 = \frac{{\omega_0}^2}{{\omega_0}^2 - \omega(\omega + j\nu)} 4\pi\epsilon_0 a^3$, where $\omega_0 = \omega_p/\sqrt{3}$ is the plasma resonance frequency of the sphere.

The quasi-static dipole polarizability given only includes absorption loss (due to ϵ'') since the radiation reaction has been neglected [19]. The extinction cross section of a particle is given by $C_{ext} = \frac{1}{\epsilon_0 k^2} \Re(S(0))$, where $S(0)$ is the amplitude function (scattering matrix), which describes the amplitude and phase of a scattered wave. In our case $S(0)$ is the forward directed amplitude function, which is given by $S(0) = ik^3\alpha$. For our quasi-static polarizability $\Re(S(0)) = 0$ for real α . We can include the radiation reaction as follows:

The electric field of a scattered wave is $E = \frac{1}{4\pi\epsilon_0} \frac{k^2 p \sin\varphi}{r} e^{-jkr}$, where φ is the angle between the scattered wave and *p*. The corresponding intensities of the incident and scattered radiation are given by the Poynting vector as $I_0 = \frac{c\epsilon_0}{2}|E_0|^2$ and

$I = \frac{c\,\epsilon_0}{2}|E|^2$, and integrating *I* over a large sphere gives total scattered power

$W = \frac{c}{3(4\pi\epsilon_0)}k^4|p|^2$. Dividing by incident intensity gives scattering cross section

$C_{scat} = \frac{k^4}{6\pi\epsilon_0^2}|\alpha|^2$.

The amplitude function due to absorption is $S(0) = jk^3\alpha$, hence

$C_{abs} = 4\pi k\Re(j\alpha)$, $C_{ext} = C_{abs} + C_{scat}$, so $S_{total}(0) = jk^3\alpha + \frac{1}{(24\pi^2\epsilon_0)}k^6\alpha^2$, or

transforming to account for radiation reaction and scattering , $\frac{1}{\alpha} \rightarrow \frac{1}{\alpha} - j\frac{1}{(6\pi\epsilon_0)}k^3$ [35].

With this more general polarizability expression, given

$\alpha(\omega) = \frac{\omega_0^2}{\omega_0^2 - \omega(\omega + j\nu)}4\pi\epsilon_0 a^3$, then $\frac{1}{\alpha(\omega)} = \frac{\omega_0^2 - \omega(\omega + j\nu)}{\omega_0^2 4\pi\epsilon_0 a^3}$ and, transforming to

account for radiation reaction and scattering:

$$\frac{1}{\alpha} \rightarrow \frac{1}{\alpha} - j\frac{1}{(6\pi\epsilon_0)}k^3 = \frac{\omega_0^2 - (\omega^2 + j\nu\omega)}{\omega_0^2 4\pi\epsilon_0 a^3} - j\frac{2}{3\cdot 4\pi\epsilon_0}k^3$$

$$= -\frac{a^{-3}}{4\pi\epsilon_0}\left[\frac{\omega^2}{\omega_0^2}\left(1 + \frac{2}{3}j\omega\frac{\omega_0^2}{c^3}a^3\right) + \frac{j\omega\nu}{\omega_0^2}\right] + \frac{a^{-3}}{4\pi\epsilon_0}$$

So finally for the two mode polarizabilities we have,

Longitudinal:

$$\frac{1}{\alpha} = -\frac{a^{-3}}{4\pi\epsilon_0}\left[\frac{\omega^2}{\omega_0^2}\left(1 + \frac{2}{3}j\omega\frac{\omega_0^2}{c^3}a^3\right) + \frac{j\omega\nu}{\omega_0^2}\right] + \frac{a^{-3}}{4\pi\epsilon_0}$$

$$= \sum_{n=1}^{\infty} \frac{1}{\pi \epsilon} \left[\frac{1}{n^3 d^3} + \frac{jk}{n^2 d^2} \right] \cos(k n d) e^{-jknd}$$

$$\frac{\omega^2}{\omega_0^2} \left(1 + \frac{2}{3} j \omega \frac{\omega_0^2}{c^3} a^3 \right) + \frac{j \omega \nu}{\omega_0^2} = 1 - \sum_{n=1}^{\infty} 4 a^3 \left[\frac{1}{n^3 d^3} + \frac{jk}{n^2 d^2} \right] \cos(k n d) e^{-jknd}$$

Transverse:

$$\frac{1}{\alpha} = \frac{-a^{-3}}{4 \pi \epsilon_0} \left[\frac{\omega^2}{\omega_0^2} \left(1 + \frac{2}{3} j \omega \frac{\omega_0^2}{c^3} a^3 \right) + \frac{j \omega \nu}{\omega_0^2} \right] + \frac{a^{-3}}{4 \pi \epsilon_0}$$

$$= \sum_{n=1}^{\infty} \frac{1}{2 \pi \epsilon} \left[\frac{-k^2}{n d} + \frac{jk}{n^2 d^2} + \frac{1}{n^3 d^3} \right] \cos(k n d) e^{-jknd}$$

$$\frac{\omega^2}{\omega_0^2} \left(1 + \frac{2}{3} j \omega \frac{\omega_0^2}{c^3} a^3 \right) + \frac{j \omega \nu}{\omega_0^2} = 1 - \sum_{n=1}^{\infty} 2 a^3 \left[\frac{-k^2}{n d} + \frac{jk}{n^2 d^2} + \frac{1}{n^3 d^3} \right] \cos(k n d) e^{-jknd}$$

Before continuing, lets evaluate these relations by comparing their quasi-static limit to the relation derived using the nearest neighbor approximation in the previous section. The quasi-static response of a lossless metal sphere corresponds to $\nu = 0$ and $c = \infty$, then the dispersion relations become:

Longitudinal:

$$\frac{\omega^2}{\omega_0^2} = 1 - \sum_{n=1}^{\infty} 4 \frac{a^3}{n^3 d^3} \cos(k n d) e^{-jknd}$$

Transverse:

$$\frac{\omega^2}{\omega_0^2} = 1 + \sum_{n=1}^{\infty} 2 \frac{a^3}{n^3 d^3} \cos(k n d) e^{-jknd}$$

Which results in the following plot:

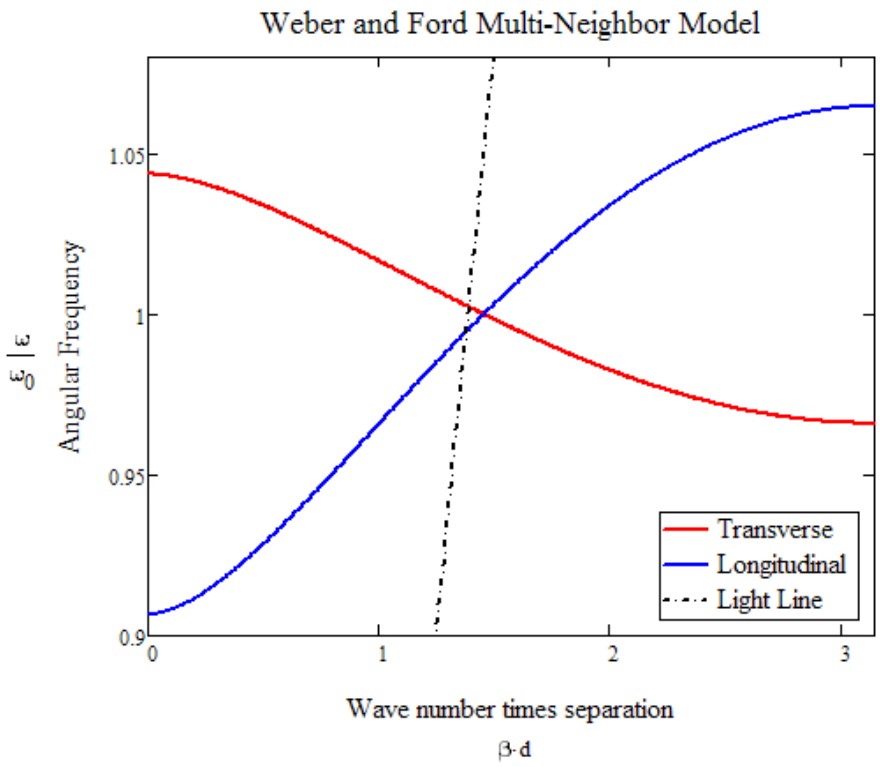

Fig. 2-8 Weber and Ford Multi-Neighbor Model Dispersion Diagram in Terms of ω/ω_0 vs. βd

A comparison to the previous nearest neighbor model can be made if it is recognized that reducing the quasi-static limit of the multi-neighbor model to only its two nearest neighbors makes the models functionally identical, except for differences in assumptions of material parameters used by each group. These different assumptions can be removed by adjusting ω_1 of the nearest neighbor approximation by a factor of 1.2. This is valid, as we aren't evaluating the material parameter assumptions of each group at

the moment, just the behavior of the models. In fact, note both groups are wrong in their material assumptions, as Brongersma and Atwater assume a frequency independent constant effective mass of the free electron in the silver, and as previously mentioned, Weber and Ford assume a Drude model with $\epsilon_\infty = 1$ instead of a more accurate $\epsilon = 6$, amongst other choices. These assumptions can be factored away by normalizing the previous nearest neighbor model to match the nearest neighbor limit of the multi-neighbor model by multiplying ω_1 by the mentioned factor. Doing so and comparing to the multi-neighbor model we have:

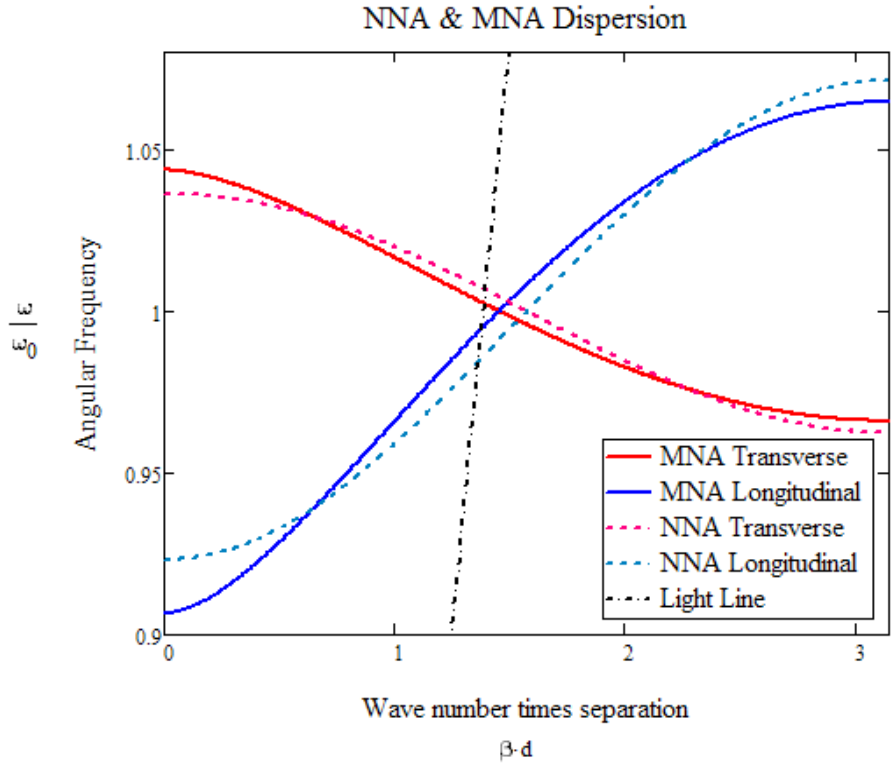

Fig. 2-9 Dispersion Relation ω/ω_0 vs. βd for NNA and MNA

What this shows is that in the limit of nearest neighbor approximation and same material parameter assumptions, the two methods match, while the new method permits more terms (farther apart neighbor's) to be included, and also takes into account additional dynamic effects.

2.5 Finite Chain with Full Coupling

As mentioned in the previous section, the derived dispersion relations do not converge for $\Im(\omega)<0$, where normal mode frequencies occur. One way this may be accounted for is by applying analytic continuition into the complex plane as shown by Engheta and Alu [14], which requires recasting the relations in terms of polylogarithms. A second and easier method is to just acknowledge that any real world structure would be finite in extent, permitting evaluation using more traditional methods and functions, and ignoring some of these concerns exhibited in the infinite structure. This also allows us to avoid the pitfalls pointed out by Conforti and Guasoni.

For a finite chain of *N* spheres, we have *N* coupled equations in the *N* unknown moments of the spheres conforming to the original equations:

Longitudinal:

$$p_n = -\alpha(\omega) \sum_{m,m\neq n} \frac{1}{2\pi\epsilon}\left[\frac{1}{|n-m|^3 d^3}+\frac{jk}{|n-m|^2 d^2}\right] e^{-jk|n-m|d}\, p_m \qquad n,m \in [1,N]$$

Transverse:

$$p_n = \alpha(\omega) \sum_{m,m\neq n} \frac{1}{4\pi\epsilon}\left[\frac{k^2}{|n-m|d}+\frac{jk}{|n-m|^2 d^2}-\frac{1}{|n-m|^3 d^3}\right] e^{-jk|n-m|d}\, p_m \qquad n,m \in [1,N]$$

These *N* equations can be represented in matrix form $\boldsymbol{M}\,\boldsymbol{p} = 0$ where $\boldsymbol{p}$ is an *N*-rowed column vector representing the p_m terms in the given equations, and $\boldsymbol{M}$ is given by:

$$M_{n,n} = -\frac{4\pi\epsilon a^3}{\alpha(\omega)} \qquad n \in [1, N]$$

$$M_{n,m\neq n} = -2\frac{a^3}{d^3}(1 + jk|n-m|d)\frac{e^{-jk|n-m|d}}{|n-m|^3} \quad \text{Longitudinal}$$

$$M_{n,n\neq m} = \frac{a^3}{d^3}(1 + jk|n-m|d - k^2|n-m|^2)\frac{e^{-jk|n-m|d}}{|n-m|^3} \quad \text{Transverse}$$

Solutions to which may be solved numerically by stimulating one of the spheres in the chain, and observing how the other spheres are polarized by inversion of the matrix M. That is to say $\boldsymbol{p} = M_{n,m}^{-l} \cdot \boldsymbol{v}$, where *v* is just a vector of all zeros except for the first term, which is 1, to excite the first sphere. For comparison with the previously derived quasi-static limit results, we choose radius $a = 25\,nm$, separation $d = 75\,nm$, and per the method prescribed in the literature, fix ω_p and ν to give the optical constants of Ag at resonance frequency $\hbar\omega_0 = 3.5\,eV$, or $\bar{h}\omega_p = \bar{h}\sqrt{3}\omega_0 = 6.19\,eV$ and $\bar{h}\nu = 0.7\,eV$. Also for the first case we consider ideal metal (lossless) with $\bar{h}\nu = 0\,eV$ [30].

We make the finite chain reasonably long to give enough distance for it to behave like the infinitely long chain. A chain of 20 spheres is considered long enough, *assuming a wave is actually coupled to the chain.* The literature assumes this, and we will evaluate based on this assumption, and in later sections evaluate whether such assumptions are valid.

The relation is evaluated by inserting values of *kd* into the relation and optimizing to find the zeros of the determinant of the matrix M. When $det[M] \to 0$,

$\boldsymbol{p} = M_{n,m}^{-l} \cdot \boldsymbol{v} \to \infty$, implying the frequency is the one best supported by the chain. The values of *kd* used are defined by: $(kd)_n = \frac{(N-2)n+1}{N(N-1)}\pi$, where N is the number of spheres in the chain.

Given a 20 sphere chain, and following the recipe as outlined in the literature, we have the following dispersion diagrams for longitudinal and transverse modes, for both the lossless metal case and silver (at resonance and according to Weber and Fords Drude model), compared to the multi neighbor approximation with retardation from the previous section.

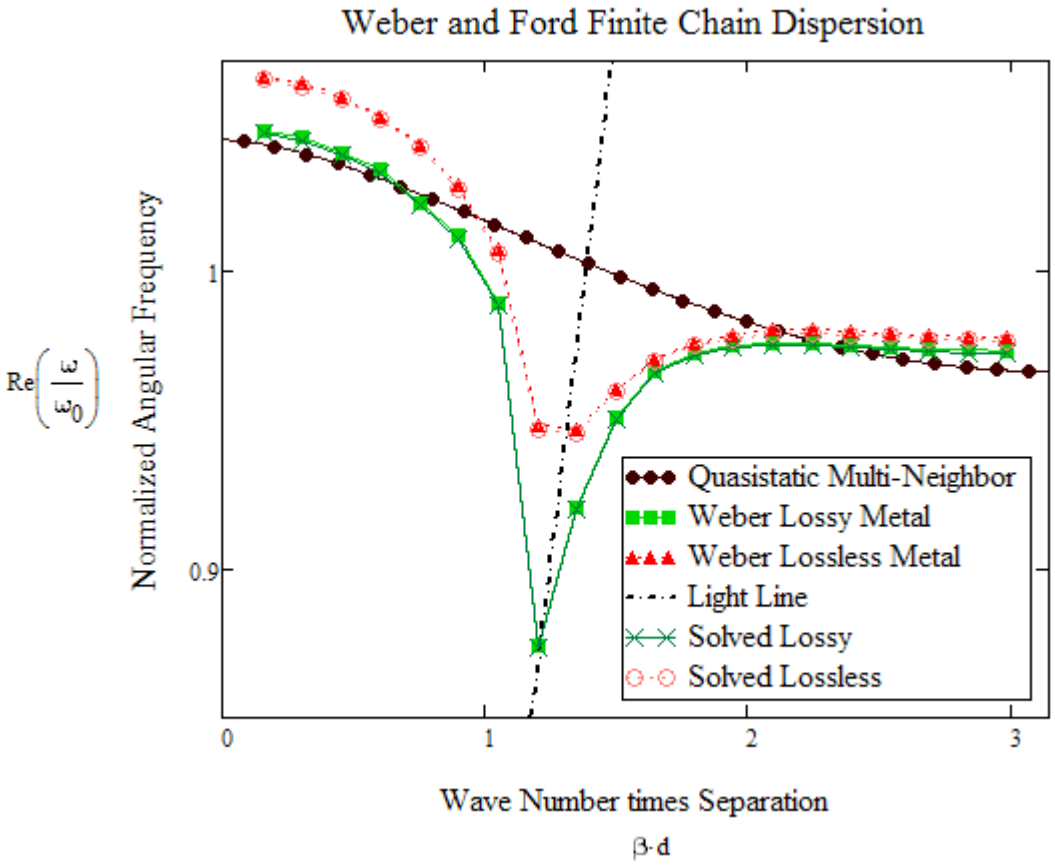

Fig. 2-10 Real Part of Complex Angular Frequency vs. βd for Transverse Modes, for the Quasi-static Case (black), Lossy Silver (Green), and Lossless Ideal Metal (Red)

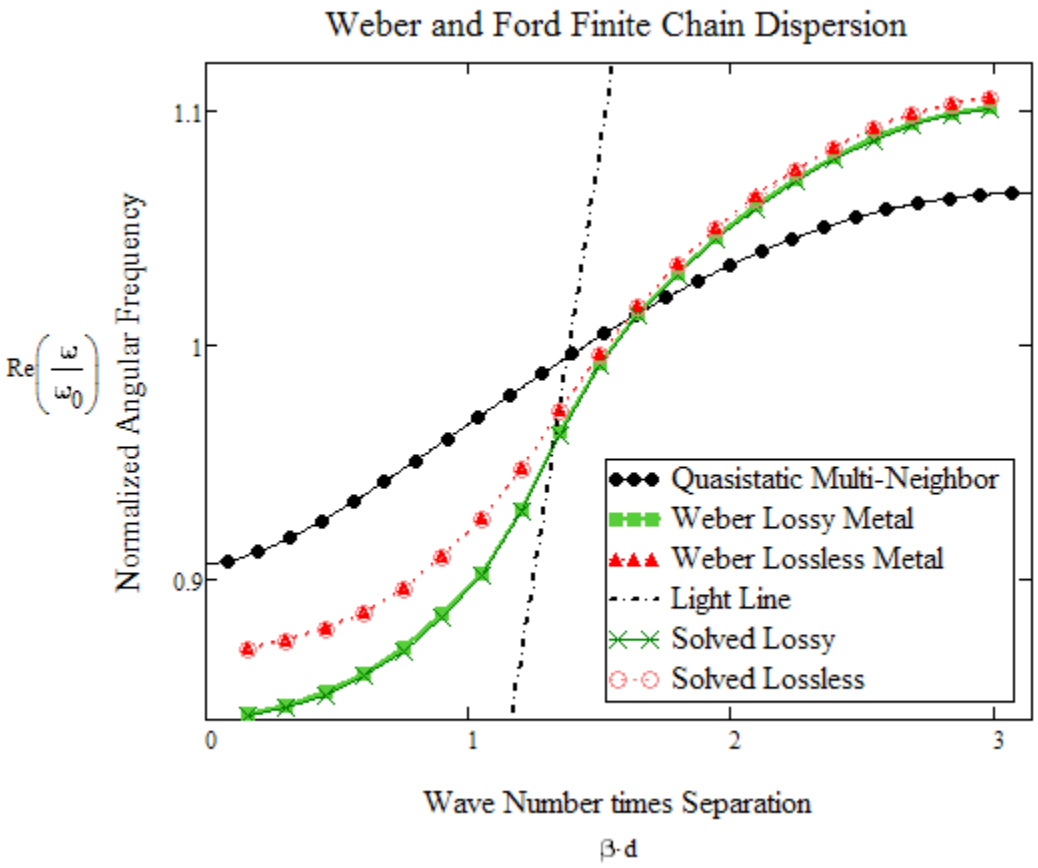

Fig. 2-11 Real Part of Complex Angular Frequency vs. βd for Longitudinal Modes, for the Quasi-static Case (black), Lossy Silver (Green), and Lossless Ideal Metal (Red)

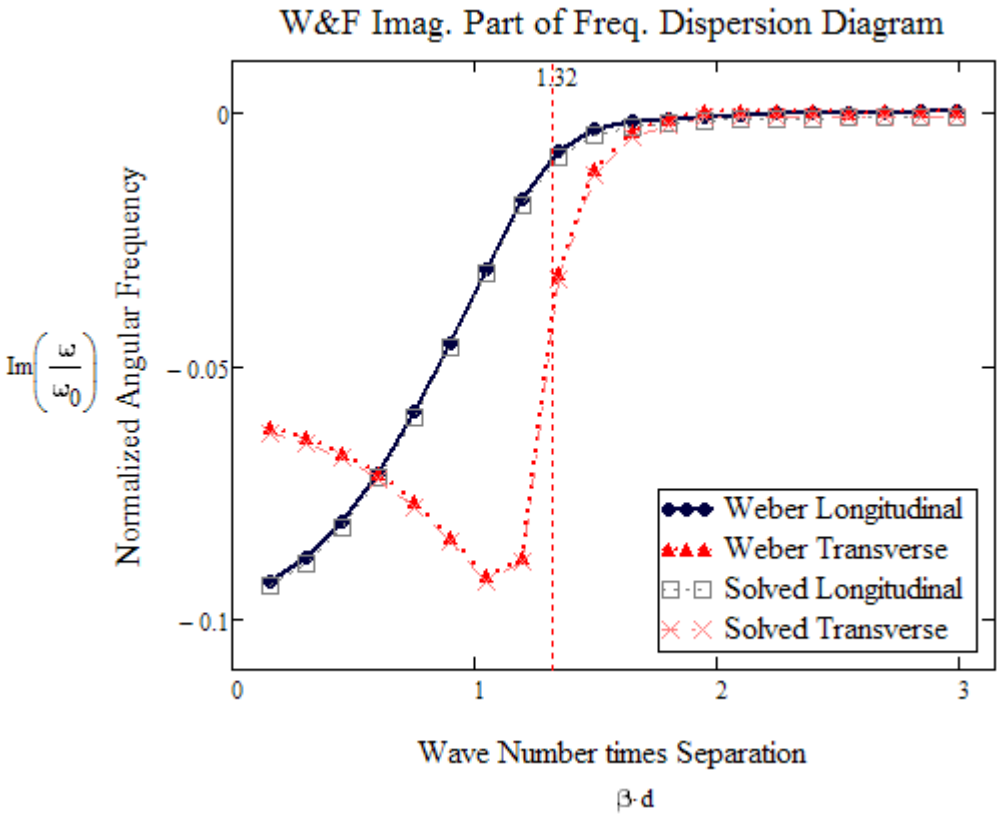

Fig 2-12 Imaginary Part of Complex Angular Frequency vs. βd for Lossy Longitudinal and Transverse Modes

Note that if we heed Conforti and Guasoni's admonition regarding this complex frequency method, the data to the left of the lightline (dot dash line) in the above figures is meaningless. To the right, it appears Weber and Ford are trying to demonstrate with this graph that the imaginary part of the complex frequency is very small, implying that the real part of the complex frequency is very close to what the completely real frequency would be given the problem was solved with a completely real frequency and complex propagation constant $k = \beta - j\alpha$.

To determine the completely real frequency vs. complex propagation constant, (instead of a complex frequency), the model calls for application of the relation $\boldsymbol{p} = M_{n,m}^{-l} \cdot \boldsymbol{v}$, and solving for $\boldsymbol{p}$ at various real test frequencies. Note this is in contrast to the method just previously described which lead to a relation between a complex frequency and propagation constant by inserting values of kd and finding the complex frequencies that maximize $\boldsymbol{p}$. For real frequency vs. propagation, $\boldsymbol{p}$ is numerically solved for at a given test frequency, and its intensity plotted in a semi-log scale, since on such a scale a decay of the form $e^{-\alpha z}$ appears as a straight line. Now we have returned to the notation of using α to represent attenuation. Then the assumption by Weber and Ford is that given enough distance of propagation, only the dominant mode will remain supported, and the intensity will then become linear, with a line of slope equal to the attenuation constant.

To do this, a 50-sphere chain was stimulated, and the polarization intensity observed. For the two orientations we have the following:

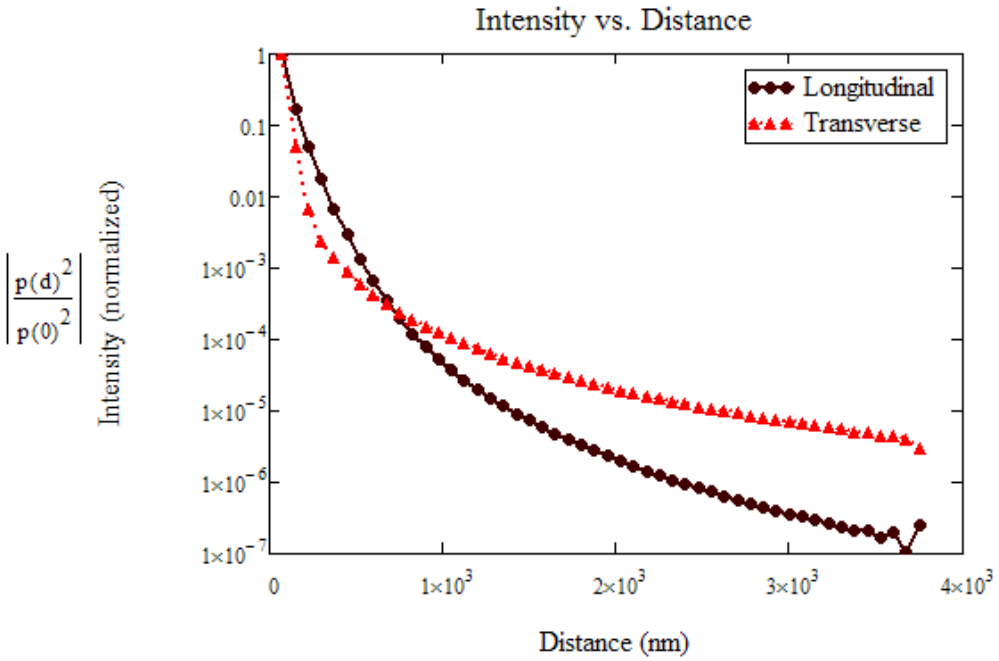

Fig. 2-13 Intensity of Sphere Polarization vs. Distance For Longitudinal and Transverse Modes

Note the rapid drop off towards the start of the chain, near where the initial stimulated dipole is located. Weber and Ford assume that this is the “non linear” region of the plot. Then towards the end of the line the data appears to be close to linear (on a log scale) shape. Also note the end of chain effects in the last few spheres. These effects must be avoided when determining parameters applicable to the infinite chain. The slope of the curves in their linear regions is assumed to be the attenuation. As is admitted in the literature, picking what area of the curve to fit the attenuation constant to is somewhat arbitrary.

With an attenuation constant, we are now prepared to find the propagation constant by fitting the calculated dipole moment to the expected form $p(z) = A e^{-jkz-\frac{\alpha}{2}z+\varphi}$ along a region toward the end of the chain, to determine the parameters of what the literature believes is a guided mode. α is known from our intensity line fit, *A* and φ are arbitrary, leaving *k* to be determined by appropriate fit. In the literature, it appears a hand-fit was performed. Using Weber and Ford's fit parameters, we see in Figure 2-14 a reasonable fit to our own calculated sphere polarization results.

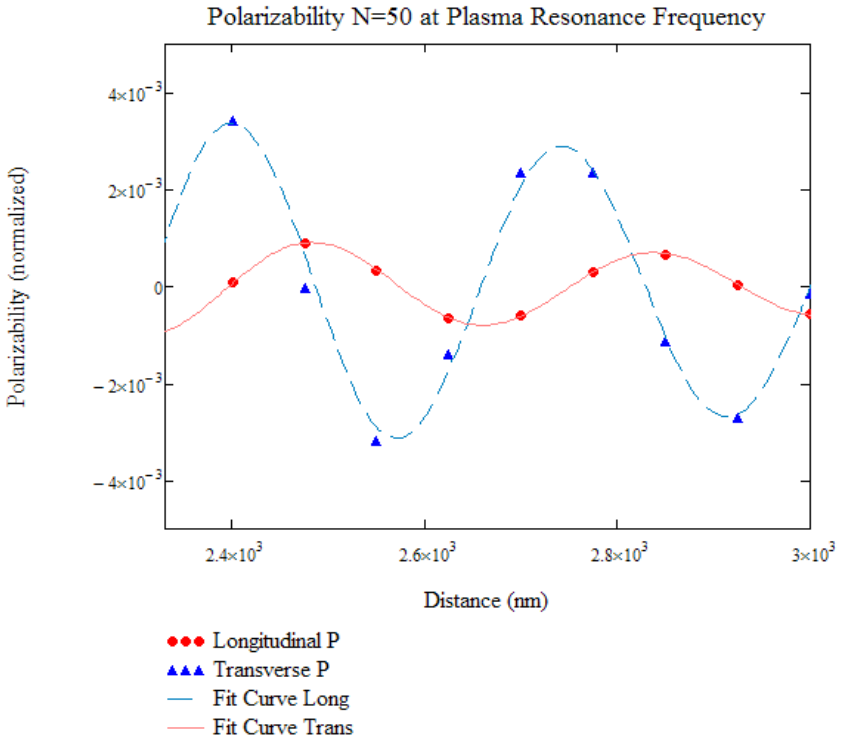

Fig. 2-14 Fit of $p(z) = Ae^{-jkz-\frac{\alpha}{2}z+\varphi}$ to Polarization of Spheres for both Longitudinal (Red) and Transverse Modes (Blue) Near the Plasma Frequency

In their paper, Weber and Ford only solve for this single frequency to obtain a "real frequency" solution that yields alpha and beta (k). It appears that after checking this result as a point in the graphs of Figures 2-11 and 2-12, and finding a close fit for this one point, the assumption was made by Weber and Ford that the rest of the points so derived would agree with the rest of the dispersion relation determined from the complex frequency argument. This assumption will be evaluated in the next chapter.

Chapter 3

EVALUATION OF MODELS AND INHERENT PROBLEMS

3.1 Are the models in the literature consistent?

Examples in the literature, including but not limited to those outlined in Chapter 2, generally conclude that their models are accurate within a reasonable degree, subject perhaps to the accuracy of their Drude metal model. However, as shown in section 2.2, the results from the different models in the literature do not necessarily agree, either in the magnitude of the attenuation, or in the shape of the dispersion diagrams.

One would assume the method-of-moments-like solution of Weber and Ford would be the most accurate, within the assumption that only the dipole moment is relevant (ignore higher order multipoles), as it takes into account more known effects, such as retardation per Mie theory analysis. In fact, their approach is indistinguishable from the Discrete Dipole Approximation, a method that has been used extensively in optical scattering and that can be shown to be equivalent to the Volume Integral Equation version of MoM [41]. The only approximation made in this case by Weber and Ford is that each sphere can be adequately modeled by a single dipole.

However, if we compare Weber and Ford's method of moment solution to their own eigenvalue solution of exactly the same particle interaction model we reach a disturbing conclusion, they do not agree with each other.

3.2 Is a Guided Wave Really Being Stimulated?

Recall the dispersion diagram for the longitudinal mode (Fig 2-12). If we follow the method prescribed in fitting for the wave number to the equation $p(z) = Ae^{-jkz-\frac{\alpha}{2}z+\varphi}$ as previously described in the preceding section, at the single frequency given, and plot the single data point (brown cross) onto the dispersion diagram showing the real part of complex frequency vs. normalized wave number, we see the point is somewhat close to the implied expected value in the literature.

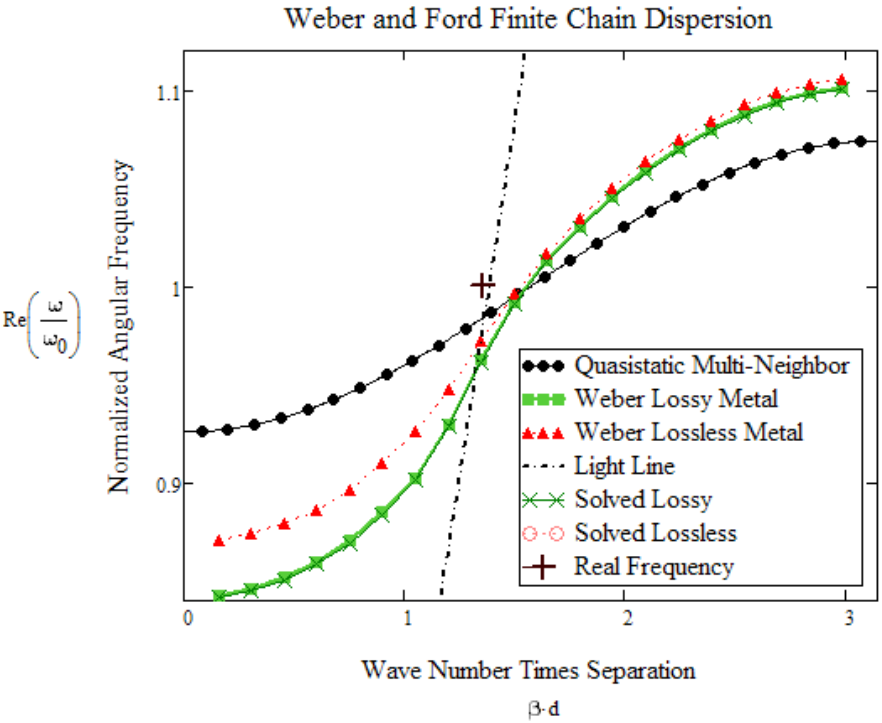

Fig. 3-1 Real Part of Complex Angular Frequency vs. βd for Longitudinal Modes, for the Quasi-static Case (black), Lossy Silver (Green), and Lossless Ideal Metal (Red), Compared to the Single Completely Real Frequency Data Point (Brown Cross)

This is where Weber and Ford stopped. If we continue using an automatic solver, under the assumption that solutions are near the $\Re(\frac{\omega}{\omega_0})$ vs. βd curve, as is implied in the paper, we fail miserably, as is shown in Fig 3-2.

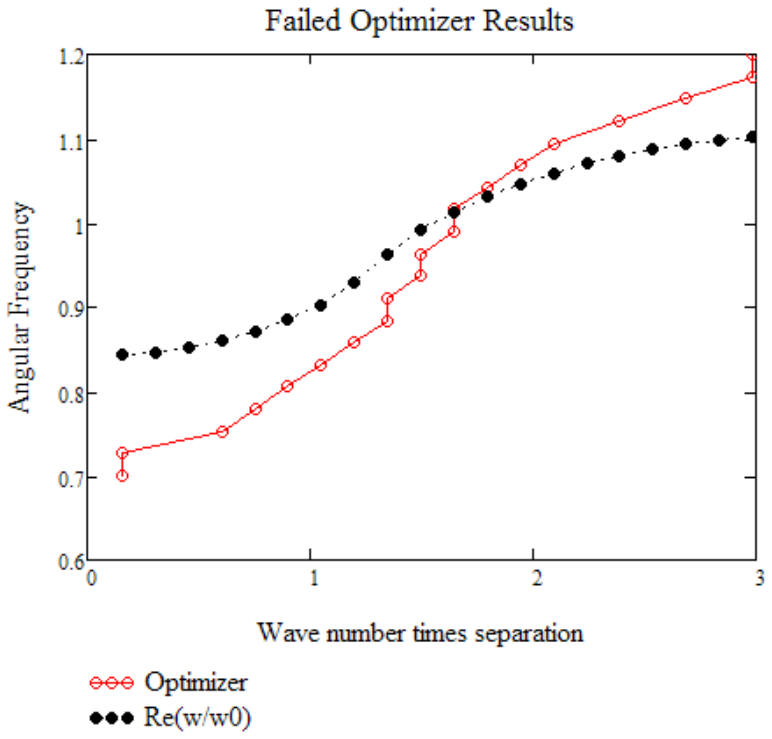

Fig. 3-2 Failed Optimizer Results in Search for Completely Real Frequency Dispersion Relation

Output from the optimizer reports no solutions found for most points. Multiple runs with adjustment of search parameters also fail in different fashions, but it was observed that the solution search kept leading to a possible solution with a much steeper slope than expected.

Instead of using an automatic least-squares optimizer, to get a handle on what is really happening, it should be possible to assume the determined attenuation constant was correct, and then attempt to fit the dipole moment versus position decaying sinusoid "by hand". Such an attempt actually succeeds as shown in Figs 3-3 and 3-4.

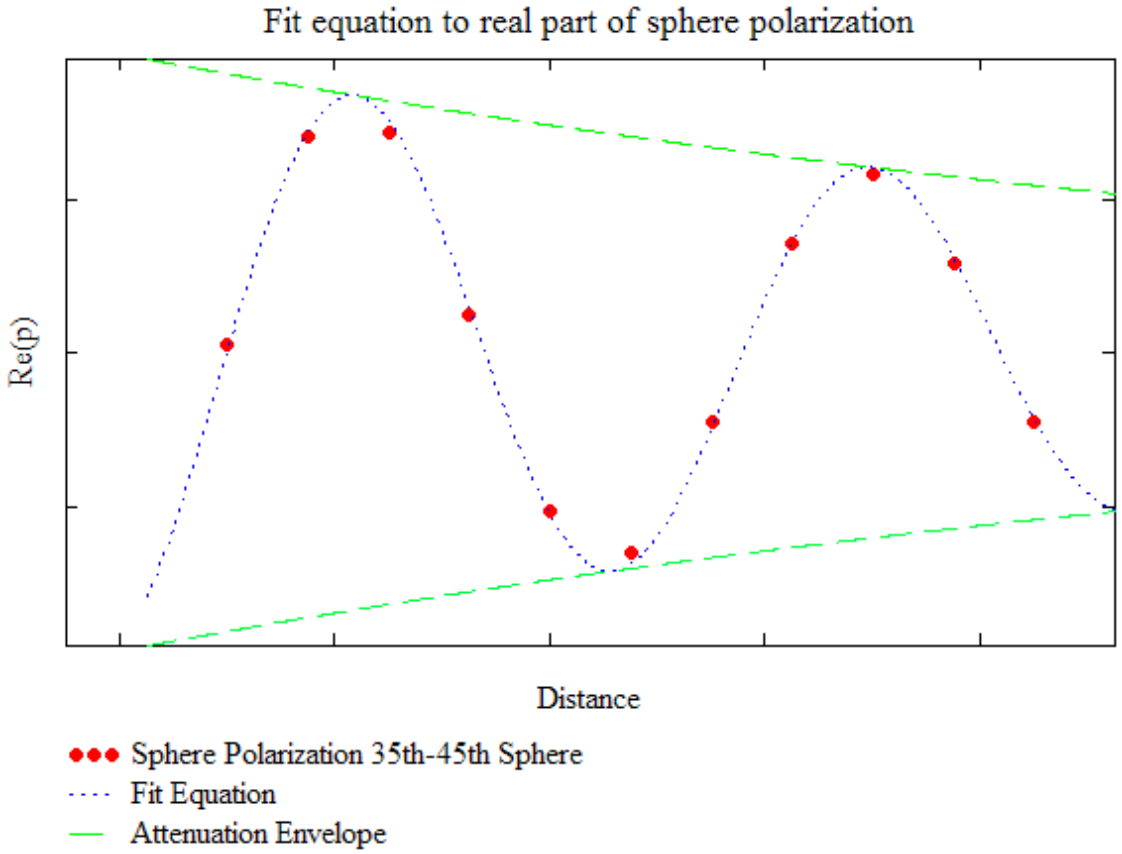

Fig 3-3 One of Twenty Hand Fit Equations for Sphere Polarizability

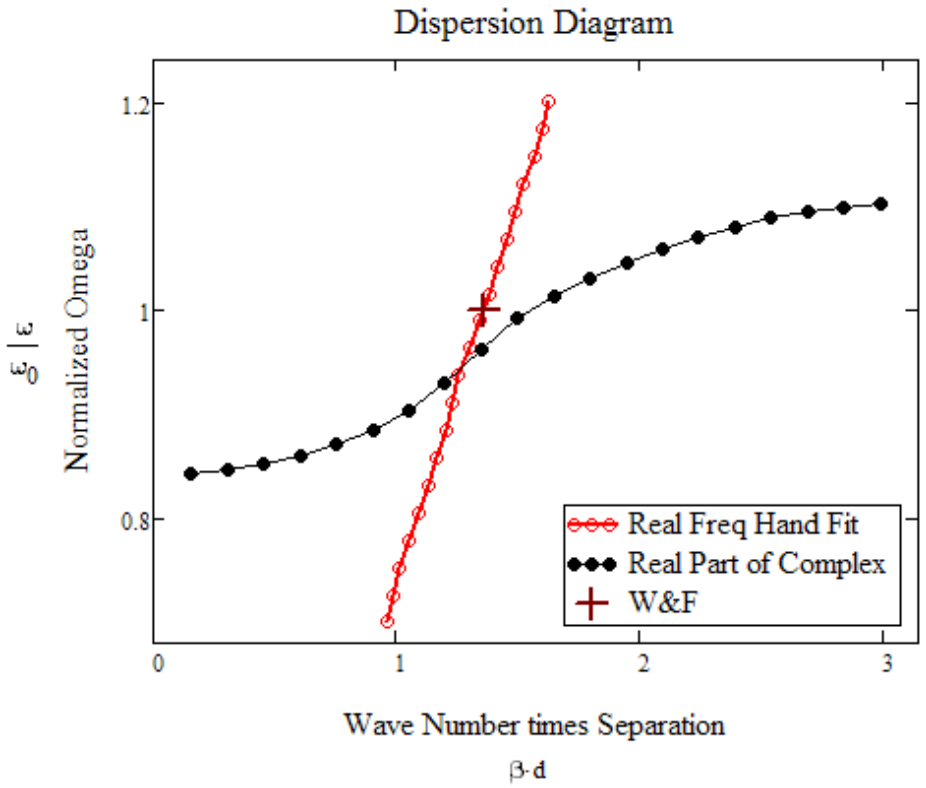

Fig 3-4 Full Dispersion Diagram Using Hand Fit Equations (red) for Completely Real Frequency vs. βd , Compared to Real Part of Complex Frequency vs. βd (black)

Note the location of the single point calculated by Weber and Ford, and how it lies exactly on our plot. Then, plotting the fit results on the original dispersion diagram in Fig 3-4 shows why the optimizer was failing; the search area was nowhere near the expected location.

But there has to be a bigger problem. Why would an optimizer that in principle "weighs" all the data be less accurate than the human eye? One hypothesis has to be that the information given the optimizer was wrong. The optimizer was asked to fit the data to

an exponentially decaying sinusoid. Is it possible that the results of the Method-of-Moments simulation do not fit such a function?

To check this hypothesis, and avoid the subjective bias of hand fits, instead of fitting to the expected equation in a least-squares sense as was previously tried and failed, we choose to apply a Prony-based method [21] for instantaneous frequency estimation, to examine the local wavelength of the propagation phenomenon along the line as a function of position. The resulting propagation constant then leads to the dispersion diagram of Figure 3-5.

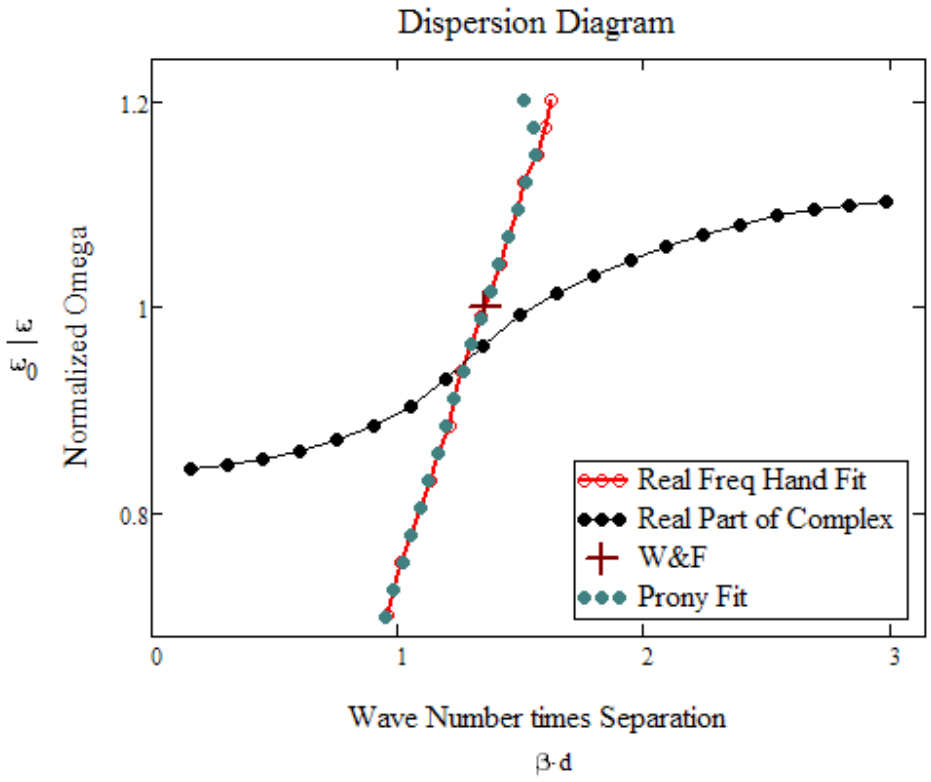

Fig. 3-5 Frequency Estimator (Prony-like method) Fit

The hand fit was accurate over most of the band. Now that the real frequency dispersion diagram has been determined, it looks very familiar. Calculating the slope from the 5th through 15th point of the new diagram, we find a velocity $v = 2.992 \times 10^8 m/s$. The dispersion diagram is just the light line! It appears the result being measured in the method of moments solution is not that of a wave being guided by the chain, but a wave traveling in free space and polarizing the spheres of the chain as it passes by. All the other steps are just measuring how this free space wave stimulates the other spheres, *not an example of a wave being guided by the spheres coupling together*. Adding the light line to the plot confirms.

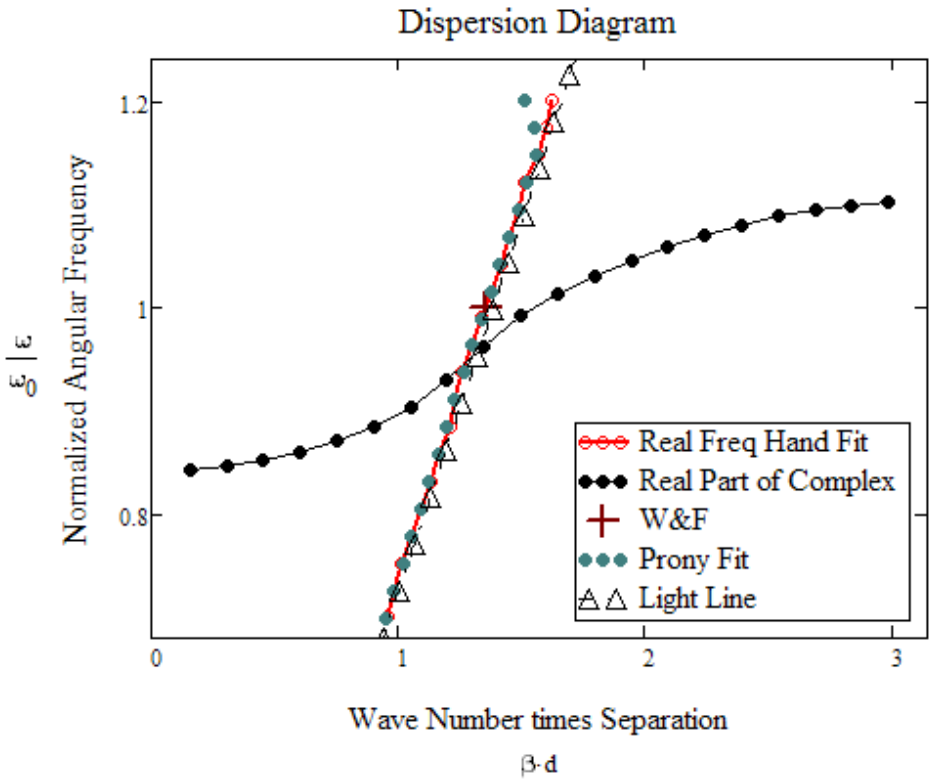

Fig. 3-6 Light Line Superimposed on Dispersion Diagram

3.3 Is There a Guided Wave Inside this MOM Solution?

This interpretation of largely only seeing the dipolar radiation of the first sphere in the chain needs to be verified. To do so, the first and eleventh frequencies of the dispersion diagram were plotted and laid over the fields along the z-axis of a dipole at the origin, scaled to the polarization of the spheres towards the end of the chain, as shown in Figs. 3-6 and 3-7.

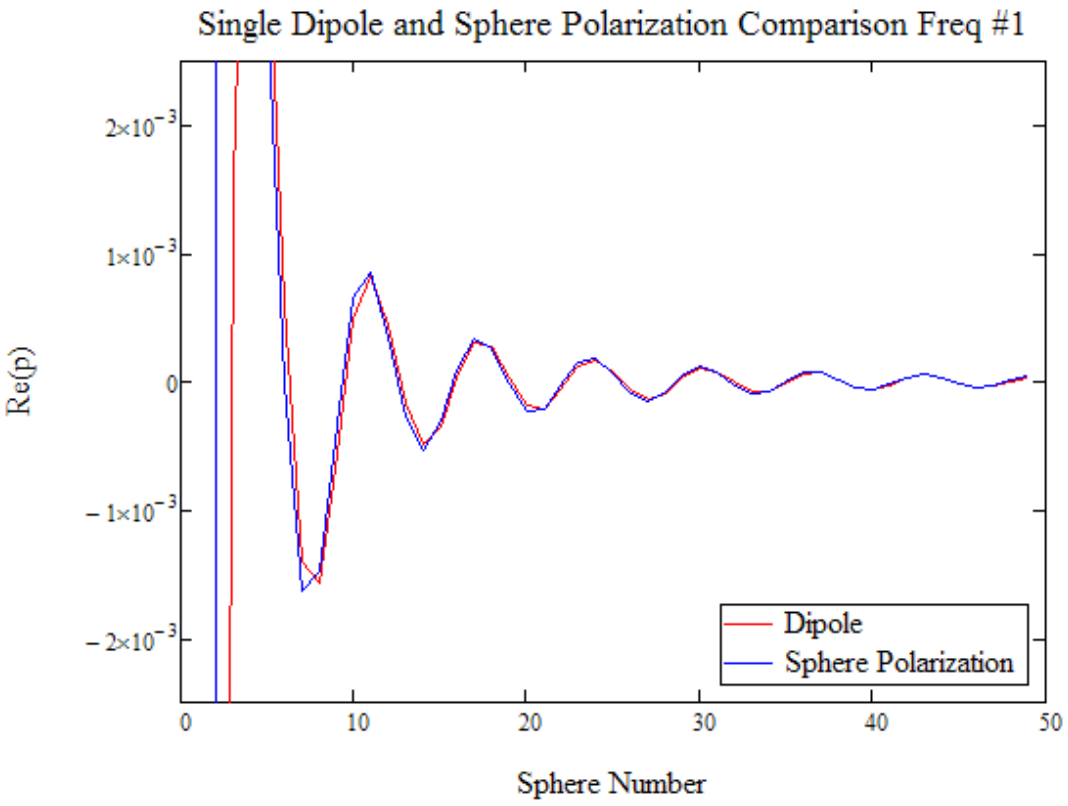

Fig. 3-7 Fields Along z-axis of Dipole at Origin Compared to Polarization of Spheres for Frequency #1 of the Dispersion Diagram

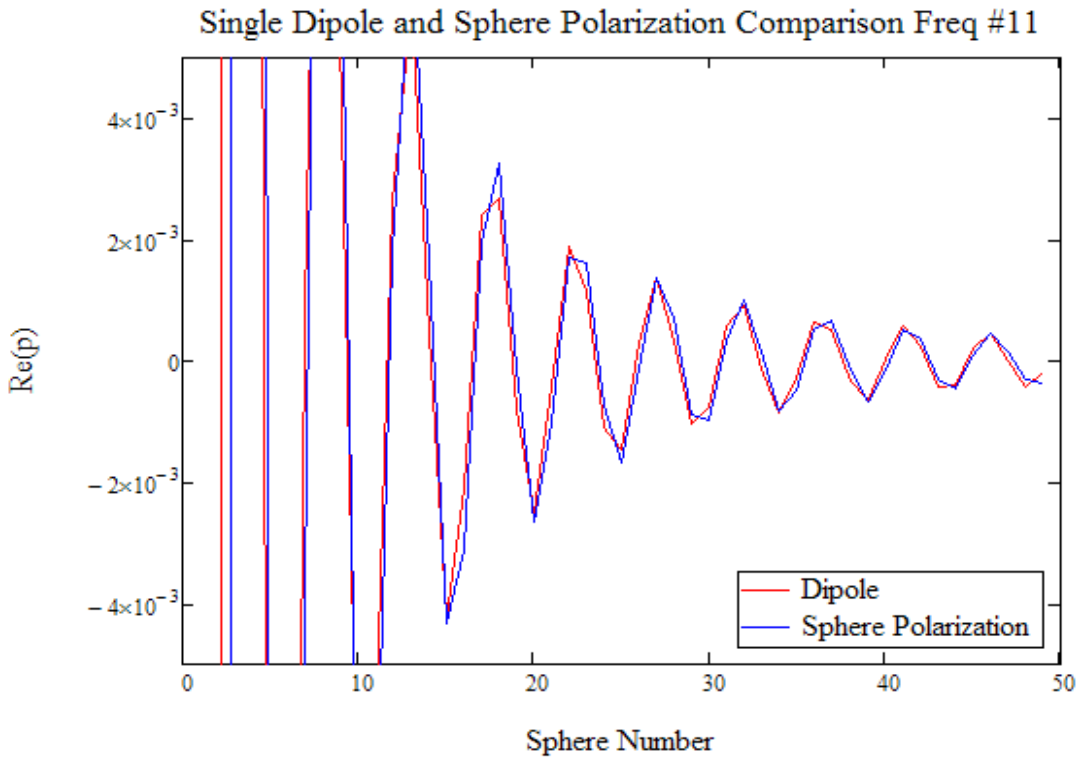

Fig. 3-8 Fields Along z-axis of Dipole at Origin Compared to Polarization of Spheres for Frequency #11 of the Dispersion Diagram

The results being so close, it is apparent that it is the direct wave from the dipole radiation of the driven first sphere scattering off the spheres towards the end of the chain that we are seeing, and not polarization due to a wave being guided by the chain and inter-sphere interactions going all the way down the chain. It must be emphasized that the assumed exponential decay is nothing else than the $1/r^2$ and $1/r^3$ dependence of the source field.

If this is all we are observing towards the end of the line, where is the guided wave? It must be overshadowed by this direct radiation. And, probably it must be so strongly attenuated that it essentially vanishes below the numerical noise over most of the line. To test this hypothesis we can attempt to subtract the radiated field we have just observed near the end of the line, and see if there is anything remaining near the beginning of the line that in some way could be interpreted as a guided mode.

Because we expect to be running up against numerical noise we model the source dipole field as seen along the line using three scaling parameters: a total strength, phase factor, and slight variations of the Prony-estimated propagation constant. These parameters may be “tweaked” and the expression subtracted from the sphere polarization data until we reduce the results near the end of the line as low as possible. (Smallest answer means we've removed most of the dipole wave). We hope then that the result remaining near the start of the chain begins to resemble a straight line on a semi-log plot, for then it would imply a truly exponentially decaying (guided) wave.

As Figures 3.9 and 3.10 show this procedure succeeds in reducing the data at the end of the line by an order of magnitude and in revealing a linear slope region near the front of the line. For the frequency in Figure 3-9, we obtain an intensity attenuation of 0.82 per sphere unit cell, and for the frequency in Figure 3-10, an intensity attenuation of 0.47 per sphere unit cell. For comparison to previously stated values, for frequency #1, that's an intensity attenuation of 23.74 dB/500nm, or 3dB/63.2nm.

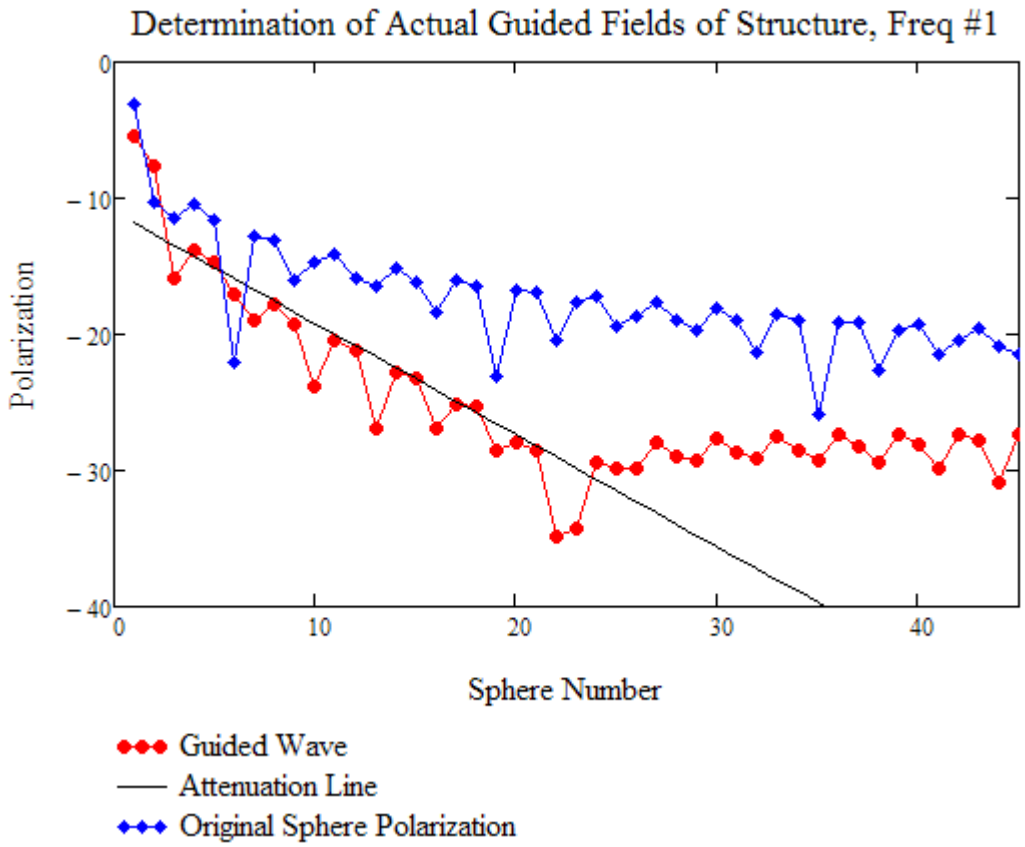

Fig. 3-9 Adjustment and Fitting to Remove Dipole Radiation from Data for Frequency #1

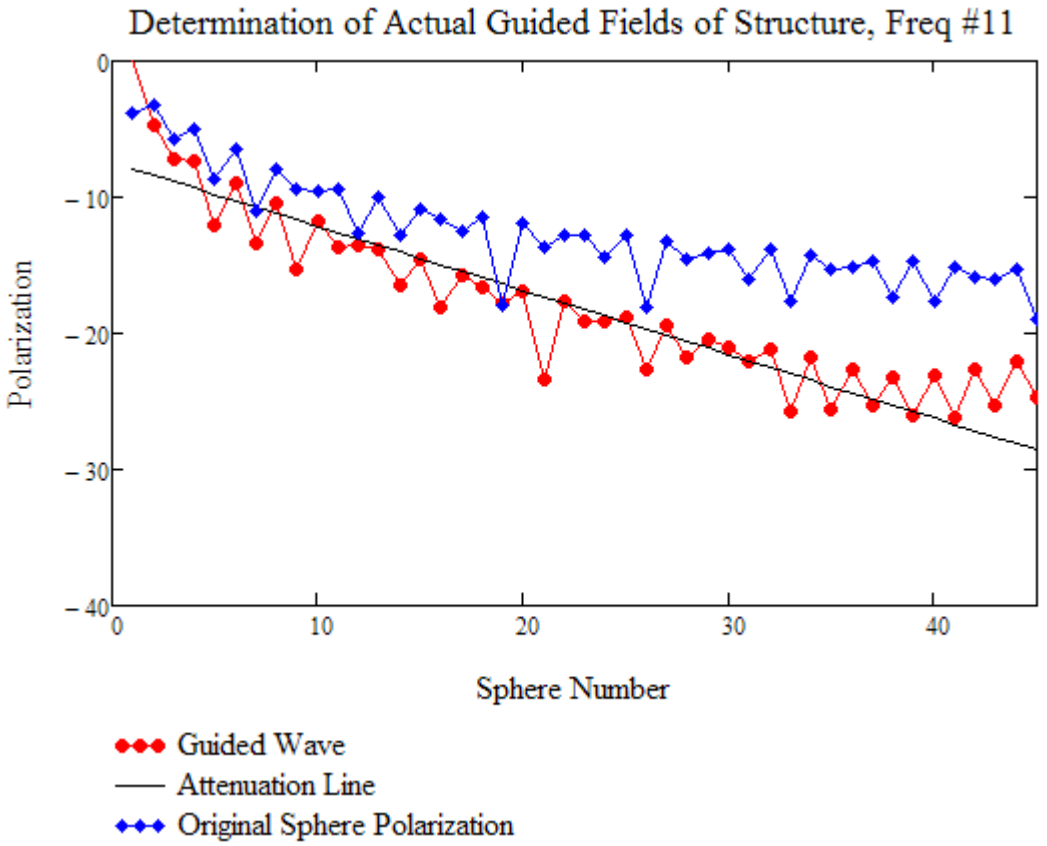

Fig. 3-10 Adjustment and Fitting to Remove Dipole Radiation from Data for Frequency #11

For frequency #11, we see an attenuation of 13.6 dB/500nm, or 3dB/110 nm.

Compare to reported attenuation constants in section 2.2, and we see the expected attenuation, when removing the fields of non-guided waves, is much greater than often predicted in the literature.

Given our removal of the free space dipole wave, we should be able to take the new data and once again apply Prony's method to rigorously find the propagation

constant for such a wave. To do so we remove the effects of attenuation from the data, by multiplying by $e^{+\alpha_{determined}\, z}$, a "dicey" proposition given that this function "blows up" at infinity. But all we want to see is if it recovers a sinusoid recognizable by Prony's method.

In the application of Prony's method to frequency identification, only 4 neighbors are used, meaning the result is only good from about sphere 6 to 18, as can be seen in Figures 3-11 and 3-12. The resulting propagation constants suggest that at frequency #1, the true propagation constant is below that of free space, meaning a fast wave. For frequency #11, we see a significantly higher propagation constant, hence a slow wave. The new results after removal of the dipole wave are compared to the previous results with the dipole effects still included in Fig 3-13.

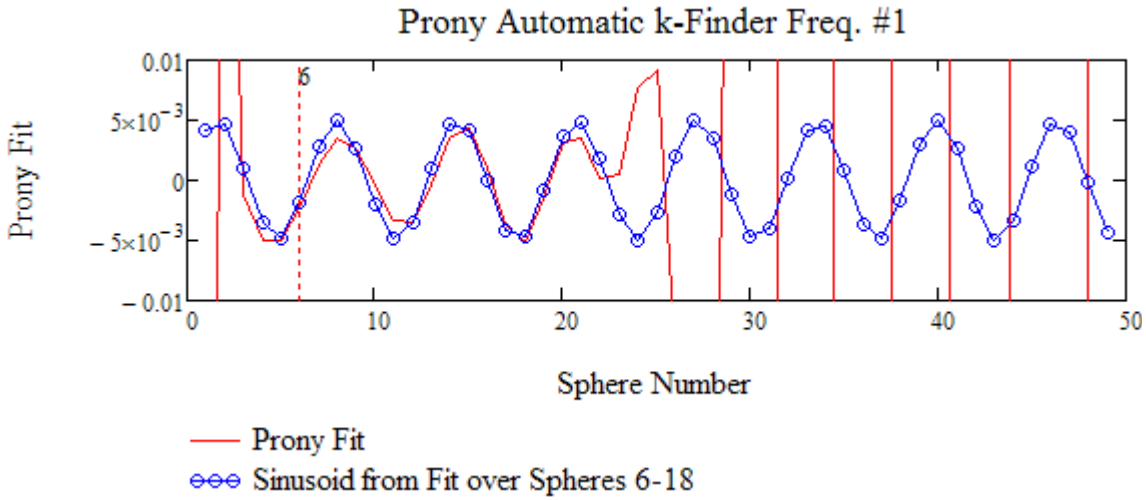

Fig. 3-11 k-Finder for Frequency #1 and Region of Solution Convergence

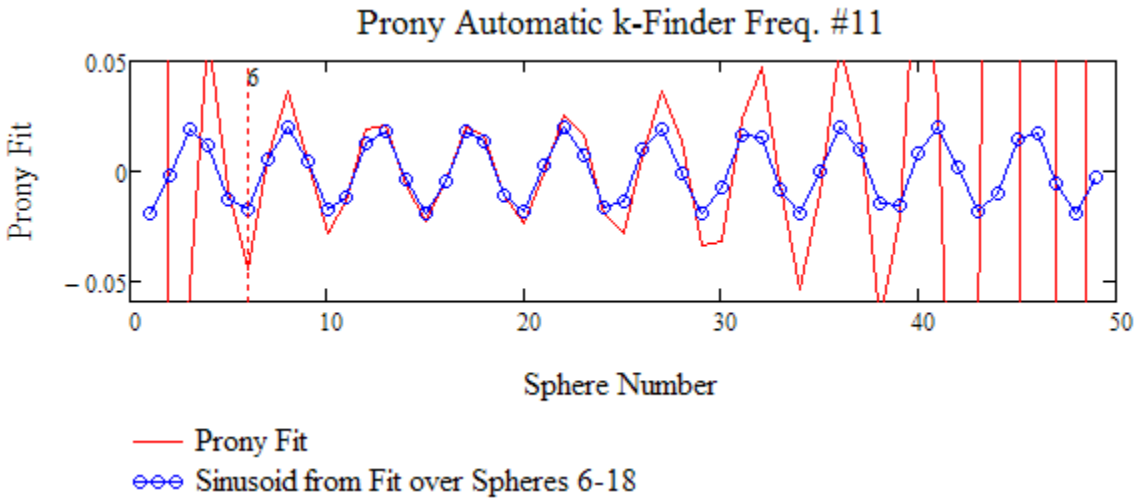

Fig. 3-12 k-Finder for Frequency #11 and Region of Solution Convergence

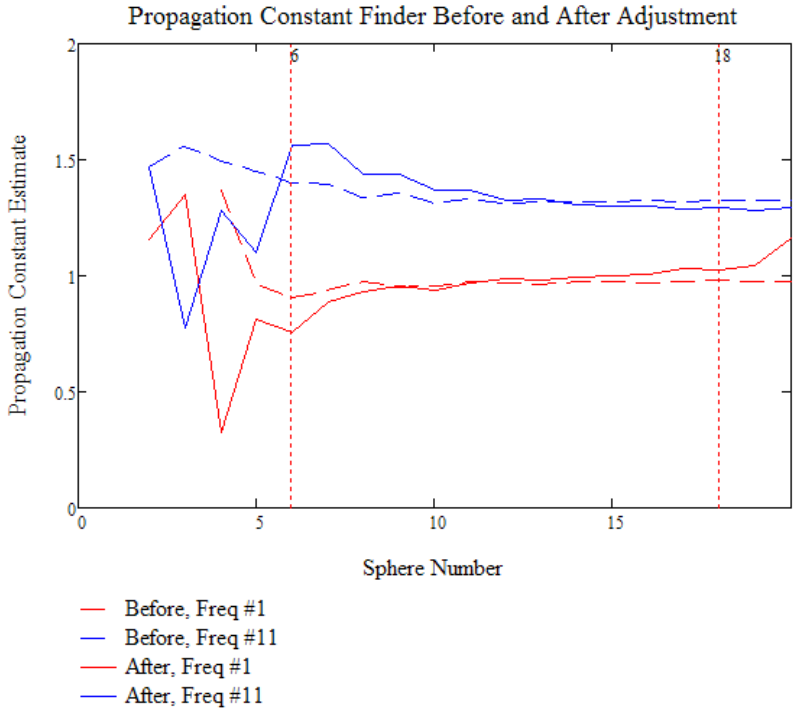

Fig. 3-13 k Estimates Using k-finder Based on Prony's Method Before and After Adjustment to Remove Free Space Dipole Wave

The method applied by Weber and Ford in and of itself is not flawed, as it does give the fields of the system, but the interpretation of what the results mean is flawed. The method of solution confounds guided wave (if there is one) with the free space wave due to the first dipole radiating; the latter severely over shadows the guided wave. We can adjust the results to try to remove the super imposed dipole wave, but increasing elements of uncertainty in the results are a concern as the data is manipulated.

Furthermore if the "guided wave" only exists within the first few spheres and its attenuation is of the order of -8dB per sphere, do we really know we have a true guided mode? After all, we can expect electromagnetic "turbulence" near the excited sphere. In a conventional closed (metal) waveguide we say this turbulence can extend up to a quarter wave down the line (the reason coax to waveguide transitions have a standard length). For open waveguides where higher order modes are not cutoff the "turbulence" distance may be longer. For this chain of spheres, with a highly inhomogeneous spatial distribution of material that encourages scattering effects, the distance may be even longer. This means that the field within the first two spheres and possibly within the first three may be an unreliable gauge of the actual waveguiding properties of this structure.

Realizing this, we may then wonder if we are better off using an eigenvalue solution of the infinite chain. However, Conforti and Guasoni's objection still stands unchallenged. We have just seen that the attenuation along the line is in no way a perturbation on the propagation constant, it is of the order of the propagation constant. Therefore not even Engehta and Alu's polylogarithm method can come to our rescue.

But more importantly we do not know yet at which frequency there is guided wave onset. Without knowing that, we do not know a priori when our results are to the left or the right of the light line. Under these conditions the validity of an eigenvalue solution is open to question. First of all, the fundamental assumption in the eigenvalue solution is that the wave is guided. If it is not, and we encounter leaky waves, it turns out that there is no physical parameter guideline to tell us when these leaky waves first become unphysical.

For instance, in Kim et al [20], the leaky dispersion characteristics in cylindrical dielectric rods are considered. Figure 3-14 below shows a plot from their paper including both the propagation constant and the attenuation constant. Notice the smoothness of the curves below onset. There is no clue in those curves when the results become invalid, yet by the time we calculate a $\beta > k_0$ with a positive real attenuation constant, we are claiming to have a slow leaky wave in a lossless waveguide. This is impossible. If the waveguide is lossless the only loss mechanism is radiation; but slow waves cannot radiate from a uniform infinite open waveguide.

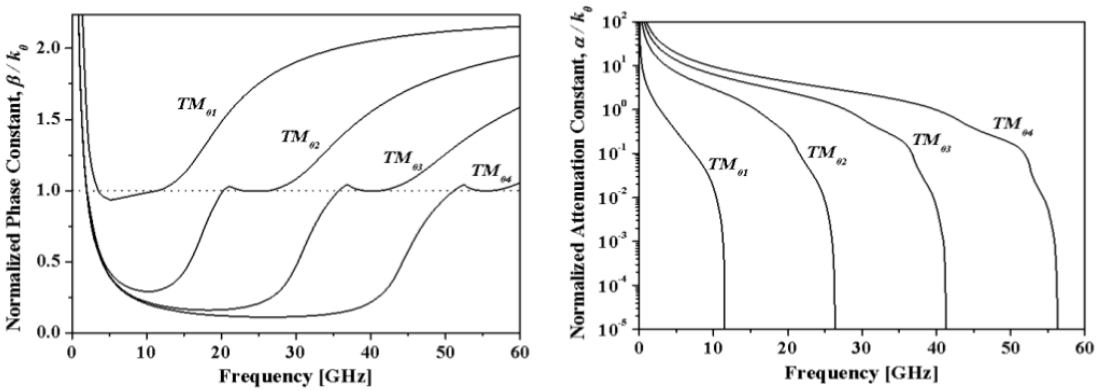

Figure 3-14 (a) Normalized Phase Constants and (b) Normalized Attenuation Constants when Dielectric Constant and Radius of Dielectric Rod are 5.0 and 5.0 mm, Respectively [20]

We need an alternate robust method that will allow us to unambiguously examine the surface wave spectrum of the chain of Noble metal spheres. Such an approach is the subject of the next chapter.

Chapter 4

EFFECTIVE MEDIUM APPROACH

4.1 Effective Medium Models

In the analysis of plasmonic nanosphere waveguides by the various models in the literature, a straight forward possibility has been overlooked. After all is said and done, with the Floquet mode formulation of the structure, the modes of practical interest are the low order modes, the first longitudinal and first transverse modes. If the guided wavelength of these modes is greater than several unit cells, it stands to reason that we are expecting the waveguide to act in some sense like an equivalent homogeneous waveguide. If this is true, then why don't we homogenize the waveguide before performing the analysis?

For the lowest order modes, a chain of waveguiding spheres should be equivalent to a lossy dielectric cylindrical waveguide of material with physical parameters determinable by an effective medium model of the unit cell. This is provided that the quasi-static assumption is satisfied in the unit cell. As has already been discussed in Chapter 2 and shown in Figures 2-2 and 2-3, this quasi-static assumption is justified, hence the approach should be valid.

In a recent paper about to be published [38], Panaretos et al show that a sub-wavelength plasmonic nanosphere smaller than the unit cell in a uniform FDTD space

can be accurately modeled by filling that unit cell with an effective medium that rigorously accounts for the presence of the sphere within the unit cell volume. The filled unit cell not only correctly scatters like the isolated sphere, a chain of three such "spheres" separated by intervening single cells of free space scatter the same way as a finely discretized model of the three sphere chain. Therefore we proceed with replacing the unit cell of the chain with an effective medium model, focusing on the longitudinal mode case.

In [38] it is shown that the classic Clausius Mossotti effective medium model of a spherical inclusion within a cubical unit cell of space is equivalent to a partially filled capacitor model. As a consequence we have two potentially valid models of the chain and we expect them to behave similarly. In the first model the equivalent rod is supposed to have exactly the same radius as the spheres a, and therefore the partially filled capacitor model is a cylindrical capacitor of length equal to the unit cell d, where the lower portion is filled with the correct volume of Noble metal to the depth:

$$x = \frac{4\pi a^3}{3} \cdot \frac{1}{\pi a^2}$$

(See Figure 4-1) The balance of the capacitor $d - x$ is filled with air. The relative effective permittivity of the rod of radius $a = 25\text{nm}$ is then given by the series sum of these capacitances:

$$\epsilon_{eff} = \left(\frac{x}{\epsilon_{metal}} + \frac{d-x}{1} \right)^{-1} \cdot d$$

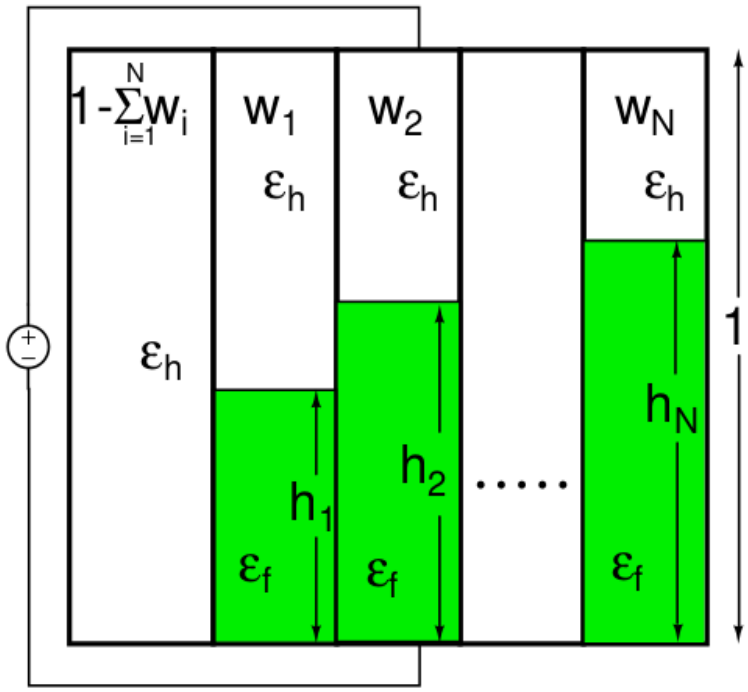

Fig. 4-1 PFC Model [38]

The second possible model uses the Clausius Mossotti expression where the sphere of volume $V_s = \frac{4\pi a^3}{3}$ is placed inside the unit cell volume $V_{cell} = d^{3.}$ Such that the volume fraction of material is $vf = \frac{V_s}{V_{cell}}$ and this is used in the CM expression for the effective permittivity. Then the volume of the cylinder of air with sphere in the center that makes up a unit cell is the same as the cube:

$$V_{cyl} = \pi a_2^2 d = V_{cell}$$

So the equivalent radius of the cylinder for our example of 25nm radius spheres at 75nm separation is:

$$a_{CM} = \sqrt{\frac{V_{cell}}{\pi d}} = 42.3\,nm$$

And the volume fraction fill ratio:

$$p = 0.155$$

Then:

$$\epsilon_{CM} = \frac{1+2\,p\left(\frac{\epsilon_{metal}-1}{\epsilon_{metal}+2}\right)}{1-p\left(\frac{\epsilon_{metal}-1}{\epsilon_{metal}+2}\right)}$$

To make a one to one comparison with our analysis of Weber and Ford's model, we must use the same Drude model for the metal, remembering that this is not necessarily the most accurate representation of Silver, and remembering that even the published data on Silver properties varies significantly (e.g. compare Palik [26] to Johnson and Christy [30]).

The two effective medium models above then yield the relative permittivity plots of Figure 4-2. As a sanity check, since the onset frequency of the conventional modes of a dielectric rod depend on the quantity $a(\epsilon_r - 1)$ we expect these two models to give a similar result. Looking at the low frequency real dielectric constant, the partially filled capacitor model gives $(2.4-1)\cdot 25 = 35$ while the CM model gives $(1.8-1)\cdot 42.3 = 34$ for this quantity. A similar calculation using the peak ϵ'' (without subtracting 1 since this is pure imaginary) gives for both approximately 93. So

indeed to first order these two dielectric rod models should be equivalent. But we may expect differences in the precise frequency at which maximum loss shows up given that the spectra in Figure 4-2 are different.

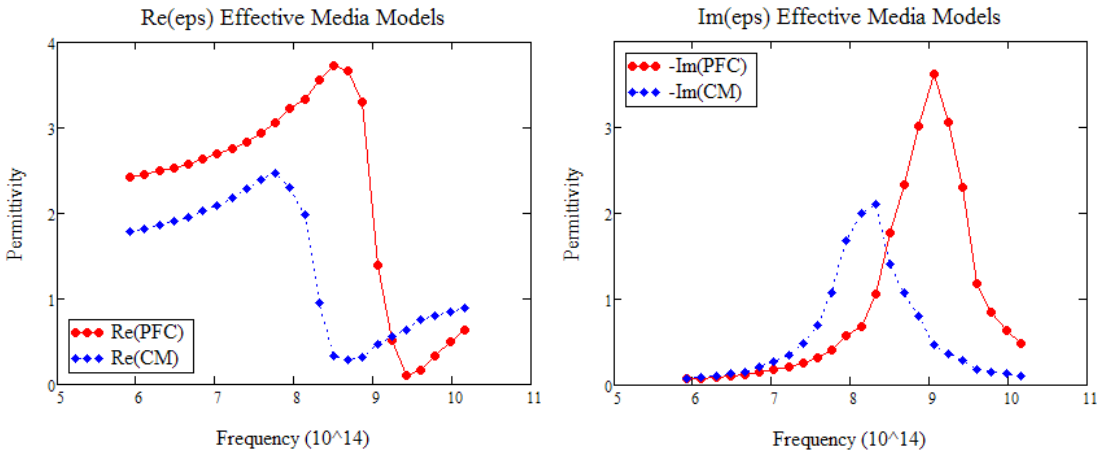

Figure 4-2 Permittivity from Effective Media Models

Since we have called into question an eigenvalue problem solution of these highly lossy dielectric rods, we turn to the solution of the Green function problem. Since this solution involves only numerical integration of the k-space spectrum and no matrix inversion, it is possible to compute the fields in an arbitrarily long region of the rod and examine their propagation as a result of a “current band” excitation at the origin.

4.2 Green Function Solution

The conventional guided mode eigenvalue solution for a lossless rod assumes purely guided waves inside the dielectric associated with evanescent waves outside.

When the rod is lossy we are faced with the question of what we should assume for the complex propagation constants that have to arise in both regions. Inside the rod there must be attenuation to account for the loss in the medium. Thus the propagation constant of the phenomenon at the boundary of the rod in the z direction must be complex. Since by the assumptions of the eigenvalue problem this propagation constant tangent to the surface must be the same in both media, the constraint equation in free space forces the external field to not only have attenuation in the radial direction, it must also have a phase constant. But a phase constant in the radial direction implies a wave is traveling either away or towards the rod. We are then left with the ambiguous question, do we assume leaky waves or do we assume energy is traveling from outside above the surface and being "sucked" into the rod?

The answer to this question eventually becomes truly puzzling when we consider the results of Kim already cited in Section 3.2, which show that even for the lossless rod we can have leaky slow solutions that are clearly unphysical. The problem then becomes, when do we know our eigenvalue solution has crossed the line into unphysicality since there is no obvious discontinuity in Kim's solution?

The Green function approach avoids all these questions. We make no assumption about the properties of the propagation constant on each space, we allow them to be whatever they need to be as long as they represent properly traveling waves (that is k is always of the form $\beta - j\alpha$ in the direction of propagation) inside and outside that must satisfy the source condition at the surface of the rod. The source is then assumed to be a

spectrum of surface magnetic current waves propagating along the z axis with purely real propagation constant ranging in value from –infinity to infinity. This is the plane wave spectrum approach, an approach that we know to be valid and that provides us a with a complete basis to represent any current flowing on the surface of the rod.

The source current in physical space is assumed to be a uniform (in φ) current band of small width at the origin. Its spectrum is calculated by a Fourier Transform and for every current wave in the spectrum the source condition and boundary conditions at the surface of the rod are satisfied. Once all the field components for every current wave are determined, the fields in spatial domain are reconstructed by taking the inverse Fourier transform. This Transform is really an integration along the real axis of *k*-space. As is well known, we can expect to have poles near that axis, but because this is a lossy cylinder, those poles are not on the axis. We avoid them by either integrating very finely along the axis to make sure the rapid variation of the function in their neighborhood is correctly accounted for, or if necessary by deforming the integration path at those poles. (We can determine their position a priori.)

The details of the derivation are given in Appendix E. To illustrate the kinds of results that are obtained with this approach, consider a lossless rod of 25 nm radius with a nearly purely real permittivity of 4, of the order of the largest value we saw in Figure 4-2. Figure 4-3 shows the amplitude versus position plot of the total current (displacement in this case) inside the rod in a semi log plot for excitation frequencies 1016, 1723, 2385, and 3048 THz, labeled (a), (b), (c), and (d) respectively. These were chosen on purpose to

show an example of a mode significantly below onset, curve (a), a mode beginning to approach onset (b), a mode very close to onset (c) and finally a well guided mode(d). Figure 4-4 shows the phase versus position plots including a light line in free space. We see (a) has a fast wave phase with noise, (b) is clearly a fast wave, (c) fast wave approaching the speed of light (d) guided slow wave.

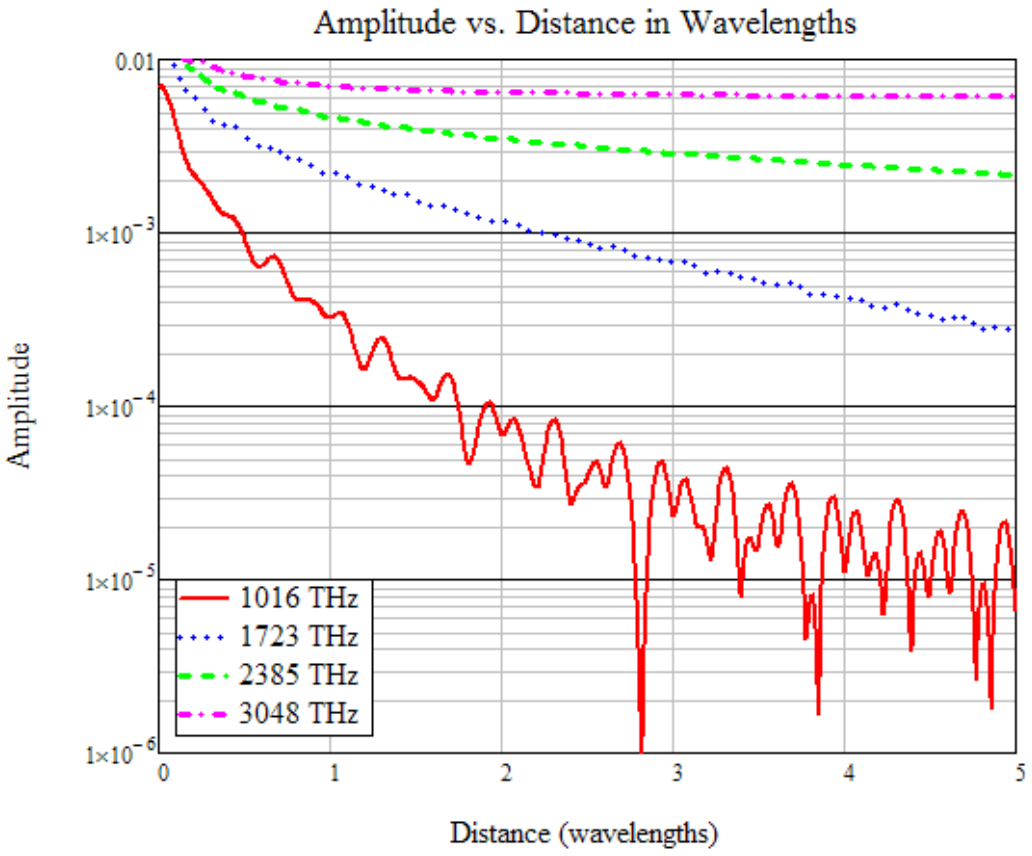

Figure 4-3 Amplitude of Current Wave vs. Distance in Wavelengths for Four Frequencies of 25nm Radius Dielectric Rod With Relative Permittivity $\epsilon_r = 4 - j \cdot 0.001$

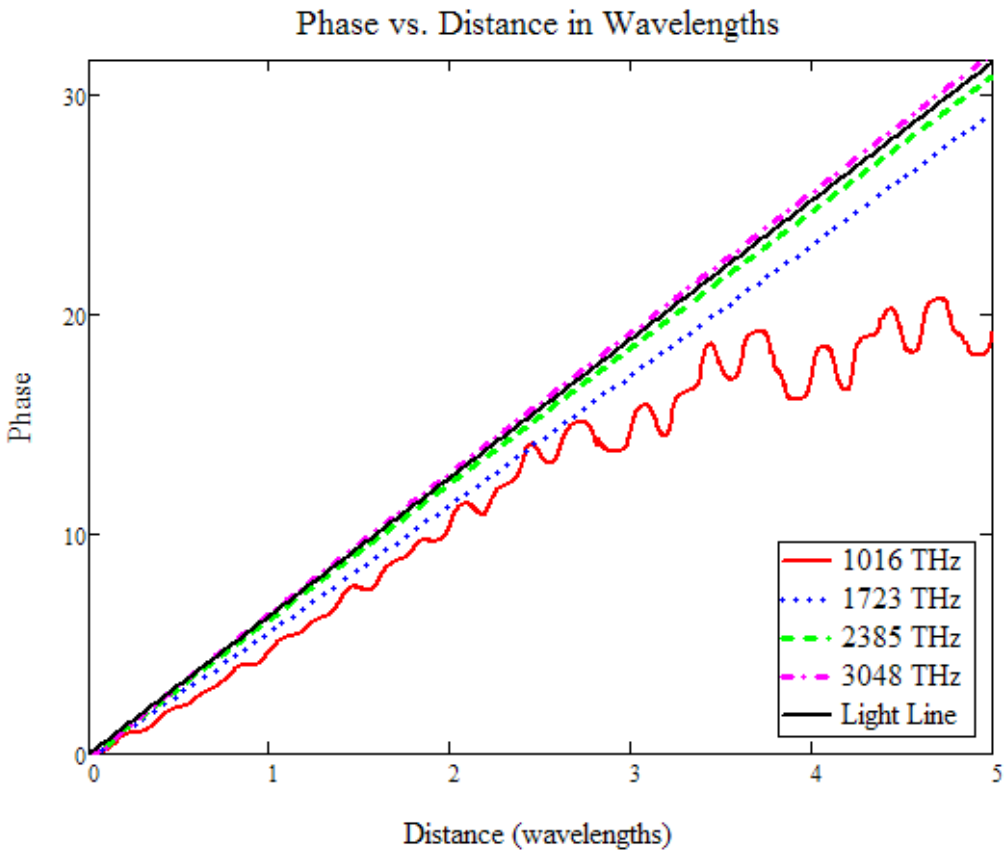

Figure 4-4 Phase vs. Distance in Wavelengths for Four Frequencies of 25nm radius Dielectric Rod With Relative Permittivity $\epsilon_r = 4 - j \cdot 0.001$

Note that to stimulate guidance of the dielectric rod with the given permittivity, the stimulating light was well into the ultraviolet, much higher in frequency than desired. What has been demonstrated is how the software works, and how results may be interpreted.

Now we proceed to apply this approach to model the effective medium rod that should be the equivalent to Weber and Ford's case by using the same Drude model as

they did, that is to say $\epsilon(\omega) = 1 - \frac{\omega_p^2}{\omega(\omega + j\nu)}$, where $\omega_p = 6.18\,eV/\hbar$,

$\nu = 0.7\,eV$, and inserting this Drude material into a Claussius-Mossotti effective medium for the dielectric rod, then varying ω over the same range as their dispersion diagram at 24 test points. The results are shown below:

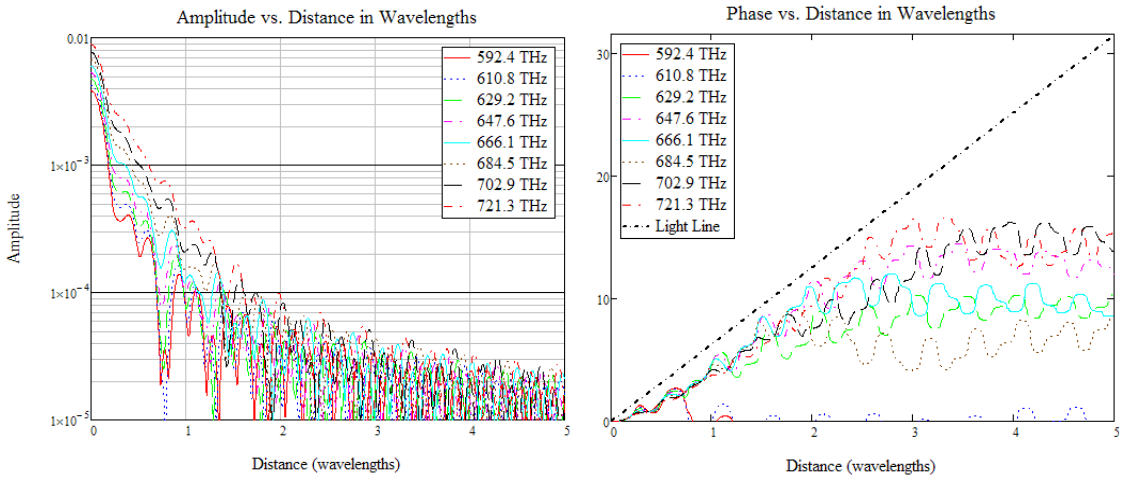

Figure 4-5 Weber and Ford Drude Model Applied to Effective Media Over First Third of Dispersion Diagram Frequency Band

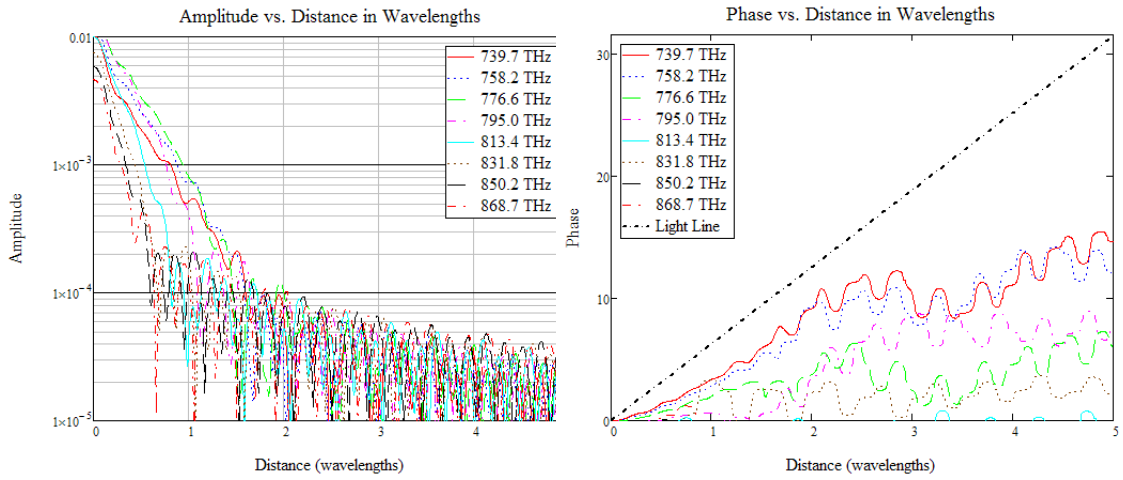

Figure 4-6 Weber and Ford Drude Model Applied to Effective Media Over Second Third of Dispersion Diagram Frequency Band

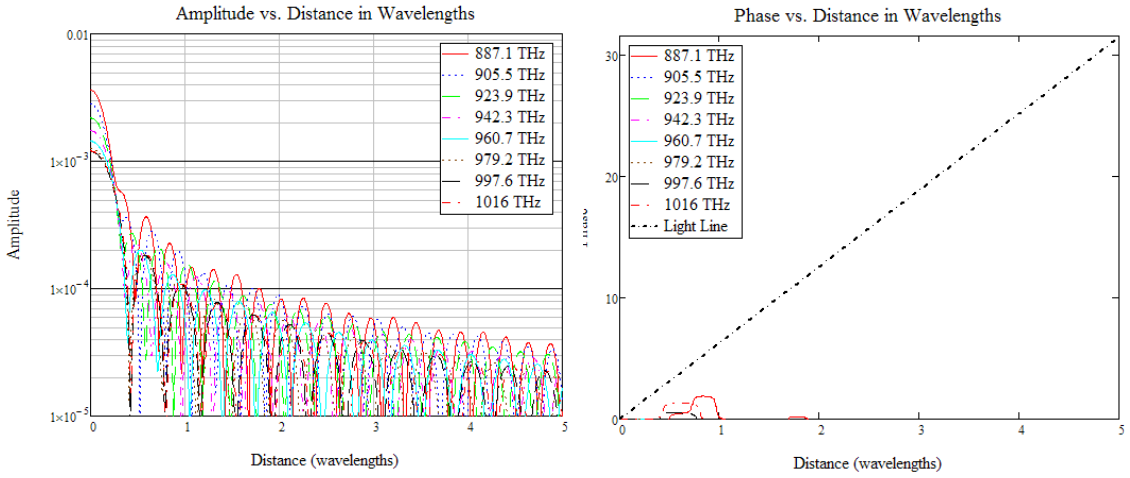

Figure 4-7 Weber and Ford Drude Model Applied to Effective Media Over Final Third of Dispersion Diagram Frequency Band

Note that these results show the effective medium rod, which is equivalent to Weber and Ford's chain of nanospheres *is not guiding*. Recall the adjustments and fitting

shown in Figures 3-9 and 3-10 to remove the dipole radiation from the data. If we take those data, and overlay the results from the effective dielectric rod at the two same frequencies (called Frequency #1 and #11 in section 3.3), we see the slope of the attenuation predicted by the adjusted data more closely matches the slope of the amplitude of the current wave of the effective rod near the point of stimulation. Note that because the material is lossy, the attenuation is high and the noise floor is raised. The initial magnitude of each data set is arbitrary, so they are offset to be spaced in the vertical for ease of viewing (no overlaping).

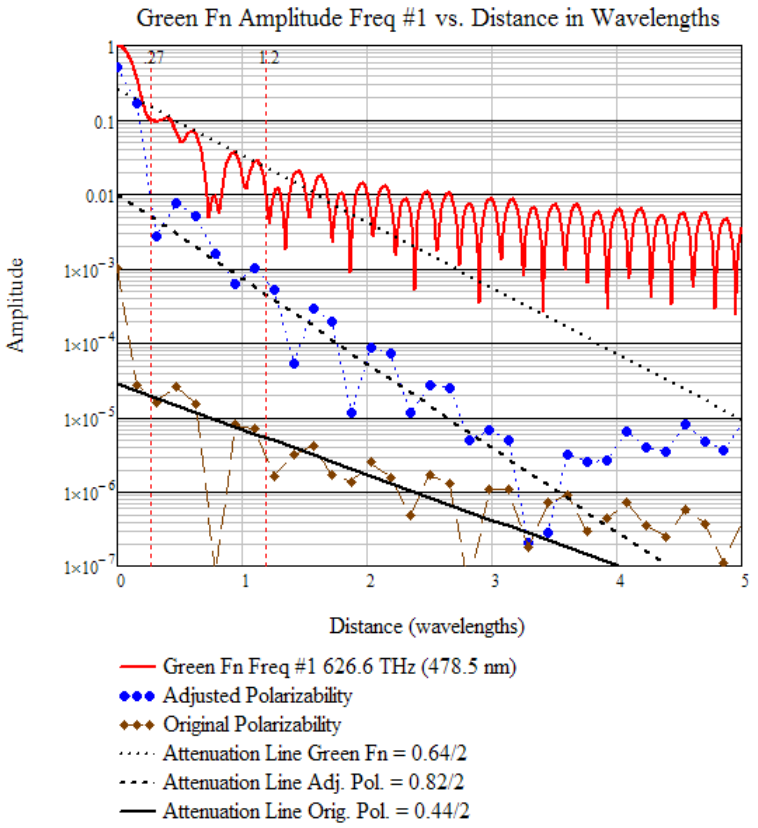

Figure 4-8 Unadjusted and Adjusted Weber and Ford Polarization Data Compared to Effective Dielectric Rod Guided Current Wave Amplitude for Freq #1

The effective dielectric rod (red) shows initial turbulence from the stimulating current source, high attenuation, then the noise floor is reached after a little over a wavelength. Vertical red markers show the region considered where the wave is attenuated, and beyond is noise. The attenuation of the current wave was 0.64/2=0.32 per unit cell (75 nm), which is $18.53\text{dB}/500\text{nm}$, or $3\text{dB}/162\text{nm}$. Note that our method of adjusting the results of Weber and Ford's method as outlined in section 3.3 led to a perceived attenuation constant of 0.82/2= 41 per unit cell near the start of the chain, which is $23.74\text{dB}/500\text{nm}$, or $3\text{dB}/126\text{nm}$. On the other hand, if one tries to fit a straight line attenuation to the *original* Weber and Ford data near the start of the chain, they would be lead to believe the attenuation was 0.44/2=21 per unit cell, which is $12.16\text{dB}/500\text{nm}$ or $3\text{dB}/247\text{nm}$. The actual attenuation is nearly in the middle. This is overlooking the fact that according to Weber and Ford's paper, the polarization well down the line is believed to show the guided wave's ture attenuation, when in fact the attenuation for the *guided* wave occurs at the start of the line, and all that is seen well down the chain of spheres is the dipolar radiation into free-space of the initially stimulated sphere. Measuring the dipolar radiation $1/r^2$ and $1/r^3$ fall off as attenuation resulted in their belief that the intensity attenuation was much lower than reality. This can be better seen at frequency #11, which is the same as their test frequency, and is shown in Figure 4-9.

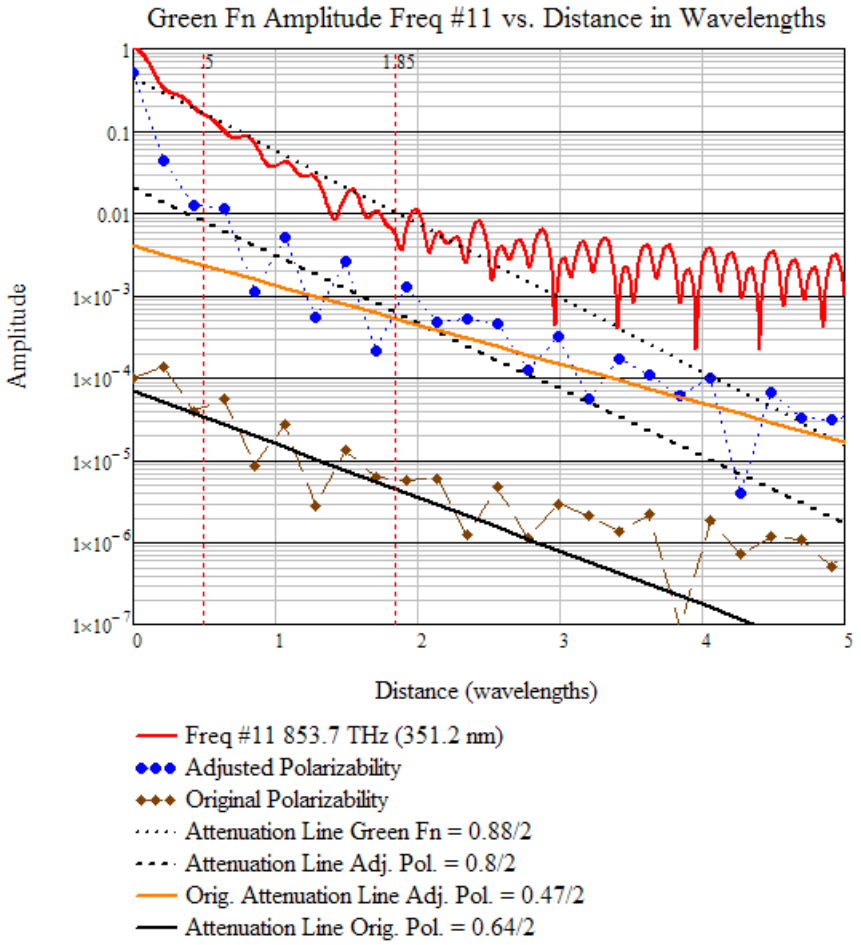

Figure 4-9 Unadjusted and Adjusted Weber and Ford Polarization Data Compared to Effective Dielectric Rod Guided Current Wave Amplitude for Freq #11

Again, we must select a region slightly past the start of the chain to avoid turbulence from the stimulating current source of the rod, and ignore the region affected by noise. These regions are marked by vertical red lines. The attenuation originally determined for the adjusted polarizability data in section 3.3 considered spheres well along the chain. It is evident we were capturing effects from the dipolar radiation which

we had tried to remove, as the attenuation determined (orange line) is not nearly steep enough in the region close to the start of the chain. The effective dielectric rod shows the attenuation is 0.88/2 = .44 per unit cell, which is $25.5\text{dB}/500\text{nm}$, or $3\text{dB}/118\text{nm}$. This enables us to compare to Weber and Ford, who calculated a power attenuation of 1.44×10^{6} per meter at the same frequency, which is $3.127\text{dB}/500\text{nm}$ or $3\text{dB}/480\text{nm}$. The actual attenuation is more than 22 dB greater.

For additional comparison, the *original* polarization intensity data from Weber and Ford's method, implies a loss of 0.64/2 = 0.32 per unit cell near the start of the line, which is $18.5\text{dB}/500\text{nm}$, and the first attempt at adjusting this data was in error, as we see the slope of the old attenuation line (orange) was trying to fit to too many spheres down the line. The flawed measurement was 0.47/2 = 0.235 per unit cell, which is $13.6\text{dB}/500\text{nm}$. Clearly the accurate line is the black dashed line, with 0.8/2 = 0.4 per unit cell, which is $23.2\text{dB}/500\text{nm}$.

There is no guided wave over the entire band given in the dispersion diagram in Weber and Ford's paper. The question now becomes, if the chain is not guiding, what *will* guide? Is the lack of guidance due to their Drude model? What can make the chain work?

Chapter 5

GUIDING STRUCTURES

5.1 Unrealistically Low Loss Silver

Part of the reason the wave is not guided given Weber and Ford's model, is the Drude metal representation used. As previously noted, they chose a Drude represented by $\epsilon(\omega) = 1 - \frac{\omega_p^2}{\omega(\omega + j\nu)}$, where $\omega_p = 6.18 eV/\hbar$, $\nu = 0.7 eV$, and apparently $\epsilon_\infty = 1$. It is known that a material may be completely modeled by a sum of Lorentz and Debye terms [29], and in the visible spectrum, for a Drude metal, aside from the Drude (Lorentz) pole $\frac{\omega_p^2}{\omega(\omega + j\nu)}$, these additional terms are nearly constant, adding together to give $\epsilon_\infty > 1$. Fitting to measured data as described in Appendix A shows $\epsilon_\infty \approx 6$ for silver. We may also fit to measured data for ω_p (which gets significantly shifted by the new ϵ_∞) and ν, also denoted γ in the appendix. Making this adjustment, which increases the permittivity, may help the object being modeled achieve guidance. Beyond adjusting the parameters of the model being used to fit to measured data, the actual measured data being fit may be selected to be of lower loss. It is believed that the measured silver data by Palik [26] is accurate, while older measurements by Johnson and Christy [30] cite unrealistically low values for ϵ'', which are on the order

of one tenth the values reported in Palik. In the interest of exploring what *will* guide a wave, we are free to use the Johnson and Christy data, and see if it is sufficient for guidance, and to give us an idea as to by what mechanism guidance may be achieved.

Figure 5-1 shows a Drude fit, which is also adjusted for mean free path effects, to Johnson and Christy's silver data. From these data 24 points are selected to use in 24 test frequencies to cover the same band as shown in previous dispersion diagrams.

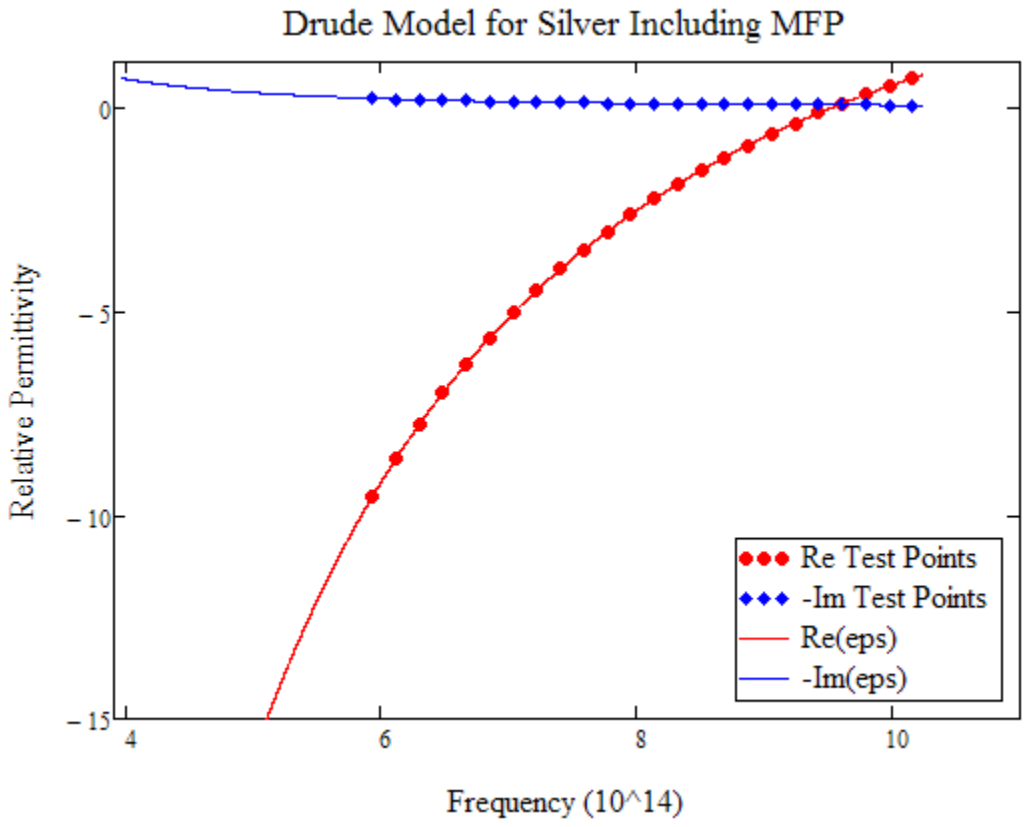

Figure 5-1 Drude Model from Fit to Johnson and Christy's Silver Data and Points Selected for Evaluation

To create an effective medium for the dielectric rod, the Drude model for silver is used for the inclusion in the previously described Claussius-Mossotti model, resulting in the Lorentz material in Figure 5-2. In particular note how “peaky” this material is at resonance, especially when compared to the same model of Figure 4-2, which used Palik's silver data.

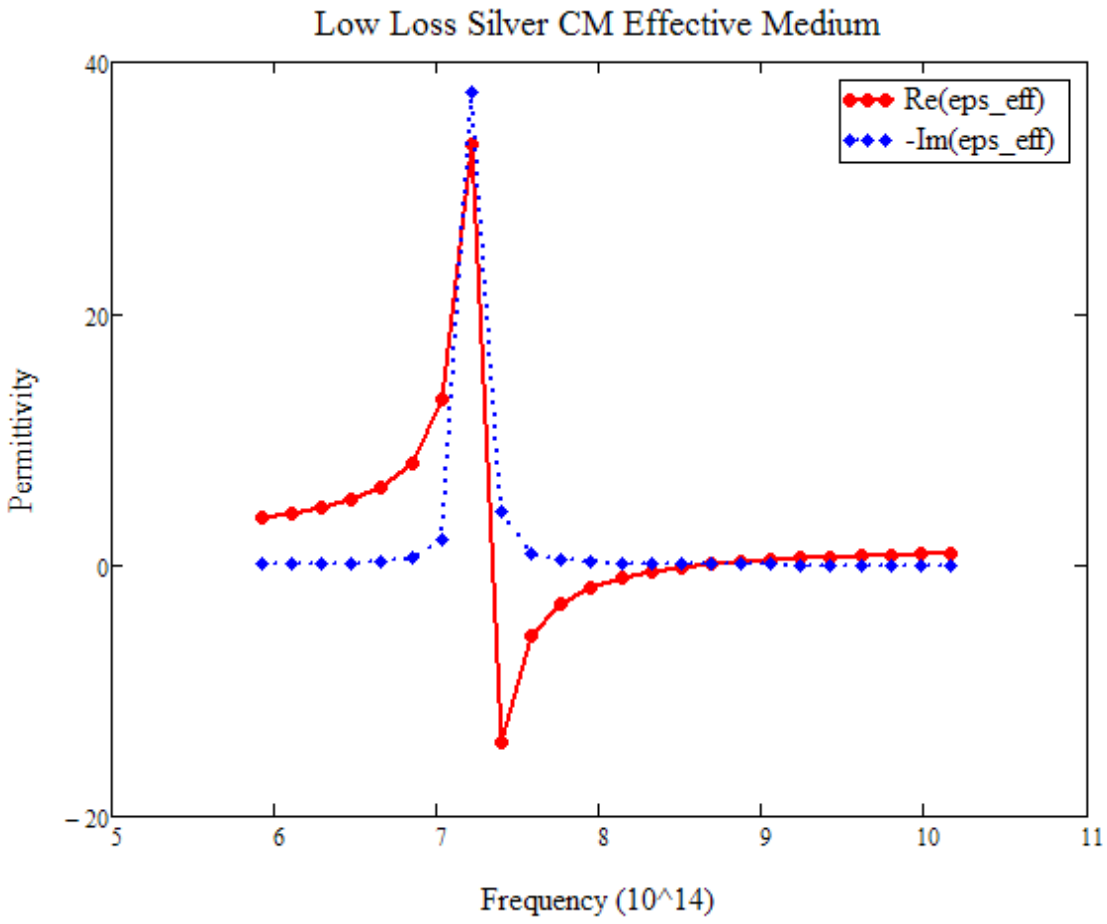

Figure 5-2 Unrealistically Low Loss CM Drude Silver Model

The simulation of the effective cylinder composed of this effective material results in Figures 5-3 through 5-5.

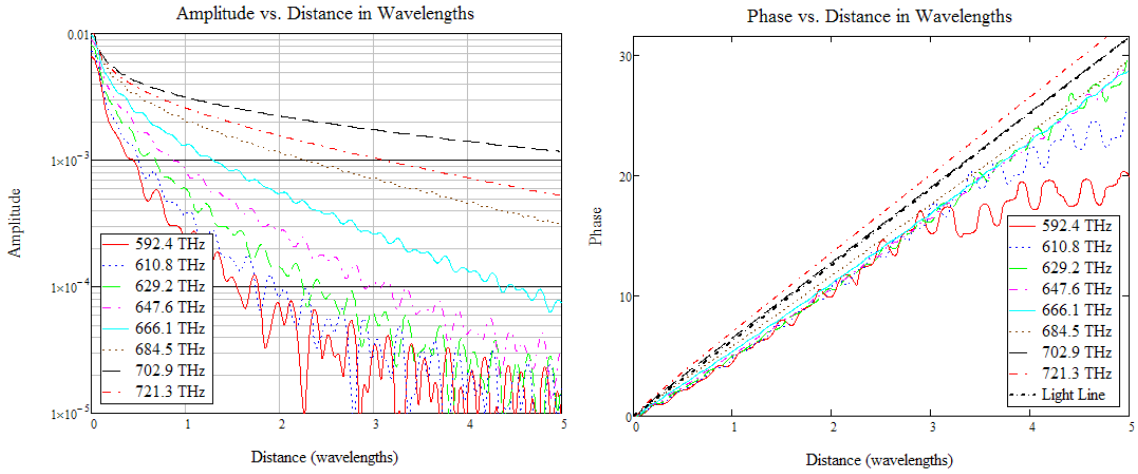

Figure 5-3 Low Loss Claussius-Mossotti 592.4 - 721.3 THz

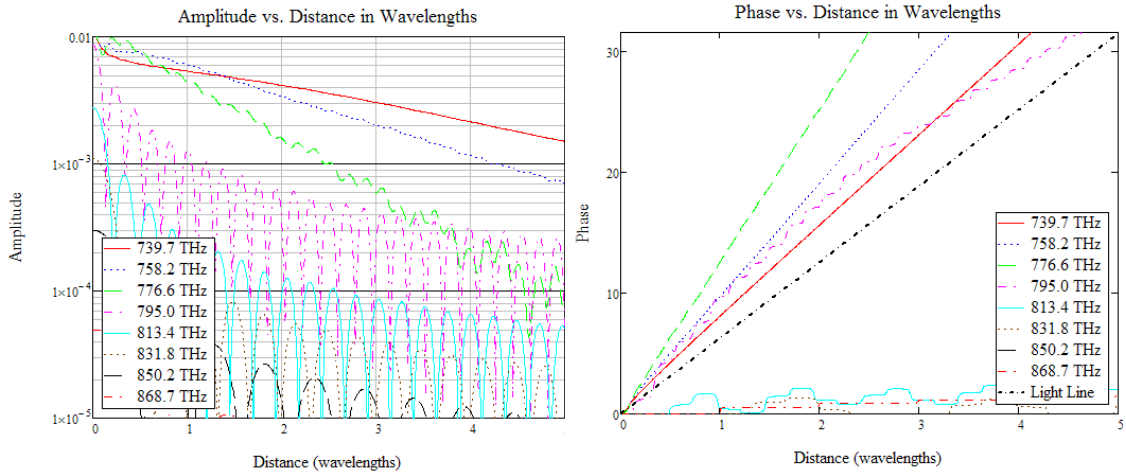

Figure 5-4 Low Loss Claussius-Mossotti 739.7 – 868.7 THz

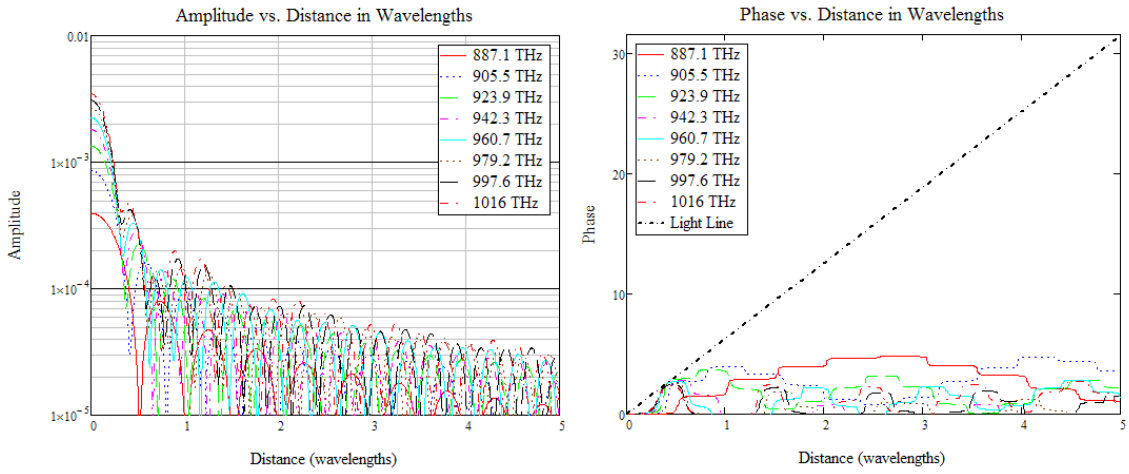

Figure 5-5 Low Loss Claussius-Mossotti 887.1 – 1016 THz

We have guidance with this structure. Onset occurs near 702.9 THz, and we have guidance support through 758.2 THz. At 776.6 THz, the next highest order mode starts interfering, causing the rippling observed in the amplitude, which is worse at 795.0 THz. Once past this frequency we enter a band of non propagation.

Observe which points on the Lorentz material permitted guidance:

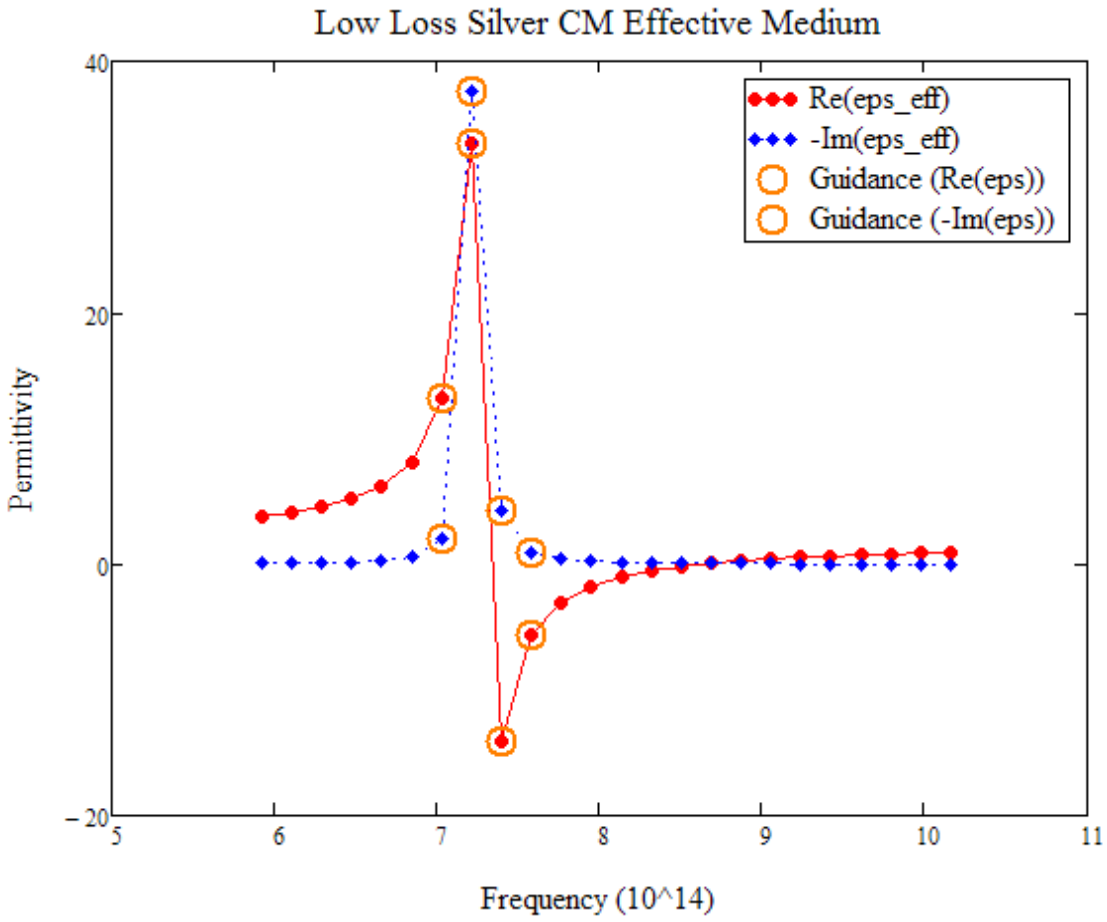

Figure 5-6 Permittivity Values of Effective Media Dielectric Rod that Support Guidance in the Band of Interest

Given low enough loss in the model of silver, or high enough real part of permittivity, the chain of spheres can guide in the region of interest. From the slope of the amplitude plots, we may determine the attenuation of the guided modes at the simulated frequencies, and from the slope of the phase plots, the propagation constant.

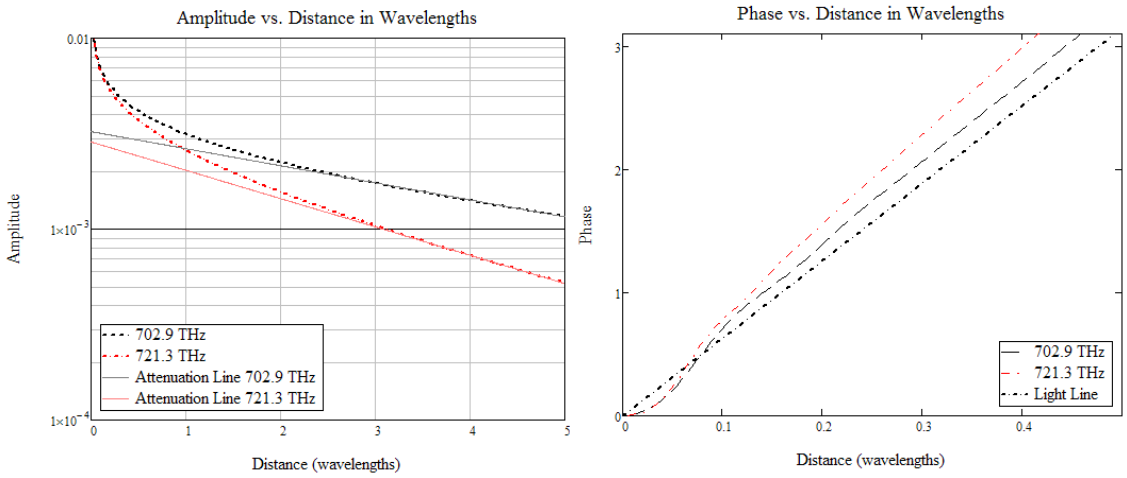

Figure 5-7 First Two Guided Frequencies and Slopes Leading to Attenuation and Propagation Constants

In a similar manner, we may find the attenuation and propagation constant for the next two frequencies, resulting in a dispersion diagram and attenuation vs. frequency plot.

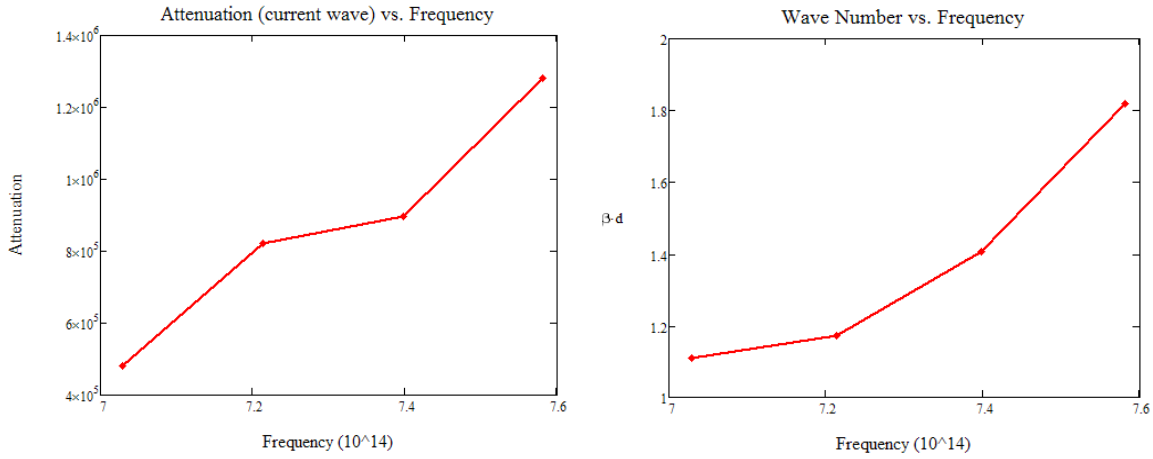

Figure 5-8 Attenuation vs. Frequency and Wave Number vs. Frequency

For comparison to previous groups results, the attenuation may be determined in dB/500nm. Also, the phase velocity may be determined from the dispersion diagram.:

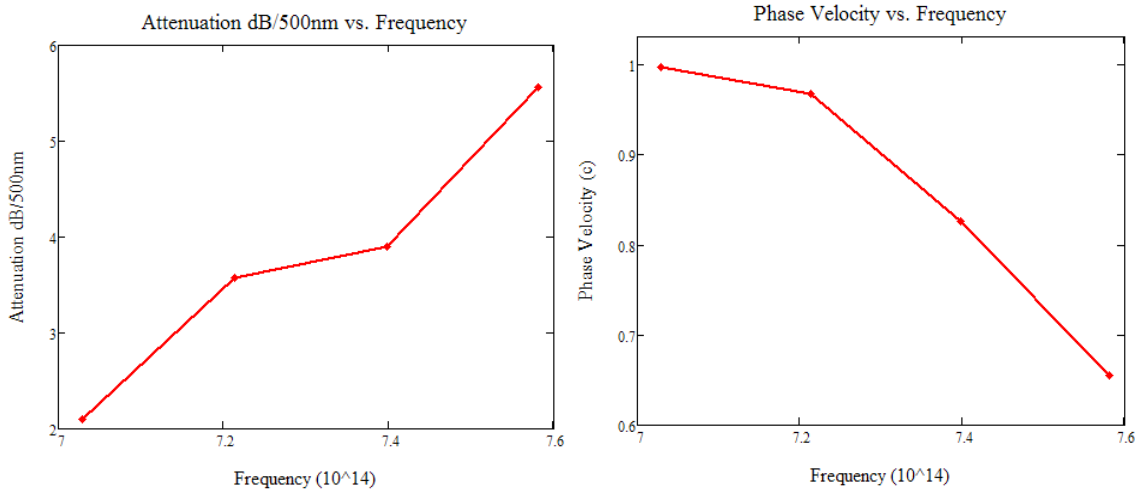

Figure 5-9 Attenuation in dB/500nm and Phase Velocity in units of the Speed of Light c vs. Frequency

We see an attenuation of 2.10, 3.57, 3.89, and 5.57dB per 500nm, and phase velocity of 0.996, 0.967, 0.826, and 0.655 times the free space speed of light, at the frequencies 702.9, 721.3, 739.7, and 758.2 THz. The group velocity could be determined by applying the Green function approach in smaller increments of frequency across the band to approximate a continuum, or estimated from the material parameters of the effective medium.

If the dielectric rod equivalent to a chain of spheres with Johnson and Christy silver spheres will guide in the region of interest, what about more realistic data from Palik?

5.2 Realistic Loss Silver

In a similar manner to section 5.1, a Claussius-Mossotti effective medium using Palik's silver data, with mean free path effect offset, was made.

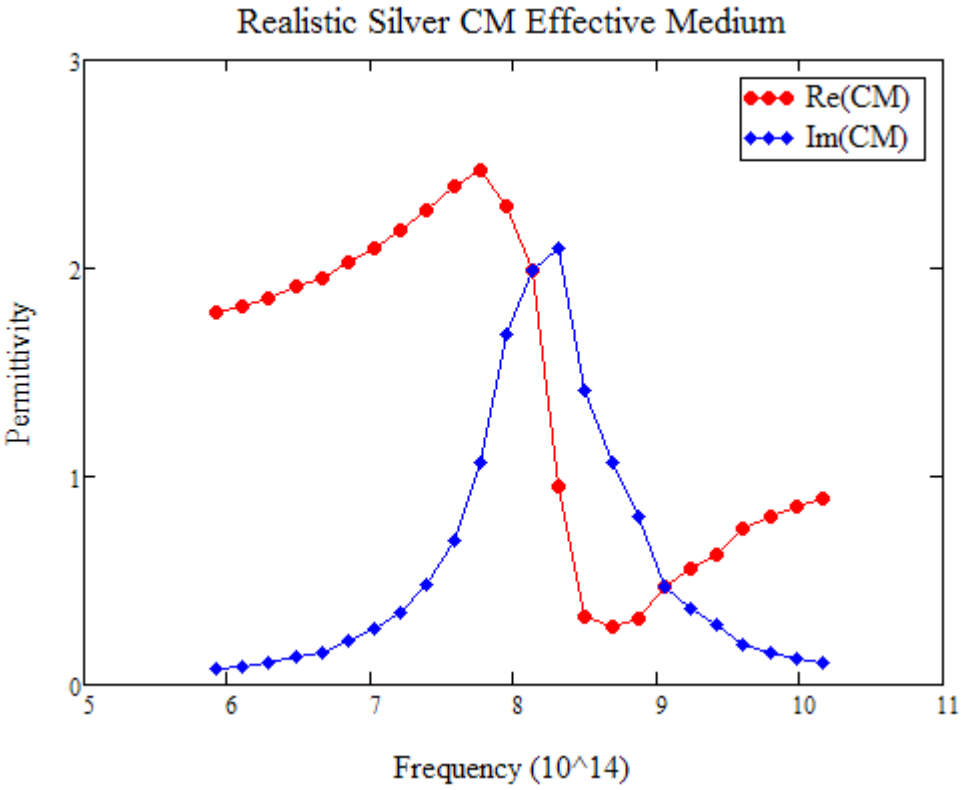

Figure 5-10 Realistic Loss Silver CM Effective Material

Note how significantly lower the peak of the resonance is compared to the low loss version in Figure 5-5. Given where there was guidance, and where there was not, in section 5.1, it can be predicted that there will be no guidance over the band of interest with this effective material, which was confirmed by simulation.

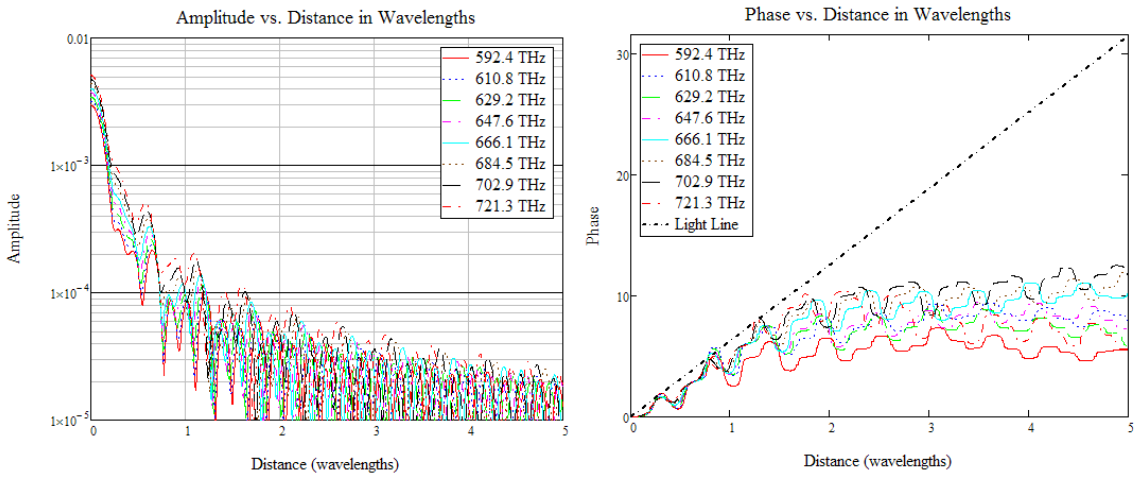

Figure 5-11 Realistic Claussius-Mossotti 592.4 - 721.3 THz

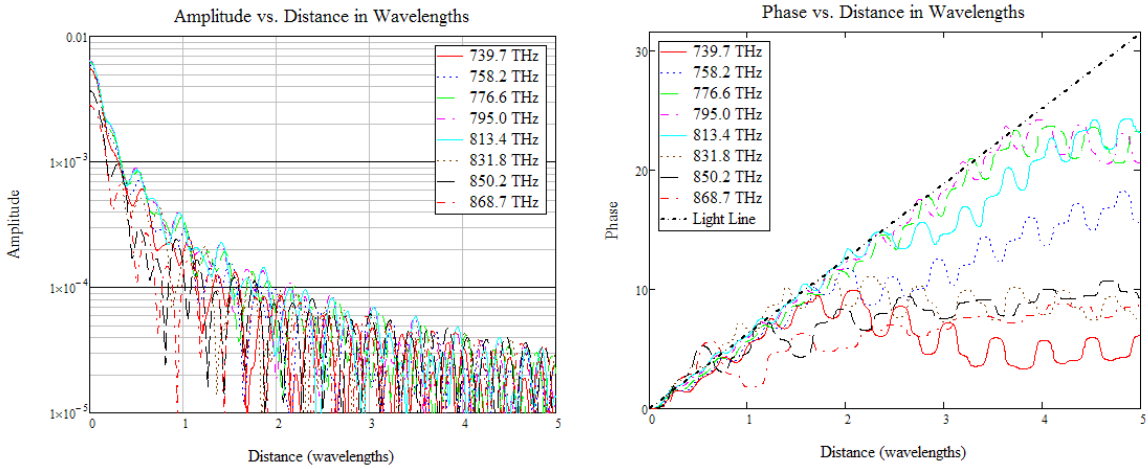

Figure 5-12 Realistic Claussius-Mossotti 739.7 – 868.7 THz

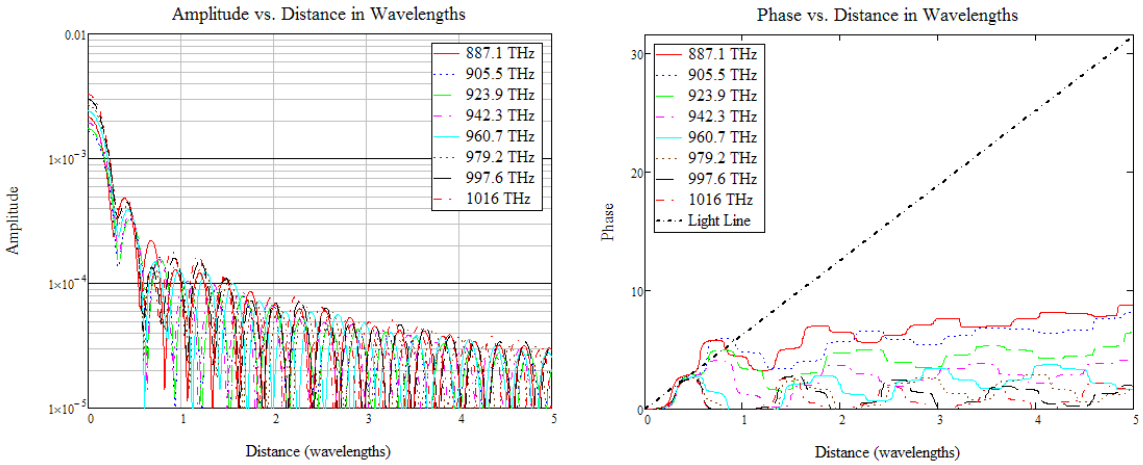

Figure 5-13 Realistic Claussius-Mossotti 887.1 – 1016 THz

Information can still be gathered from the results, for instance the envelope of the amplitude peaks in the region near the start of the chain, before the noise floor, can be considered, giving an attenuation constant as described in section 4.2 and shown in figures 4-8 and 4-9. But the consideration at hand is simply if such a structure will guide in the band of interest given realistic material parameters, and it clearly will not. It is apparent that the sharp resonance of the unit cell of the effective medium is necessary to guide.

5.3 Realistic Silver Nano-wire

What if we simply filled our equivalent lossy dielectric cylinder with silver instead of an effective permittivity as made by a spherical inclusion? 24 data points from

the permittivity function from a Drude fit to Palik's silver data, with mean free path adjustment, were used to fill a 25 nm radius cylinder.

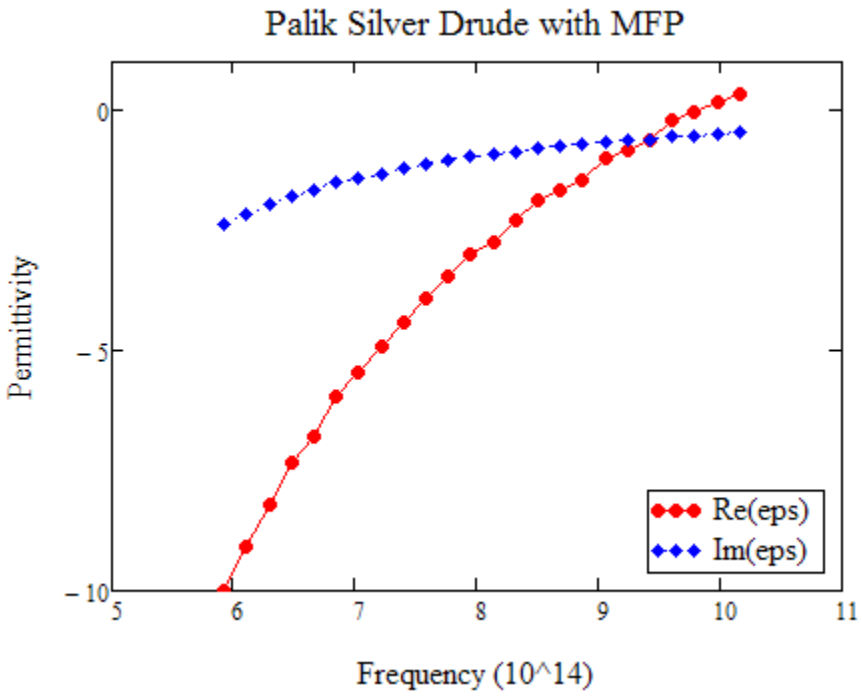

Fig 5-14 Sample Points from Palik Silver Drude Model with Mean Free Path Adjustment

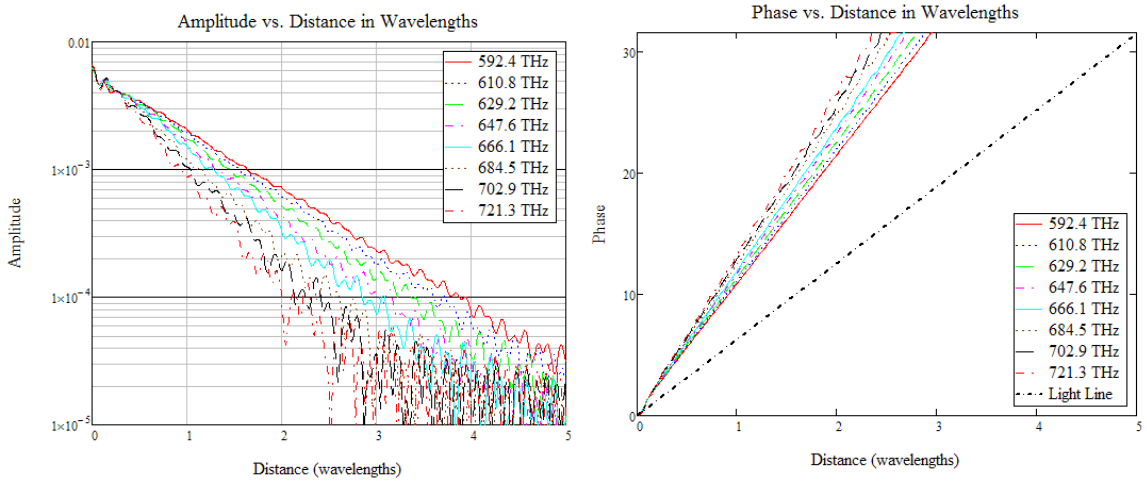

Figure 5-15 Realistic Silver Cylinder 592.4 - 721.3 THz

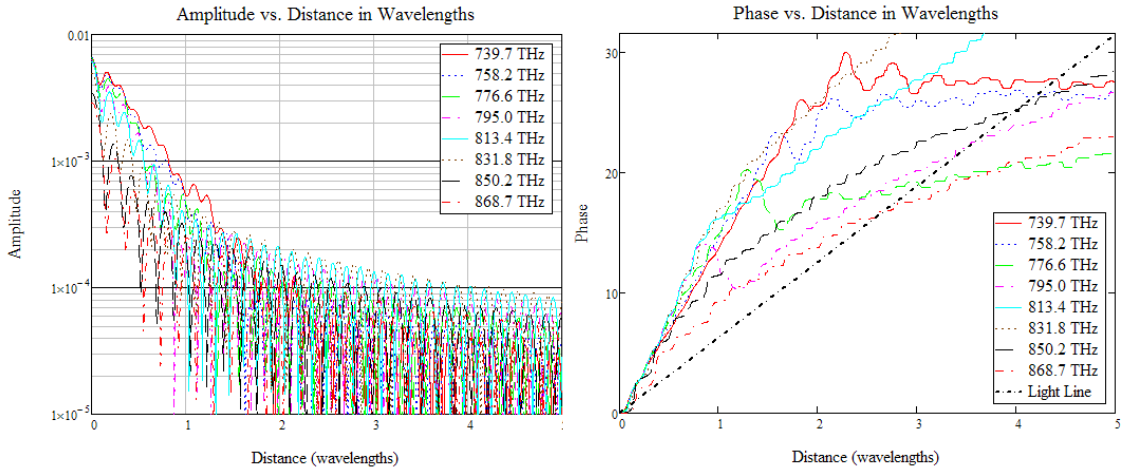

Figure 5-16 Realistic Silver Cylinder 739.7 – 868.7 THz

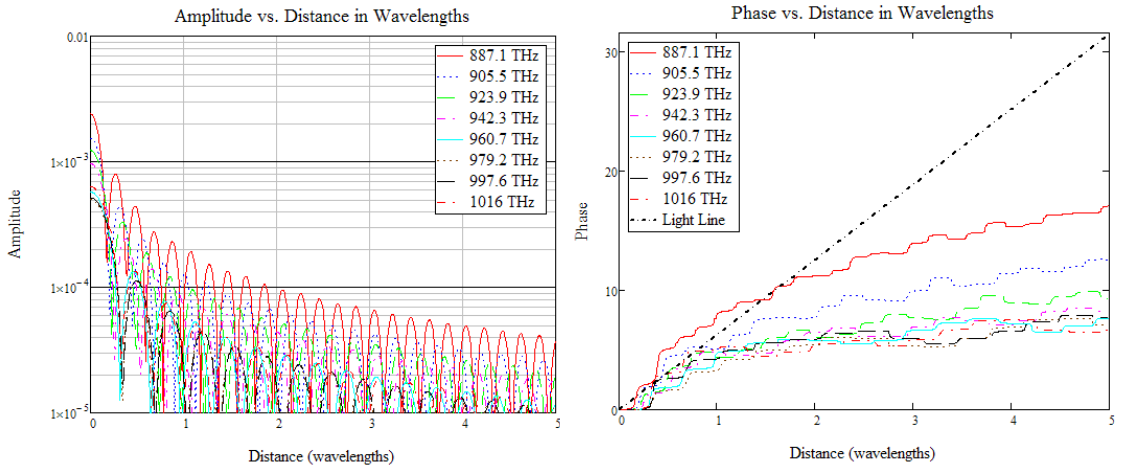

Figure 5-17 Realistic Silver Cylinder 887.1 – 1016 THz

The realistic silver wire does guide, but much like a plane wave traveling over a lossy Earth, the wave on the surface of the rod appears to be drawn into the wire and damped. The lowest frequency tested, 592.4 THz, has the lowest attenuation, which is $9.10\,dB/500\text{nm}$, with wave number $\beta d = 1.585$, and phase velocity 0.587c. After 721.3 THz, the wave does not appear to be guided much past a wavelength. At this

frequency the attenuation is $22.3\,dB/500\text{nm}$, wave number $\beta d = 2.362$, and phase velocity $0.480c$.

5.4 Unrealistically Low Loss Silver Nano-wire

In section 5.3 we saw a realistic structure that does guide, the silver nano-wire. In section 5.1 we saw that a chain of spheres with unrealistically low loss silver guides as well. To compare the structures, consider a nano-wire similar to that of section 5.3, except now composed of the same Drude model fit to Johnson and Christy mean free path adjusted low loss silver, such as was used for the material of the chain of spheres in section 5.1. Doing so, and we see better guidance than the realistic nano-wire of section 5.3, as can be expected due to the lower loss, yet similar damping behavior as the frequency increases. We also see a lower onset frequency than the chain of spheres of the same material as was shown in section 5.1, with higher cutoff, and less attenuation.

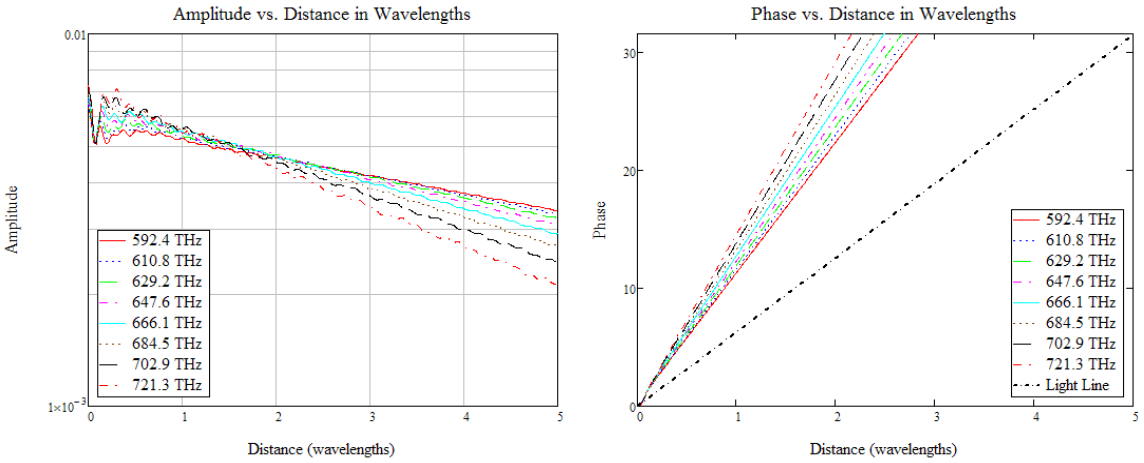

Figure 5-18 Low Loss Silver Cylinder 592.4 - 721.3 THz

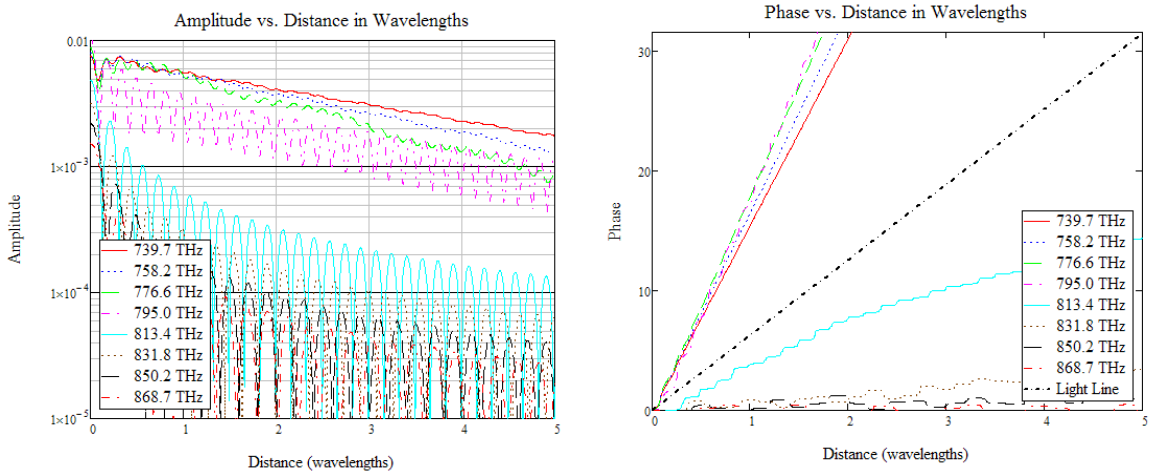

Figure 5-19 Low Loss Silver Cylinder 739.7 – 868.7 THz

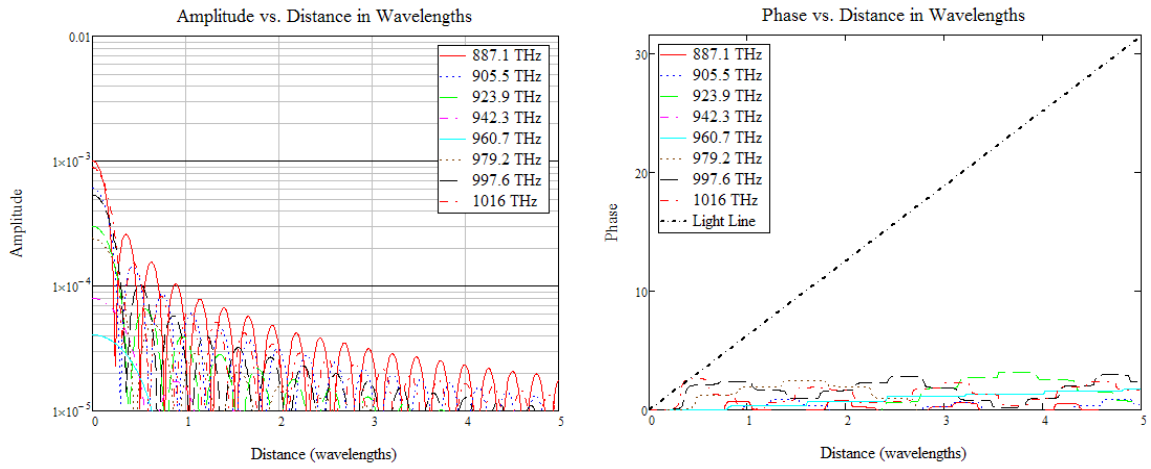

Figure 5-20 Low Loss Silver Cylinder 887.1 – 1016 THz

Again, from the slope of the amplitude plots, we may determine the attenuation of the guided modes at the simulated frequencies, and from the slope of the phase plots, the propagation constant.

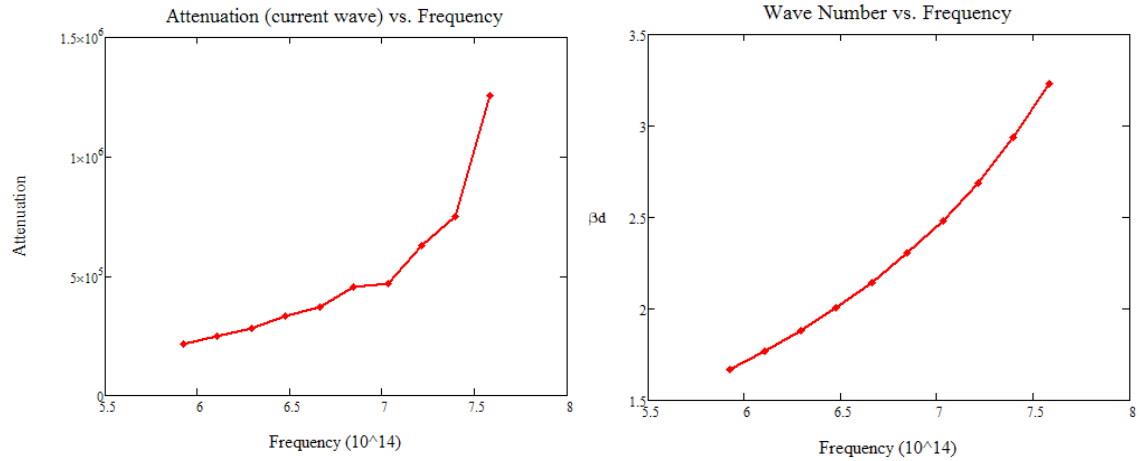

Figure 5-21 Attenuation vs. Frequency and Wave Number vs. Frequency

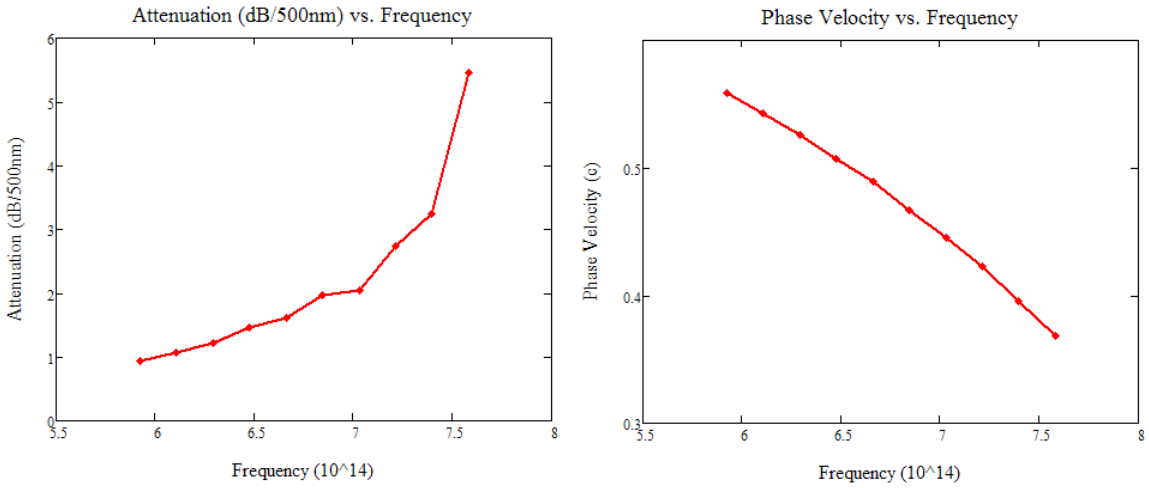

Figure 5-22 Attenuation in dB/500nm and Phase Velocity in units of the Speed of Light c vs. Frequency

So from 592.4 to 758.2 THz, the attenuation varies from 0.93 to 7.58 dB/500nm, and the phase velocity from 0.558 to 0.369 c.

In both low loss and realistic cases, we see the nanowire has lower onset, wider band, slower wave, and less attenuation.

Chapter 6

CONCLUSION

A method for small scale imaging using visible wavelength light was proposed, which called for a material or structure to slow the wave sufficiently for high resolution. Recent models in the waveguiding potential of plasmonic nanospheres implied their usability in this application, but evaluation introduced uncertainty in their validity. A method in evaluating the waveguiding properties of an equivalent cylinder conforming to effective media theory was proposed utilizing a Green function approach, which confirmed the concerns in the original models, and introduced an improved method of modeling such structures.

The results in the literature, though not necessarily unanimous, claimed attenuation constants as low as $3.13\mathrm{dB}/500\mathrm{nm}$. The results in the literature have been shown here to be in all likelihood spurious either because of misinterpretation of measured total fields on a line of spheres as being due only to a guided wave, or violation of validity conditions for the eigenvalue solution methods used.

The Green function solution with an effective medium model is shown to unambiguously demonstrate whether or not there is guidance by considering not only the amplitude, but also the phase of the guided phenomenon. Slow waves can be excited on a silver chain of spheres of the usual construction assumed in the literature if and only if the loss of the silver is assumed to be extraordinarily low. In this case the lowest

attenuation observed in the same band as evaluated in the literature for a wave which could even be considered guided was $9.10\,dB/500\text{nm}$, with attenuation of the order $22.3\,dB/500\text{nm}$ observed near the region in which the literature believed the attenuation was of the order $3.13\,dB/500\text{nm}$.

More realistic material properties preclude guidance with these chain parameters (25nm radius spheres and 75nm center-to-center separation). Other chain configurations can readily be modeled.

It is also shown that a pure silver rod of the same diameter does guide under both realistic or idealized silver parameters with attenuation of 9.10 to 22.3 $dB/500\text{nm}$ for the realized and 0.93 to 7.58 $dB/500\text{nm}$ for the idealized.

Chapter 7

FUTURE WORK

- Finite-Difference Time-Domain Simulation to verify results seen with Green function solution for both chain of spheres and nanowire.
- Evaluation of plasmonic chain of spheres model by Alu and Engheta [14] and comparison to Green function solution.
- Evaluation of adjustment of particle geometry (radius and separation) for effect on guidance
- Evaluation of the third type of waveguiding media, the cylinder made from bulk colloidal sphere effective media (Fig. 2-6)
- Evaluation of attenuation and dispersion for all waveguiding devices with respect to radar-like imaging applications
- Exploration and evaluation of other high resolution methods, such as transverse resolution achieved by twin transmission line with small line separation, instead of by slow longitudinal wave

REFERENCES

[1] C. Bai, *Scanning Tunneling Microscopy and its Applications,* New York: Springer Publishing. 2000, pp. 2.

[2] M. J. Rost *et al*, "Scanning Probe Microscopes Go Video Rate and Beyond", *AIP Review of Scientific Instruments,* vol. 76, pp. 053710-19, April 2005.

[3] M. Ohtsu, K. Kobayashi, "Origin of Limits: Diffraction of Light", *Optical Near Fields*, New York: Springer Publishing. 2004, pp. 6-9.

[4] A. Tseng *et al*, "Fabrication of Microbowtie Structures for Optical Probing of Nanoscale Objects", *Microsystem Tecnologies*, vol. 9, num. 5, pp. 335-9, 2003.

[5] R. E. Diaz, "Proof of Feasibility for sub-10nm Optical Defect Detection", Internal ASU White-Paper, ECEE Dept., Arizona State University, 2005.

[6] R. E. Diaz *et al*. "Coherent Evanescent Wave Imaging," U.S. Patent 6 980 716, Dec. 27, 2005.

[7] R. E. Diaz, "ORION Preproposal", Internal document of AESIR research lab, received 8/15/2008.

[8] L. M. Liz-Marzan, "Tailoring Surface Plasmons through the Morphology and Assembly of Metal Nanoparticles", *Langmuir, The ACS Journal of Surface and Colloids,* vol. 22, pp. 32-41, 2006.

[9] S. A. Tretyakov, A. J. Viitanen, "Line of Periodically Arranged Passive Dipole Scatterers", *Electrical Engineering*, vol 82, issue 6, pp. 353-61, Nov. 2000.

[10] M. Quinten, A. Leitner, J. R. Krenn, and F. R. Aussenegg, Opt. Lett. 23, 1331 1998.

[11] S. A. Maier et al, "Optical pulse propagation in metal nanoparticle chain waveguides", *Physical Review B,* vol 67, pp. 205402-7 , May 2003.

[12] M. L. Brongersma, J. W. Hartman, H. A. Atwater, "Plasmonics: Electromagnetic energy transfer and switching in nanoparticle chain-arrays below the diffraction limit," *Physical Review B,* vol 62, pp. 16356-9, Dec. 2000.

[13] W.H. Weber, G.W. Ford, "Propagation of Optical Excitations by Dipolar Interactons in Metal Nanoparticle Chains", Physical Review B, vol. 70, no 12, pp 125429-1, Sept. 2004.

[14] A. Alu, N. Engheta, “Theory of linear chains of metamaterial/plasmonic particles as subdiffraction optical nanotransmission lines ”, *Physical Review B,* vol 74, pp. 205436-54, Nov. 2006.

[15] D. J. Griffiths, "Special Techniques," in *Introduction to Electrodynamics*, 3rd ed, Upper Saddle River, NJ: Prentice Hall, 1999, pp. 146-55.

[16] B. W. Van Der Meer, G. Coker III, S.-Y. S. Chen, "Förster Theory," in *Resonance Energy Transfer*, New York: VCH Publishers, 1994, pp. 35.

[17] J. D. Jackson, “Radiative Reaction Force from Conservation of Energy”, *Classical Electrodynamics,* 3rd ed, New York: Wiley, 1998, pp. 746.

[18] C. Kittel, "Fermi Surfaces and Metals," in *Introduction to Solid State Physics*, New York: John Wiley & Sons Inc. 1967, pp. 228.

[19] H. C. van de Hulst, "Particles Small Compared to Wavelength," in Light Scattering by Small Particles, New York: Dover Publications Inc. 1981, pp. 66.

[20] K. Y. Kim, H-S. Tae, J-H. Lee, “Leaky Dispersion Characteristics in Circular Dielectric Rod Using Davidenko's Method”, Journal of the Korea Electromagnetic Engineering Society, vol 5, no. 2, June 2005.

[21] L. B. Fertic, J. H. McClellan, “Instantaneous Frequency Estimation Using Linear Prediction with Comparisons to the DESAs”, *IEEE Signal Processing Letters,* vol 3, no. 2, Feb. 1996.

[22] R. E. Diaz, “Dielectric Rod Notes – Fixed”, Internal document of AESIR research lab, received 6/15/2011.

[23] R. E. Diaz, "Towards a Pseudo-Conductor Transmission Line with a Designed Propagation Constant", Internal document of AESIR research lab, received 12/15/2012.

[24] R. E. Diaz, "Modeling the permeable rod", Internal document of AESIR research lab, received 12/15/2012.

[25] C. A. Balanis, “Dielectric Waveguides and Resonators”, *Advanced Engineering Electromagnetics,* 2nd Ed., John Wiley & Sons Inc., New York, pp. 513, 1989.

[26] E. D. Palik, “Optical Constants of Metals: Silver (Ag)”, Handbook of Optical Constants of Solids, Academic Press, San Diego, 1991.

[27] W. W. Bell, "Legendre Polynomials and Functions," in *Special Functions for Scientists and Engineers,* Mineola, NY: Dover Pub. Inc., 2004, pp. 48.

[28] R. P. Lucht, "Drude Model for Dielectric Constant of Metals", Online Reference from Purdue University, Online [http://optics.hanyang.ac.kr/~shsong/27-Metals.pdf] Accessed: 6/15/2012.

[29] R. E. Diaz, N. G. Alexopoulos, “An Analytic Continuation Method for the Analysis and Design of Dispersive Materials”, *IEEE Transactions on Antennas and Propagation,* vol 45, no. 11, pp. 1602-10, Nov. 1997.

[30] P. Johnson, R. Christy, "Optical Constants of the Noble Metals", Phys. Rev. B, vol 6, no. 12, 1972.

[31] W. Zhang et al., "Influence of the electron mean free path on the resistivity of thin metal films", Microelectronic Engineering, vol 76, pp. 146-52, Aug. 2004.

[32] C. F. Bohren, D. R. Huffman, "Absorption and Scattering by a Sphere", *Absorption and Scattering of Light by Small Particles,* John Wiley & Sons, Inc., New York, 1998.

[33] M. Abramowitz, I.A. Stegun, *Handbook of Mathematical Functions with Formulas, Graphs, and Mathematical Tables*, Dover, New York, 1965, pp. 360, 439.

[34] F. Capolino, "Single Dipole Approximation for Modeling Collections of Nanoscatterers", *Theory and Phenomena of Metamaterials*, Vol 1, CRC Press, Boca Raton, 2009, pp. 87.

[35] H. C. van de Hulst, “Conservation of Energy and Momentum”, Light Scattering by Small Particles, Dover, New York, 1981, pp. 11.

[36] S.Y. Park, D. Stroud, “Surface-plasmon dispersion relations in chains of metallic nanoparticles: an exact quasistatic calculation”, Physical Review B, vol 69, pp. 125418-25, 2004.

[37] C. Kittel, *Introduction to Solid State Physics*, Wiley, New York, 1986, p. 134.

[38] A. H. Apanaretos, R. E. Diaz, “Incorporating Effective Media in the Finite-Difference Time-Domain Method for Spherical Nanoparticle Modeling”, unpublished.

[39] T. Sebastian, “Magneto-dielectric antenna theory and design”, unpublished.

[40] M. Conforti, M. Guasoni, “Dispersive properties of linear chains of lossy metal nanoparticles”, J. Opt. Soc. Am. B, vol 27, no. 8, Aug. 2010.

[41] R. Schmehl, B. M. Nebeker, E. D. Hirleman, “Discrete-dipole approximation for scattering by features on surfaces by means of a two-dimensional fast Fourier transform technique”, JOSA A, vol 14, no. 11, pp. 3026-3036, 1997.

APPENDIX A

DRUDE MODEL

The Drude Model for the permittivity function of a material is based on the Lorentz model (harmonic oscillator) without restorative force (IE free electrons not bound to a particular nucleus) [28]. Perturbation of the electron modeled as a harmonic oscillator (Lorentz):

$$m_{e^-} a_{e^-} = F_{E-Local} + F_{Damping} + F_{Spring} \Rightarrow m_{e^-} \frac{d^2 \vec{r}}{dt^2} + m_{e^-} \gamma \frac{d\vec{r}}{dt} + C\vec{r} = -e\vec{E}_L$$

For motion of *free* electron, which is not bound to a particular nucleus, $C = 0$ and the Lorentz model becomes the Drude model.

$$m_{e^-} \frac{d^2 \vec{r}}{dt^2} + m_{e^-} \gamma \frac{d\vec{r}}{dt} + C\vec{r} = -e\vec{E}_L \Rightarrow m_{e^-} \frac{d\vec{v}}{dt} + m_{e^-} \gamma \vec{v} \Rightarrow \frac{d\vec{v}}{dt} + \gamma \vec{v} = -\frac{e}{m_{e^-}} \vec{E}_L$$

Note $\gamma = \frac{1}{\tau}$ where τ is the relaxation time, typically on the order of 10^{-14} s. Current density is defined $\vec{J} = -Ne\vec{v}$ where *N* is the number of electrons per meter squared, *-e* is the charge of an electron, and $\vec{v}$ is the electron velocity. Back substitution into the equation of motion gives:

$$\frac{d\vec{J}}{dt} + \gamma \vec{J} = \frac{Ne^2}{m_{e^-}} \vec{E}_L$$

Assume applied electric field and conduction current density are given by:

$$\vec{E} = \vec{E}_0 e^{j\omega t} \qquad \vec{J} = \vec{J}_0 e^{j\omega t}$$

Back substitute into equation of motion:

$$\frac{d\left(\vec{J}_0 e^{j\omega t}\right)}{dt} + \gamma \vec{J}_0 e^{j\omega t} = \frac{Ne^2}{m_{e^-}} \vec{E}_0 e^{j\omega t} \Rightarrow \left(j\omega + \gamma\right)\vec{J}_0 = \frac{Ne^2}{m_{e^-}} \vec{E}_0$$

At DC, $\omega = 0$ and : $\vec{J} = \left(\frac{Ne^2}{m_{e^-}\gamma}\right)\vec{E} = \sigma\vec{E}$ so static conductivity $\sigma = \frac{Ne^2}{m_{e^-}\gamma}$.

General case for oscillating applied field:

$$\vec{J} = \left[\frac{\sigma}{1 + j\,\omega/\gamma}\right]\vec{E} = \sigma_\omega \vec{E} \quad \text{where} \quad \sigma_\omega \quad \text{is the dynamic conductivity.}$$

Maxwell's equations give us the following wave equation for metals:

$$\nabla^2 \vec{E} = \frac{1}{c^2}\frac{\partial^2 \vec{E}}{\partial t^2} + \frac{1}{\epsilon_0 c^2}\frac{\partial \vec{J}}{\partial t} \quad \text{because} \quad \vec{P} = 0 \qquad \vec{J} \neq 0$$

As determined, $\vec{J} = \left[\frac{\sigma}{1 + j\,\omega/\gamma}\right]\vec{E}$, so back substitution:

$$\nabla^2 \vec{E} = \frac{1}{c^2}\frac{\partial^2 \vec{E}}{\partial t^2} + \frac{1}{\epsilon_0 c^2}\frac{\partial}{\partial t}\left(\frac{\sigma}{1 + j\,\omega/\gamma}\vec{E}\right)$$

The wave equation is of course satisfied by electric fields of form $\vec{E} = \vec{E}_0 e^{j(\omega t - \vec{k}\cdot\vec{r})}$,

where $k^2 = \frac{\omega^2}{c^2} + j\left[\frac{\sigma\,\omega\,\mu_0}{1 + j\,\omega/\gamma}\right] \qquad c^2 = \frac{1}{\epsilon_0 \mu_0}$.

$k^2 = \omega^2 \epsilon\,\mu = \frac{\omega^2}{c^2}\epsilon_r$ given $\mu_r = 1$, so:

$$\epsilon_r \frac{\omega^2}{c^2} = \frac{\omega^2}{c^2} + j\left[\frac{\sigma\,\omega\,\mu_0}{1 + j\,\omega/\gamma}\right] \Rightarrow \epsilon_r = 1 - \frac{\gamma\,\sigma\,\mu_0 c^2}{\omega^2 - j\,\omega\,\gamma}$$

This is the effective permittivity of the Drude material. Define the plasma frequency

$\omega_p^2 = \gamma\,\sigma\,\mu_0 c^2$ so that when $\omega \gg 1$ the ω^2 term in the denominator dominates, and

ϵ_r changes sign when $\omega = \omega_p$. Then $\epsilon_r = 1 - \frac{\omega_p^2}{\omega^2 - j\,\omega\,\gamma}$.

Given a material is *strictly* Drude, this model is appropriate. In reality, all materials have other mechanisms which affect their permittivity [29]. Define these other

effects $F(\omega)$, then the permittivity function becomes $\epsilon_r = 1 - \frac{\omega_p^2}{\omega^2 - j\omega\gamma} + F(\omega)$.

Rigorous study of materials has shown that for silver, these other effects are nearly constant over the visible spectrum, making $F(\omega) \approx \epsilon_\infty - 1$, a constant. Then a usable model for silver becomes $\epsilon_r = \epsilon_\infty - \frac{\omega_p^2}{\omega^2 - j\omega\gamma}$, where ϵ_∞ , ω_p^2 , and γ are parameters to be optimized so that the given equations are accurate over the frequency range of interest.

Using the measured data for silver from Johnson and Christy [30] we can use a numeric optimizer (lsqnonlin function in MATLAB 2012a) to solve for the best fit Drude model parameters over the entire range. Using an educated "guess" of $\epsilon_\infty = 6$ and the measured data, we determine the best fit shown in Figure B-1 with parameters $\omega_p = 1.4684 \times 10^{16} rad/s$, and $\gamma = 4.9942 \times 10^{13} rad/s$.

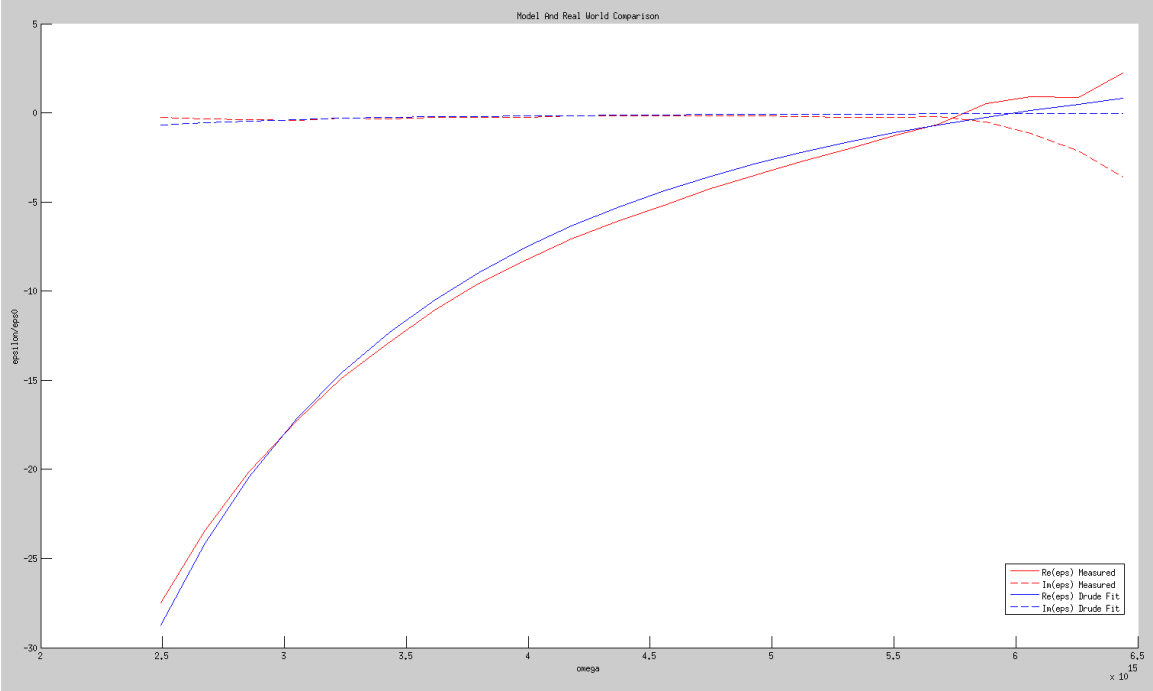

Figure B-1 Drude Model Fit to Measured Data

This Drude model for various particle radii gives the same ω_p for all the spheres:

$$\omega_p = 1.4684 \times 10^{16}$$

Note that in fitting the data, although ω_p remains a constant value to the 4th significant figure, the parameter γ varies between 4.99×10^{13} to 5.77×10^{13} when the particle radius varies from 25nm to 100nm. Labeling this parameter "plasmon resonance" is a misnomer. Recall the equation for the permittivity using the Drude model:

$$\epsilon_r(\omega) = \epsilon_\infty - \frac{\omega_p^2}{\omega^2 - j\omega\gamma}$$

In traditional derivations, we assume no (nearly) constant effects from Lorentz or Debye terms in the model, which would make $\epsilon_\infty = 1$. However, in fitting the Drude model, we saw that over our band of interest, the effects of other Lorentz or Debye terms which are occurring far from the center of our band have the effect of offsetting ϵ_∞ in our band of interest. Trial and error in fitting the model showed $\epsilon_\infty = 6$ is appropriate for silver. This makes the Drude model:

$$\epsilon_r(\omega) = 6\left(1 - \frac{\omega_p^2}{6\,\omega^2 - j\,6\,\omega\,\gamma}\right)$$

For a bulk infinite material resonance occurs when $\epsilon_r = 0$, or when $\omega \approx \omega_p/\sqrt{6}$. So $\omega_{pole} \approx \frac{1.468\times10^{16}}{2.45} = 5.992\times10^{15}$. Which implies resonance should occur at the wavelength:

$$\lambda = \frac{c}{\frac{\omega}{2\pi}} = \frac{2\pi\cdot2.998}{5.992}\times10^{-7} = 314\,nm$$

Note that Brongersma and Atwater's nearest neighbor model [12] uses, without proof, $\omega_{res} \approx 5\times10^{15}$. Using this value in the Drude model, we see resonance should occur at the wavelength:

$$\lambda_{Atwater} = \frac{c}{\frac{\omega}{2\pi}} = \frac{2\pi\cdot2.998}{5}\times10^{-7} = 377\,nm$$

For a *sphere* of silver, in the quasi-static approximation (Appendix D), we expect resonance to occur when $\epsilon_r = -2$, which means:

$$-2 = 6\left(1 - \frac{\omega_p^2}{6\omega^2 - j6\omega\gamma}\right) \Rightarrow \frac{\omega_p^2}{6\omega^2 - j6\omega\gamma} = \frac{4}{3} \Rightarrow \frac{\omega_p^2}{\omega^2} = 8$$

That is when:

$$\omega \approx \omega_p/\sqrt{8}$$

$$\omega_{pole} \approx \frac{1.468\times10^{16}}{3.464} = 5.192\times10^{15}$$

$$\lambda = \frac{c}{\frac{\omega}{2\pi}} = \frac{2\pi\cdot2.998}{5.192}\times10^{-7} = 363\,nm$$

This means we have a parameter ω_p , often called the *Drude plasmon resonance*, which we solve for by fitting a Drude model to measured data. Although this value is *called* the plasmon resonance, the frequency at which we actually observe plasmon resonance is usually this fitted value multiplied by some factor as determined by ϵ_∞ and the geometry of the system. As noted, for silver, at visible frequencies, we know $\epsilon_\infty = 6$. The geometry of the object comes into play by noting that for an infinite homogeneous medium, resonance occurs when $\epsilon_r = 0$; for a semi-infinite distribution $\epsilon_r = -1$; and for a spherical distribution, the distribution of interest in our case, $\epsilon_r = -2$. To clarify whether we are discussing a resonance of the material (plasmon resonance of bulk silver), or resonance of an object (a nanoscale sphere of silver), introduce ω_{pole} , which for a silver sphere is as was determined, $\omega_{pole} = \frac{\omega_p}{\sqrt{8}}$.

The Drude model is a quasi-static approximation. Using the Drude model, for a spherical particle we expect resonance at $\omega_{pole} = \frac{\omega_p}{\sqrt{8}}$, but this may be shifted in a

dynamic system. This is where the Mie theory solution to the scattering of a sphere may be used to exactly model the resonance of a sphere and find at what frequency it occurs for different size spheres. From the quasi-static approximation, we expect them to be near $\lambda \approx 363\text{nm}$.

Also note that the measured silver data from Johnson and Christy has been used, but upon further analysis, the data provided by Palik is expected to be more representative of reality. The method remains the same, just the measured data being fit to may be interchanged.

APPENDIX B

ADJUSTMENT FOR MEAN FREE PATH EFFECT

While the Drude model works reasonably well for bulk material, the effects of the mean free path of the electron becomes significant when a dimension of the material used approaches the order of the length of the electron's free mean path. [31]

This effect changes the observed resistivity of the material, which of course is proportional to the imaginary part of the permittivity. Hence the Drude model must be adjusted for this effect to be sufficiently accurate for our purposes.

Reference [31] shows the adjusted resistivity is given by:

$$\rho = \rho_{bulk}\left[1-\frac{3}{2k}(1-p)\int_1^{\infty}\left(\frac{1}{t^3}-\frac{1}{t^5}\right)\frac{1-e^{-kt}}{1-p\,e^{-kt}}\,dt\right]^{-1}$$

Where ρ_{bulk} is the bulk resistivity of the material of interest, $k = \frac{d}{\lambda}$, where d is the thickness of the film (or diameter of the sphere), and p is the surface scattering factor of the material. Since the particular material placement method to be used has yet to be determined, an average of the resulting *p*'s from different material placement methods will be used.

First, the bulk resistivity may be determined from the imaginary part of the measured permittivity. $\epsilon = \epsilon' - j\epsilon'' = \epsilon' - j\frac{\sigma}{\omega} = \epsilon' - j\frac{1}{\rho\omega}$ so

$$\epsilon'' = \frac{1}{\rho\omega} \Rightarrow \rho = \frac{1}{\epsilon''\omega} \quad .$$

So measured data, such as Johnson and Christy [30], gives us *bulk* property parameters. When we fit our Drude model to their data, we are creating the Drude model

for *bulk* silver, so no offset is required. Once we have the bulk model, we need to adjust it so that it more closely resembles a material that has dimensions which are effected by the electron mean free path. This may be achieved by offsetting the Johnson and Christy resistivity by the appropriate amount, then finding the parameters for the Drude model again using this new offset data. This will give a new Drude model that contains the effects from the small dimensions on the mean free path of the electron.

So bulk resistivity is given by $\rho_{bulk} = \frac{1}{\epsilon''_{meas}\,\omega}$, then for a material with electron mean free path effects we have:

$$\rho = \rho_{bulk}\left[1 - \frac{3}{2k}(1-p)\int_1^{\infty}\left(\frac{1}{t^3} - \frac{1}{t^5}\right)\frac{1-e^{-kt}}{1-p\,e^{-kt}}\,dt\right]^{-1}$$

and:

$$\epsilon''_{meanFP} = \frac{1}{\rho\,\omega}$$

This adjustment is incorporated into the Drude model software built for Appendix A.

APPENDIX C

MIE THEORY

As demonstrated by Bohren and Huffman [32], and following established notation and time convention, assume a time-harmonic electromagnetic field in a linear, isotropic, homogeneous medium. Then the fields must satisfy the wave equation:

$$\nabla^2 \vec{E} + k^2 \vec{E} = 0 \qquad \nabla^2 \vec{H} + k^2 \vec{H} = 0$$

Where $k^2 = \omega^2 \mu \epsilon$ and since there are no free charges:

$$\nabla \cdot \vec{E} = 0 \qquad \nabla \cdot \vec{H} = 0$$

By Maxwell's equations, E and H are dependent:

$$\nabla \times \vec{E} = j\omega\mu \vec{H} \qquad \nabla \times \vec{H} = -j\omega\epsilon \vec{E}$$

Then in a similar manner to constructing solutions from vector potentials, suppose we construct a vector function $\vec{M}$ from constant vector *c* and scalar function ψ such that $\vec{M} = \nabla \times (c\psi)$. So $\vec{M}$ is the curl of a scalar function, and vector analysis shows that the divergence of the curl of a scalar function is 0:

$$\nabla \cdot \vec{M} = 0$$

Apply vector identities:

$$\nabla \times (\vec{A} \times \vec{B}) = \vec{A}(\nabla \cdot \vec{B}) - \vec{B}(\nabla \cdot \vec{A}) + (\vec{B} \cdot \nabla)\vec{A} - (\vec{A} \cdot \nabla)\vec{B}$$

$$\nabla (\vec{A} \cdot \vec{B}) = \vec{A} \times (\nabla \times \vec{B}) + \vec{B} \times (\nabla \times \vec{A}) + (\vec{B} \cdot \nabla)\vec{A} + (\vec{A} \cdot \nabla)\vec{B}$$

to get the vector wave equation:

$$\nabla^2 \vec{M} + k^2 \vec{M} = \nabla \times \left[c(\nabla^2 \psi + k^2 \psi) \right]$$

So the vector wave equation is satisfied by $\vec{M}$ if the scalar wave equation is satisfied by $\nabla^2 \psi + k^2 \psi = 0$. Writing out $\vec{M} = \nabla \times (c\psi)$ and rearranging terms shows

$\vec{M} = -c\,\nabla\times\psi$ which means $\vec{M}$ is perpendicular to *c*. Construct a second vector function $\vec{N}$ from $\vec{M}$ defined by:

$$\vec{N} = \frac{\nabla\times\vec{M}}{k}$$

Then

$$\nabla^2\vec{N} + k^2\vec{N} = \nabla\left(\nabla\cdot\vec{N}\right) - \nabla\times\left(\nabla\times\vec{N}\right) + k^2\vec{N} = -\nabla\times\left(\nabla\times\vec{N}\right) + k\,\nabla\times\vec{M}$$
$$= -\nabla\times\left(\nabla\times\left(\frac{\nabla\times\vec{M}}{k}\right)\right) + k\,\nabla\times\vec{M} = -\frac{1}{k}\nabla\times\left(\nabla\left(\nabla\cdot\vec{M}\right) - \nabla^2\vec{M}\right) + k\,\nabla\times\vec{M}$$
$$= \frac{1}{k}\nabla\times\left(\nabla^2\vec{M}\right) + k\,\nabla\times\vec{M} = \frac{1}{k}\nabla\times\left(-k^2\vec{M} + \nabla\times\left[c\left(\nabla^2\psi + k^2\psi\right)\right]\right) + k\,\nabla\times\vec{M}$$
$$= -k\,\nabla\times\left(\vec{M}\right) + k\,\nabla\times\vec{M} = 0$$

So $\nabla^2\vec{N} + k^2\vec{N} = 0$, then $-\nabla\times\left(\nabla\times\vec{N}\right) + k\,\nabla\times\vec{M} = 0$, so $\nabla\times\vec{N} = k\,\vec{M}$. What this means is that $\vec{M}$ and $\vec{N}$ have the same properties of an electromagnetic field; they satisfy the vector wave equation, are divergence-free, and the curl of one is proportional to the other and vice versa. So the vector field equations may be determined by solving the scalar wave equation. ψ is the scalar generating function of the *vector harmonics* $\vec{M}$ and $\vec{N}$, and the *guiding* or *pilot* vector is denoted by *c*.

The choice of appropriate generating function ψ is governed by the symmetry of the problem at hand. For scattering by a sphere (as is the interest in Mie theory), ψ should be functions that satisfy the wave equation in spherical coordinates. Choice of pilot vector *c* may not be obvious, but note if the radius vector *r* is used for *c*, then $\vec{M}$ is a solution to the vector wave equation in spherical coordinates.

So $\vec{M} = \nabla \times (r\psi)$, $\vec{N} = \frac{\nabla \times \vec{M}}{k} = \frac{\nabla \times \nabla \times (r\psi)}{k}$. Note $\vec{M}$ is tangential to *r*, so $r \cdot \vec{M} = 0$, i.e. $\vec{M}$ is everywhere tangential to any sphere $|r| = constant$.

The scalar wave equation in spherical coordinates:

$$\frac{1}{r^2}\frac{\partial}{\partial r}\left(r^2\frac{\partial \psi}{\partial r}\right)+\frac{1}{r^2\sin\theta}\frac{\partial}{\partial \theta}\left(\sin\theta\frac{\partial \psi}{\partial \theta}\right)+\frac{1}{r^2\sin\theta}\frac{\partial^2 \psi}{\partial \varphi^2}+k^2\psi = 0$$

In the typical fashion, assume separation of variables $\psi(r,\theta,\varphi) = R(r)\Theta(\theta)\Phi(\varphi)$ which results in:

$$\frac{d^2\Phi}{d\varphi}+m^2\Phi = 0$$

$$\frac{1}{\sin\theta}\frac{d}{d\theta}\left(\sin\theta\frac{d\Theta}{d\theta}\right)+\left[n(n+1)-\frac{m^2}{\sin^2\theta}\right]\Theta = 0$$

$$\frac{d}{dr}\left(r^2\frac{dR}{dr}\right)+\left[k^2r^2-n(n+1)\right]R = 0$$

Then $\Phi = \Phi_e+\Phi_o$, where $\Phi_e = \cos m\varphi$, $\Phi_0 = \sin m\varphi$, $\psi(\varphi) = \psi(\varphi+2\pi)$ and $m \in \mathbb{Z}$. Solutions to $\frac{1}{\sin\theta}\frac{d}{d\theta}\left(\sin\theta\frac{d\Theta}{d\theta}\right)+\left[n(n+1)-\frac{m^2}{\sin^2\theta}\right]\Theta = 0$ which are finite at the boundary conditions $\theta = 0, \pi$ are associated Legendre polynomials $P_n^m(\cos\theta)$.

Introduce variable $\rho = kr$ and define $Z = R\sqrt{\rho}$ then:

$\frac{d}{dr}\left(r^2\frac{dR}{dr}\right)+\left[k^2r^2-n(n+1)\right]R = 0$ becomes $\rho\frac{d}{d}\rho\left(\rho^2\frac{dZ}{d\rho}\right)+\left[\rho^2-(n+1/2)^2\right]Z = 0$

let $n+1/2 = \nu$ then the equation has Bessel function solutions J_ν and Y_ν , then in terms of *n* we have spherical Bessel functions:

$$j_n(\rho) = \sqrt{\frac{\pi}{2\rho}} J_{n+1/2}(\rho)$$

$$y_n(\rho) = \sqrt{\frac{\pi}{2\rho}} Y_{n+1/2}(\rho)$$

Any linear combination of the solutions are also a solution, particularly spherical Hankel functions:

$$h_n^{(1)}(\rho) = j_n(\rho) + j\, y_n(\rho)$$

$$h_n^{(2)} = j_n(\rho) - j\, y_n(\rho)$$

So the possible even and odd solutions to scalar function are:

$$\psi_{emn} = \cos m\varphi\, P_n^m(\cos\theta)\, z_n(k\,r)$$

$$\psi_{omn} = \sin m\varphi\, P_n^m(\cos\theta)\, z_n(k\,r)$$

where z_n stands for one of the four given spherical Bessel functions. Then the vector equations may be given by $\vec{M}_{emn} = \nabla\times(r\,\psi_{emn})$, $\vec{M}_{omn} = \nabla\times(r\,\psi_{omn})$,

$\vec{N}_{emn} = \dfrac{\nabla\times(\vec{M}_{emn})}{k}$, and $\vec{N}_{omn} = \dfrac{\nabla\times(\vec{M}_{omn})}{k}$.

Then substituting in the scalar wave equation we have:

$$\vec{M}_{emn} = \frac{-m}{\sin\theta}\sin m\varphi\, P_n^m(\cos\theta)\, z_n(\rho)\,\hat{a}_\theta - \cos m\varphi\,\frac{d}{d\theta}\left(P_n^m(\cos\theta)\right) z_n(\rho)\,\hat{a}_\varphi$$

$$\vec{M}_{omn} = \frac{m}{\sin\theta}\cos m\varphi\, P_n^m(\cos\theta)\, z_n(\rho)\,\hat{a}_\theta - \sin m\varphi\,\frac{d}{d\theta}\left(P_n^m(\cos\theta)\right) z_n(\rho)\,\hat{a}_\varphi$$

$$\vec{N}_{emn} = \frac{z_n(\rho)}{\rho}\cos m\varphi\, n(n+1) P_n^m(\cos\theta)\,\hat{a}_r + \cos m\varphi\,\frac{d}{d\theta}\left(P_n^m(\cos\theta)\right)\frac{1}{\rho}\frac{d}{d\rho}\left[\rho\, z_n(\rho)\right]\hat{a}_\theta$$
$$-m\sin m\varphi\,\frac{P_n^m(\cos\theta)}{\sin\theta}\frac{1}{\rho}\frac{d}{d\rho}\left[\rho\, z_n(\rho)\right]\hat{a}_\varphi$$

$$\vec{N}_{omn} = \frac{z_n(\rho)}{\rho}\sin m\varphi\, n(n+1)\, P_n^m(\cos\theta)\,\hat{a}_r + \sin m\varphi \frac{d}{d\theta}\left(P_n^m(\cos\theta)\right)\frac{1}{\rho}\frac{d}{d\rho}\left[\rho\, z_n(\rho)\right]\hat{a}_\theta$$
$$+ m\cos m\varphi \frac{P_n^m(\cos\theta)}{\sin\theta}\frac{1}{\rho}\frac{d}{d\rho}\left[\rho\, z_n(\rho)\right]\hat{a}_\varphi$$

Now any solution to the field equations can be expanded in an infinite series of these four equations.

We may now expand the incident plane wave for scattering evaluation. To do so, assume there is an *x* polarized impinging plane wave propagating in the positive *z*-direction:

$$\vec{E}_i = E_0 e^{jkr\cos\theta}\hat{a}_x$$

(note physicists time convention in this case, to match established analysis as done in the physics community, replace *j* in the results with *-j* if applying to problems with engineering time convention of e^{-jkz}), where:

$$\hat{a}_x = \sin\theta\cos\varphi\,\hat{a}_r + \cos\theta\cos\varphi\,\hat{a}_\theta - \sin\varphi\,\hat{a}_\varphi$$

and of course $r\cos\theta = z$. Suppose this wave is scattered by a sphere. For a solution, first expand the incident wave into spherical harmonics:

$$\vec{E}_i = \sum_{m=0}^{\infty}\sum_{n=0}^{\infty}\left(B_{emn}\vec{M}_{emn} + B_{omn}\vec{M}_{omn} + A_{emn}\vec{N}_{emn} + A_{omn}\vec{N}_{omn}\right)$$

Each $\vec{M}$ and $\vec{N}$ are all mutually orthogonal, so to find each coefficient proceed in the typical fashion of application of the inner product:

$$B_{emn} = \frac{\int_o^{2\pi}\int_0^{\pi}\vec{E}_i\cdot\vec{M}_{emn}\sin\theta\, d\theta\, d\varphi}{\int_o^{2\pi}\int_0^{\pi}\left|\vec{M}_{emn}\right|^2\sin\theta\, d\theta\, d\varphi} \qquad B_{omn} = \frac{\int_o^{2\pi}\int_0^{\pi}\vec{E}_i\cdot\vec{M}_{omn}\sin\theta\, d\theta\, d\varphi}{\int_o^{2\pi}\int_0^{\pi}\left|\vec{M}_{omn}\right|^2\sin\theta\, d\theta\, d\varphi}$$

$$A_{emn} = \frac{\int_o^{2\pi}\int_0^{\pi} \vec{E}_i \cdot \vec{N}_{emn} \sin\theta \, d\theta \, d\varphi}{\int_o^{2\pi}\int_0^{\pi} \left|\vec{N}_{emn}\right|^2 \sin\theta \, d\theta \, d\varphi} \qquad A_{omn} = \frac{\int_o^{2\pi}\int_0^{\pi} \vec{E}_i \cdot \vec{N}_{omn} \sin\theta \, d\theta \, d\varphi}{\int_o^{2\pi}\int_0^{\pi} \left|\vec{N}_{omn}\right|^2 \sin\theta \, d\theta \, d\varphi}$$

Orthogonality of sin and cosine means $B_{emn} = A_{omn} = 0$ for all *m* and *n*. Similarly all $B_{omn} = A_{emn} = 0$ for all $m \neq 1$ (to match the *x* directed unit vector in spherical coordinates attached to the impinging wave). We require finite fields at the origin, hence solutions with y_n are rejected for the incident field. Let superscript (1) denote vector harmonics which are solely dependent on j_n, then the expansion of incident field $\vec{E}_i$ is given by:

$$\vec{E}_i = \sum_{n=1}^{\infty} \left(B_{o1n} \vec{M}_{o1n}^{(1)} + A_{e1n} \vec{N}_{e1n}^{(1)} \right)$$

Solving $B_{o1n} = \frac{\int_o^{2\pi}\int_0^{\pi} \vec{E}_i \cdot \vec{M}_{o1n} \sin\theta \, d\theta \, d\varphi}{\int_o^{2\pi}\int_0^{\pi} \left|\vec{M}_{o1n}\right|^2 \sin\theta \, d\theta \, d\varphi}$ by application of $P_n^1 = -\frac{d P_n}{d\theta}$ and

Gegenbauer's generalization of Poisson's integral $j_n(\rho) = \frac{j^{-n}}{2} \int_0^{\pi} e^{j\rho\cos\theta} P_n \sin\theta \, d\theta$ gives:

$$B_{o1n} = j^n E_0 \frac{2n+1}{n(n+1)}$$

Integration by parts and significant rearranging gives:

$$A_{e1n} = -j E_0 j^n \frac{2n+1}{n(n+1)}$$

So the impinging incident wave may be represented:

$$\vec{E}_i = E_0 \sum_{n=1}^{\infty} j^n \frac{2n+1}{n(n+1)} \left(\vec{M}_{o1n}^{(1)} - j \vec{N}_{e1n}^{(1)} \right)$$

Now the internal and scattered fields may be accounted for. The dependence of the magnetic field on the electric gives:

$$\vec{H}_i = -\frac{j}{\omega \mu} E_0 \nabla \times \vec{E}_i = -\frac{j}{\omega \mu} E_0 \sum_{n=1}^{\infty} \frac{2n+1}{n(n+1)} \left(\nabla \times \vec{M}_{o1n}^{(1)} - j \nabla \times \vec{N}_{e1n}^{(1)} \right)$$

$$= -\frac{j}{\omega \mu} E_0 \sum_{n=1}^{\infty} \frac{2n+1}{n(n+1)} \left(k \vec{N}_{o1n}^{(1)} - j k \vec{M}_{e1n}^{(1)} \right) = \frac{k}{\omega \mu} E_0 \sum_{n=1}^{\infty} j^n \frac{2n+1}{n(n+1)} \left(\vec{M}_{e1n}^{(1)} + j \vec{N}_{o1n}^{(1)} \right)$$

and we have:

$$\vec{H}_i = = -\frac{k}{\omega \mu} E_0 \sum_{n=1}^{\infty} j^n \frac{2n+1}{n(n+1)} \left(\vec{M}_{e1n}^{(1)} + j \vec{N}_{o1n}^{(1)} \right)$$

The scattered fields $\left(\vec{E}_s, \vec{H}_s \right)$ and the fields inside the sphere $\left(\vec{E}_1, \vec{H}_1 \right)$ may also be expanded into spherical harmonics of the same form. At the boundary of the sphere the tangential components of the fields must be continuous, so we have boundary conditions:

$$\left(\vec{E}_i + \vec{E}_s - \vec{E}_1 \right) \times \hat{a}_r = \left(\vec{H}_i + \vec{H}_s - \vec{H}_1 \right) \times \hat{a}_r = 0$$

The fields inside the sphere must not be a function of y_n, otherwise the fields at the origin would not be finite. j_n is represented by $j_n(k_1 r)$, where k_1 is the wave number of the sphere. So the expansion of the interior fields are:

$$\vec{E}_1 = E_0 \sum_{n=1}^{\infty} j^n \frac{2n+1}{n(n+1)} \left(c_n \vec{M}_{o1n}^{(1)} - j d_n \vec{N}_{e1n}^{(1)} \right)$$

$$\vec{H}_1 = = -\frac{k_1}{\omega \mu_1} E_0 \sum_{n=1}^{\infty} j^n \frac{2n+1}{n(n+1)} \left(d_n \vec{M}_{e1n}^{(1)} + j c_n \vec{N}_{o1n}^{(1)} \right)$$

Outside the sphere, j_n and y_n are both finite and hence permitted solutions. It is

convenient to combine them into a Hankel function representation. In physicists time convention, a Hankel function of the first kind corresponds to an outgoing traveling wave, so the Bessel function portion of the solution will be $h_n^{(1)}$. Note that if we take the complex conjugate to get the engineering time convention, the Hankel function of the first kind transforms to a Hankel function of the second time. Let superscript (3) denote the Hankel function outward traveling wave solution as described for physicists time convention, then the expansion for the scattered field is given by:

$$\vec{E}_s = E_0 \sum_{n=1}^{\infty} j^n \frac{2n+1}{n(n+1)} \left(-b_n \vec{M}_{o1n}^{(3)} + j a_n \vec{N}_{e1n}^{(3)} \right)$$

$$\vec{H}_s = = \frac{k_1}{\omega \mu_1} E_0 \sum_{n=1}^{\infty} j^n \frac{2n+1}{n(n+1)} \left(a_n \vec{M}_{e1n}^{(1)} + j b_n \vec{N}_{o1n}^{(1)} \right)$$

(note sign in front of constants is chosen for convenience later)

Now we are able to determine scattering coefficients. To do so, apply the tangential component continuity at the surface boundary condition as done earlier:

$$E_{i\theta} + E_{s\theta} = E_{1\theta} \qquad E_{i\varphi} + E_{s\varphi} = E_{1\varphi} \qquad H_{i\theta} + H_{s\theta} = H_{1\theta} \qquad H_{i\varphi} + H_{s\varphi} = H_{1\varphi} \quad \text{at} \quad r = a$$

which results in four linear equations in the four expansion coefficients:

$$j_n(m\chi) c_n + h_n^{(1)}(\chi) b_n = j_n(\chi)$$

$$\mu \left[m\chi j_n(m\chi) \right]' c_n + \mu_1 \left[\chi h_n^{(1)}(\chi) \right]' b_n = \mu_1 \left[\chi j_n(\chi) \right]'$$

$$\mu m j_n(m\chi) d_n + \mu_1 h_n^{(1)}(\chi) a_n = \mu_1 j_n(\chi)$$

$$\left[m\chi j_n(m\chi) \right]' d_n + m \left[\chi h_n^{(1)}(\chi) \right]' a_n = m \left[\chi j_n(\chi) \right]'$$

Where prime indicates differentiation with respect to the argument in the parentheses,

$\chi = k\,a = \frac{2\pi N a}{\lambda}$ is the size parameter, N is the index of refractive index of the medium, $m = \frac{k_1}{k} = \frac{N_1}{N}$ is the relative refractive index where N_1 is the refractive index of the spherical particle.

Then solving the linear system of equations gives expansion coefficients inside the particle:

$$c_n = \frac{\mu_1 j_n(\chi)[\chi h_n^{(1)}(\chi)]' - \mu_1 h_n^{(1)}(\chi)[\chi j_n(\chi)]'}{\mu_1 j_n(m\chi)[\chi h_n^{(1)}(\chi)]' - \mu h_n^{(1)}(\chi)[m\chi j_n(m\chi)]'}$$

$$d_n = \frac{\mu_1 m j_n(\chi)[\chi h_n^{(1)}(\chi)]' - \mu_1 m h_n^{(1)}(\chi)[\chi j_n(\chi)]'}{\mu m^2 j_n(m\chi)[\chi h_n^{(1)}(\chi)]' - \mu_1 h_n^{(1)}(\chi)[m\chi j_n(m\chi)]'}$$

And outside particle:

$$a_n = \frac{\mu m^2 j_n(m\chi)[\chi j_n(\chi)]' - \mu_1 j_n(\chi)[m\chi j_n(m\chi)]'}{\mu m^2 j_n(m\chi)[\chi h_n^{(1)}(\chi)]' - \mu_1 h_n^{(1)}(\chi)[m\chi j_n(m\chi)]'}$$

$$b_n = \frac{\mu_1 j_n(m\chi)[\chi j_n(\chi)]' - \mu j_n(\chi)[m\chi j_n(m\chi)]'}{\mu_1 j_n(m\chi)[\chi h_n^{(1)}(\chi)]' - \mu h_n^{(1)}(\chi)[m\chi j_n(m\chi)]'}$$

So now we can express the expansion completely. These are the most general expressions for the coefficients.

Depending on the wavelength of illuminating light, a sphere may be electrically small, an approximations based on this assumption may prove useful. Note that if the denominator of either a_n or b_n is *small*, then the term multiplied by the coefficient is large, that is the normal mode associated with a given coefficient is dominant. We would

like to see if there is a lowest order mode supported by such a particle. If a_n is dominant, then its denominator is small and:

$$\frac{\left[\chi h_n^{(1)}(\chi)\right]'}{h_n^{(1)}(\chi)} = \frac{\mu_1\left[m\chi j_n(m\chi)\right]'}{\mu m^2 j_n(m\chi)}$$

Recall the prime means derivative with respect to the argument in parentheses, so applying the chain rule we get:

$$\left[\chi h_n^{(1)}(\chi)\right]' = [\chi]' h_n^{(1)}(\chi) + \chi\left[h_n^{(1)}(\chi)\right]' = h_n^{(1)}(\chi) + \chi\left[h_n^{(1)}(\chi)\right]'$$

and for spherical Bessel functions we have recurrence relations:

$$(2n+1)\frac{d}{dz} f_n(z) = n f_{n-1}(z) - (n+1) f_{n+1}(z)$$

$$\left[f_n(z)\right]' = \frac{1}{2n+1}\left(n f_{n-1}(z) - (n+1) f_{n+1}(z)\right)$$

$$\frac{n}{z} f_n(z) - \frac{d}{dz} f_n(z) = f_{n+1}(z)$$

$$\left[f_n(z)\right]' = \frac{n}{z} f_n(z) - f_{n+1}(z) \quad [33]$$

$$\left[h_n^{(1)}(\chi)\right]' = \frac{n}{\chi} h_n^{(1)}(\chi) - h_{n+1}^{(1)}(\chi)$$

$$\left[\chi h_n^{(1)}(\chi)\right]' = h_n^{(1)}(\chi) + \chi\left[\frac{n}{\chi} h_n^{(1)}(\chi) - h_{n+1}^{(1)}(\chi)\right] = h_n^{(1)}(\chi) + n h_n^{(1)}(\chi) - \chi h_{n+1}^{(1)}(\chi)$$
$$= (n+1) h_n^{(1)}(\chi) - \chi h_{n+1}^{(1)}(\chi)$$

Similarly:

$$\left[m\chi j_n(m\chi)\right]' = (n+1) j_n(m\chi) - m\chi j_{n+1}(m\chi)$$

also, ultimately we are interested in gold or silver spheres, so $\frac{\mu_1}{\mu} = 1$, and we have:

$$\frac{\left[\chi h_n^{(1)}(\chi)\right]'}{h_n^{(1)}(\chi)} = \frac{\left[m\chi j_n(m\chi)\right]'}{m^2 j_n(m\chi)}$$

and substituting our expression for the derivatives:

$$\frac{(n+1)h_n^{(1)}(\chi)-\chi h_{n+1}^{(1)}(\chi)}{h_n^{(1)}(\chi)} = \frac{(n+1)j_n(m\chi)-m\chi j_{n+1}(m\chi)}{m^2 j_n(m\chi)}$$

$$(n+1)-\frac{\chi h_{n+1}^{(1)}(\chi)}{h_n^{(1)}(\chi)} = \frac{(n+1)}{m^2}-\frac{\chi j_{n+1}(m\chi)}{m j_n(m\chi)}$$

Similarly, if b_n is dominant, then:

$$\frac{\left[\chi h_n^{(1)}(\chi)\right]'}{h_n^{(1)}(\chi)} = \frac{\mu\left[m\chi j_n(m\chi)\right]'}{\mu_1 j_n(m\chi)}$$

which is similar to the case for a_n , except note the missing m^{-2} term on the right side. Then again assuming nonmagnetic material:

$$\frac{\left[\chi h_n^{(1)}(\chi)\right]'}{h_n^{(1)}(\chi)} = \frac{\left[m\chi j_n(m\chi)\right]'}{j_n(m\chi)}$$

$$(n+1)-\frac{\chi h_{n+1}^{(1)}(\chi)}{h_n^{(1)}(\chi)} = (n+1)-\frac{m\chi j_{n+1}(m\chi)}{j_n(m\chi)}$$

$$\frac{h_{n+1}^{(1)}(\chi)}{h_n^{(1)}(\chi)} = \frac{m j_{n+1}(m\chi)}{j_n(m\chi)}$$

Now consider the case for a very small sphere with respect to the wavelength of the impinging field. Expanding the spherical Bessel functions gives [33]:

$$j_n(z) = \frac{z^n}{1\cdot 3\cdot 5\ldots(2n+1)}\left[1-\frac{\frac{1}{2}z^2}{1!(2n+3)}+\frac{\left(\frac{1}{2}z^2\right)^2}{2!(2n+3)(2n+5)}-\ldots\right]$$

$$y_n(z) = -\frac{1\cdot 3\cdot 5\ldots(2n-1)}{z^{n+1}}\left[1-\frac{\frac{1}{2}z^2}{1!(1-2n)}+\frac{\left(\frac{1}{2}z^2\right)^2}{2!(1-2n)(3-2n)}-\ldots\right]$$

and recall $h_n^{(1)}(z) = j_n(z) + j\,y_n(z)$. Limiting values as $z \to 0$ leads to:

$$z^{-n} j_n(z) \to \frac{1}{1\cdot 3\cdot 5\ldots(2n+1)}$$

$$z^{n+1} y_n(z) \to -1\cdot 3\cdot 5\ldots(2n-1)$$

so $h_n^{(1)}(z) \to j\,y_n(z) = -j\frac{1\cdot 3\cdot 5\ldots(2n-1)}{z^{n+1}}$ since $|y_n(z)| \gg |j_n(z)|$ when $z \to 0$.

So for b_n $\frac{h_{n+1}^{(1)}(\chi)}{h_n^{(1)}(\chi)} = (2n-1)\chi^{-1}$ and $\frac{j_{n+1}(m\chi)}{j_n(m\chi)} = \frac{m\chi}{2n+1}$ as $\chi \to 0$ so

$\frac{h_{n+1}^{(1)}(\chi)}{h_n^{(1)}(\chi)} = \frac{m\,j_{n+1}(m\chi)}{j_n(m\chi)}$ which has no solution for $\chi \to 0$. So for electrically small spheres, the supported mode(s) must be completely represented by the a_n terms. For these:

$$(n+1) - \frac{\chi h_{n+1}^{(1)}(\chi)}{h_n^{(1)}(\chi)} = \frac{(n+1)}{m^2} - \frac{\chi\, j_{n+1}(m\chi)}{m\, j_n(m\chi)}$$

$$(n+1) - (2(n+1)-1)\chi\chi^{-1} = \frac{(n+1)}{m^2} - \frac{\chi^2}{2(n+1)+1}$$

$$-n = \frac{(n+1)}{m^2} \quad \text{so} \quad m^2 = -\frac{n+1}{n} \quad \text{(for electrically small spheres)}$$

m is the relative index of refraction. Since the permittivity is a function of frequency, so too must the index $m = m(\omega)$. If we're near the frequency in which the lowest order

term is dominant, the other terms will be comparatively small and may be ignored. Also in particular note for the lowest order term $m^2 = \epsilon_r = -2$.

Hence for a sufficiently small sphere, the N_{e11} mode is dominant. Recall:

$$N_{emn} = \frac{z_n(\rho)}{\rho}\cos m\varphi\, n(n+1) P_n^m(\cos\theta)\hat{a}_r + \cos m\varphi \frac{d}{d\theta}\left(P_n^m(\cos\theta)\right)\frac{1}{\rho}\frac{d}{d\rho}\left[\rho\, z_n(\rho)\right]\hat{a}_\theta$$
$$-m\sin m\varphi \frac{P_n^m(\cos\theta)}{\sin\theta}\frac{1}{\rho}\frac{d}{d\rho}\left[\rho\, z_n(\rho)\right]\hat{a}_\varphi$$

$$N_{e11} = \frac{h_1^{(1)}(\rho)}{\rho} 2\cos\varphi P_1^1(\cos\theta)\hat{a}_r + \cos\varphi \frac{d}{d\theta}\left(P_1^1(\cos\theta)\right)\frac{1}{\rho}\frac{d}{d\rho}\left[\rho\, h_1^{(1)}(\rho)\right]\hat{a}_\theta$$
$$-\sin\varphi \frac{P_1^1(\cos\theta)}{\sin\theta}\frac{1}{\rho}\frac{d}{d\rho}\left[\rho\, h_1^{(1)}(\rho)\right]\hat{a}_\varphi$$

Recall: $P_n^m(x) = (-1)^m (1-x^2)^{m/2}\frac{d^m}{dx^m}\left(P_n(x)\right)$ [33], so

$$P_1^1(\cos\theta) = -(1-\cos^2\theta)^{1/2}\frac{d}{dx}\left(P_1(x)\right) = -(\sin^2\theta)^{1/2}\frac{d}{dx}(x) = -\sin\theta$$

and:

$$N_{e11} = -\frac{h_1^{(1)}(\rho)}{\rho} 2\cos\varphi\sin\theta\hat{a}_r - \cos\varphi\frac{d}{d\theta}(\sin\theta)\frac{1}{\rho}\frac{d}{d\rho}\left[\rho h_1^{(1)}(\rho)\right]\hat{a}_\theta$$
$$+\sin\varphi\frac{1}{\rho}\frac{d}{d\rho}\left[\rho\, h_1^{(1)}(\rho)\right]\hat{a}_\varphi$$

To evaluate how reasonable our results are, lets consider their limits. First, in the far-field, the infinitesimal sphere supporting the N_{e11} mode should appear as a dipole. Note that in the far field [32]:

$$h_n^{(1)}(p) \approx \frac{(-i)^{n+1}e^{i\rho}}{\rho} \quad \text{and} \quad \frac{d}{d\rho}\left(h_n^{(1)}(\rho)\right) \approx \frac{(-i)^n e^{i\rho}}{\rho}$$

so:

$$N_{e1n} = -2\frac{(-i)^{n+1}e^{i\rho}}{\rho^2}\cos\varphi\sin\theta\,\hat{a}_r - \cos\varphi\cos\theta\frac{1}{\rho}\left[\frac{(-i)^{n+1}e^{i\rho}}{\rho} + (-i)^n e^{i\rho}\right]\hat{a}_\theta$$
$$+\sin\varphi\frac{1}{\rho}\left[\frac{(-i)^{n+1}e^{i\rho}}{\rho} + (-i)^n e^{i\rho}\right]\hat{a}_\varphi$$

and the first term:

$$N_{e11} = 2\frac{e^{i\rho}}{\rho^2}\cos\varphi\sin\theta\,\hat{a}_r + \cos\varphi\cos\theta\frac{1}{\rho}\left[\frac{e^{i\rho}}{\rho} + i\,e^{i\rho}\right]\hat{a}_\theta - \sin\varphi\frac{1}{\rho}\left[\frac{e^{i\rho}}{\rho} + i\,e^{i\rho}\right]\hat{a}_\varphi$$

Then in the far field:

$E \propto \cos\varphi\cos\theta\frac{e^{ikr}}{r}\hat{a}_\theta - \sin\varphi\frac{e^{ikr}}{r}\hat{a}_\varphi$ which, as expected, is the same field as an infinitesimal x-directed dipole. (Recall $\rho = kr$ and that we are using physicists time convention here, resulting in the complex conjugate of the usual engineering result for the fields of a dipole). In the near-field (ρ small so sphere looks like a sphere, not a dipole) for an electrically small sphere (χ small, so the impinging field doesn't vary across the sphere) we expect the fields to be that of an electrostatic sphere.

In the near-field for electrically small sphere (quasi-static approximation):

$$h_1^{(1)}(\rho) = j_n(\rho) + i\,y_n(\rho)$$

as $\rho \to 0$

$$\rho^{-n} j_n(\rho) \to \frac{1}{1\cdot 3\cdot 5\ldots(2n+1)}$$

and:

$$\rho^{n+1} y_n(\rho) \to -1\cdot 3\cdot 5\ldots(2n-1)$$

so:

$$h_1^{(1)}(\rho) \rightarrow i\, y_1(\rho)\rho^{-2} \rightarrow -i\rho^{-2} \quad \text{for small} \quad \rho$$

Then:

$$N_{e11} \rightarrow \frac{j}{\rho^3} 2\cos\varphi\sin\theta\,\hat{a}_r - \cos\varphi\cos\theta\frac{1}{\rho}\frac{d}{d\rho}\left[\rho\left(\frac{-j}{\rho^2}\right)\right]\hat{a}_\theta + \sin\varphi\frac{1}{\rho}\frac{d}{d\rho}\left[\rho\left(\frac{-j}{\rho^2}\right)\right]\hat{a}_\varphi$$

$$= \frac{j\,2\cos\varphi\sin\theta}{\rho^3}\hat{a}_r - \frac{j\cos\varphi\cos\theta}{\rho^3}\hat{a}_\theta + \frac{j\sin\varphi}{\rho^3}\hat{a}_\varphi$$

Which is the exact functional form of the fields of a dielectric sphere.

So our derivation has the right form to properly account for already known limits, supporting our confidence in its accuracy.

Now to find the exact expression for the near-field (IE take into account the coefficient and make sure it is generating the appropriate scaling factor). Recall

$$\vec{E}_s = E_0\sum_{n=1}^{\infty} j^n \frac{2n+1}{n(n+1)}\left(-b_n\vec{M}_{o1n}^{(3)} + j\,a_n\vec{N}_{e1n}^{(3)}\right)$$

So for the N_{e11} mode we have $\vec{E}_s = -E_0\frac{3}{2}a_1\vec{N}_{e11}$, where:

$$a_1 = \frac{\mu m^2 j_1(m\chi)[\chi j_1(\chi)]' - \mu_1 j_1(\chi)[m\chi j_1(m\chi)]'}{\mu m^2 j_1(m\chi)[\chi h_1^{(1)}(\chi)]' - \mu_1 h_1^{(1)}(\chi)[m\chi j_1(m\chi)]'}$$

where *m* is the relative index of refraction, $\chi = ka$.

recall the sphere is electrically small for the electrostatic approximation, so for small

argument $\rho^{-n} j_n(\rho) \rightarrow \frac{1}{1\cdot 3\cdot 5\ldots(2n+1)}$, which means $j_1(\rho)\rightarrow\frac{\rho}{3}$, so breaking a_1

into four main pieces, we have for the first piece:

$$\mu m^2 j_1(m\chi)[\chi j_1(\chi)]' \approx \mu m^3 \frac{\chi}{3}\left[\frac{\chi^2}{3}\right]' = \frac{2}{9}\mu m^3 \chi^2$$

then the second piece:

$$\mu_1 j_1(\chi)[m\chi j_1(m\chi)]' \approx \frac{2}{9}\mu_1 m\chi^2$$

recall $h_1^{(1)}(\rho) \to i\, y_1(\rho)\rho^{-2} \to -i\rho^{-2}$ for small ρ so the third piece:

$$\mu m^2 j_1(m\chi)[\chi h_1^{(1)}(\chi)]' \approx \mu m^3 \chi\left[-i\chi^{-1}\right]' = i\mu m^3 (3\chi)^{-1}$$

fourth piece:

$$\mu_1 h_1^{(1)}(\chi)[m\chi j_1(m\chi)]' \approx \mu_1(-i\chi^{-2})[(m\chi)^2]' = -i2\mu_1 m(3\chi)^{-1}$$

recall for N_{e11} it must be the case that $m^2 = -2$ so $m = i\sqrt{2}$ and $\epsilon_r = -2$

also recall $m = \frac{k_1}{k}$ and $\chi = ka$.

So putting all 4 pieces back together and we get:

$$a_1 = \frac{\mu m^2 j_1(m\chi)[\chi j_1(\chi)]' - \mu_1 j_1(\chi)[m\chi j_1(m\chi)]'}{\mu m^2 j_1(m\chi)[\chi h_1^{(1)}(\chi)]' - \mu_1 h_1^{(1)}(\chi)[m\chi j_1(m\chi)]'}$$

$$= \frac{\frac{2}{9}\mu m^3 \chi^2 - \frac{2}{9}\mu_1 m\chi^2}{i\mu m^3 (3\chi)^{-1} + i2\mu_1 m(3\chi)^{-1}}$$

$$= -\frac{2}{3} i\chi^3 \frac{\mu m^2 - \mu_1}{\mu m^2 + 2\mu_1}$$

Assuming permittivity of the medium is that of free space, then $\mu = \mu_1$ and

$$= -\frac{2}{3} i\chi^3 \frac{m^2 - 1}{m^2 + 2}$$

substituting $m^2 = \epsilon_r$ (note this is essentially assuming the sphere has relative

permittivity ϵ_r and is suspended in free-space. If not in free space, we would need to replace with the permittivity of the sphere relative to the medium it is suspended in, not free space):

$$= -\frac{2}{3} i \chi^3 \frac{\epsilon_r - 1}{\epsilon_r + 2} = -\frac{2}{3} i (k a)^3 \frac{\epsilon_r - 1}{\epsilon_r + 2}$$

so:

$$a_1 = -\frac{2}{3} i (k a)^3 \frac{\epsilon_r - 1}{\epsilon_r + 2}$$

$$\vec{E}_s = -E_0 \frac{3}{2} a_1 \vec{N}_{e11}$$

$$\vec{N}_{e11} = \frac{j 2 \cos\varphi \sin\theta}{\rho^3} \hat{a}_r - \frac{j \cos\varphi \cos\theta}{\rho^3} \hat{a}_\theta + \frac{j \sin\varphi}{\rho^3} \hat{a}_\varphi$$

$$\rho = kr$$

$$\vec{E}_s = -E_0 \frac{3}{2} \left(-\frac{2}{3} i (k a)^3 \frac{\epsilon_r - 1}{\epsilon_r + 2} \right) \vec{N}_{e11}$$

$$\vec{E}_s = \frac{E_0 a^3}{r^3} \frac{\epsilon_r - 1}{\epsilon_r + 2} \left(2 \cos\varphi \sin\theta \hat{a}_r - \cos\varphi \cos\theta \hat{a}_\theta + \sin\varphi \hat{a}_\varphi \right)$$

So in the electrostatic limit (as the sphere becomes electrically small), we match the fields of an electrostatic polarized sphere.

To sufficiently model radiation damping, the expansion for the coefficient may be truncated to just a few terms. To do so, take the expression for a_1

$$a_1 = \frac{\mu m^2 j_1(m\chi)[\chi j_1(\chi)]' - \mu_1 j_1(\chi)[m\chi j_1(m\chi)]'}{\mu m^2 j_1(m\chi)[\chi h_1^{(1)}(\chi)]' - \mu_1 h_1^{(1)}(\chi)[m\chi j_1(m\chi)]'}$$

and recast in terms of Riccati-Bessel functions, where $\psi_n(\rho) = \rho\, j_n(\rho)$, and $\xi_n(\rho) = \rho\, h_n^{(1)}(\rho)$, then:

$$a_1 = \frac{m\psi_1(m\chi)\psi_1'(\chi) - \psi_1(\chi)\psi_1'(m\chi)}{m\psi_1(m\chi)\xi_1'(\chi) - \xi_1(\chi)\psi_1'(m\chi)}$$

$$j_n(z) = \frac{z^n}{1\cdot 3\cdot 5\ldots(2n+1)}\left[1 - \frac{\frac{1}{2}z^2}{1!(2n+3)} + \frac{\left(\frac{1}{2}z^2\right)^2}{2!(2n+3)(2n+5)} - \ldots\right]$$

$$y_n(z) = -\frac{1\cdot 3\cdot 5\ldots(2n-1)}{z^{n+1}}\left[1 - \frac{\frac{1}{2}z^2}{1!(1-2n)} + \frac{\left(\frac{1}{2}z^2\right)^2}{2!(1-2n)(3-2n)} - \ldots\right] \quad [33]$$

so expansion of each up to the first two terms:

$$\psi_1(z) = z\, j_1(z) \approx \frac{z^2}{3}\left[1 - \frac{z^2}{10}\right] = \frac{z^2}{3} - \frac{z^4}{30}$$

$$\xi_1(z) = z\, j_1(z) + iz\, y_1(z) \approx \frac{z^2}{3} - \frac{z^4}{30} - \frac{i}{z}\left[1 + \frac{z^2}{2}\right] = -\frac{i}{z} - i\frac{z}{2} + \frac{z^2}{3} - \frac{z^4}{30} \approx -\frac{i}{z} - i\frac{z}{2} + \frac{z^2}{3}$$

$$\psi_1'(z) \approx \frac{2z}{3} - \frac{2z^3}{15} \qquad \xi_1'(z) \approx \frac{i}{z^2} - \frac{i}{2} + \frac{2z}{3}$$

$$a_1 = \frac{m\left[\frac{(m\chi)^2}{3} - \frac{(m\chi)^4}{30}\right]\left[\frac{2\chi}{3} - \frac{2\chi^3}{15}\right] - \left[\frac{\chi^2}{3} - \frac{\chi^4}{30}\right]\left[\frac{(m\chi)^2}{3} - \frac{(m\chi)^4}{30}\right]}{m\left[\frac{(m\chi)^2}{3} - \frac{(m\chi)^4}{30}\right]\left[\frac{i}{\chi^2} - \frac{i}{2} + \frac{2\chi}{3}\right] - \left[\frac{-i}{\chi} - i\frac{\chi}{2} + \frac{\chi^2}{3}\right]\left[\frac{(m\chi)^2}{3} - \frac{(m\chi)^4}{30}\right]}$$

Since we are only interested in the dominant terms of a_1 , we can derive a simplified expression for them by taking the Taylor expansion of a_1 :

$$a_1 = -\frac{i2\chi^3}{3}\frac{m^2-1}{m^2+2} - \frac{i2\chi^5}{5}\frac{(m^2-2)(m^2-1)}{(m^2+2)^2} + \frac{4\chi^6}{9}\left(\frac{m^2-1}{m^2+2}\right)^2 + O(x^7)$$

Then the electric field:

$$\vec{E}_s = -E_0 \frac{3}{2} a_1 \vec{N}_{e11}$$

$$\vec{N}_{e11} = \frac{j2\cos\varphi\sin\theta}{\rho^3}\hat{a}_r - \frac{j\cos\varphi\cos\theta}{\rho^3}\hat{a}_\theta + \frac{j\sin\varphi}{\rho^3}\hat{a}_\varphi \quad \text{(far-field)}$$

$$\rho = kr \qquad \chi = ka$$

$$\vec{E}_s = -E_0 \frac{3}{2}\left(\frac{-i2\chi^3}{3}\frac{m^2-1}{m^2+2} - \frac{i2\chi^5}{5}\frac{(m^2-2)(m^2-1)}{(m^2+2)^2} + \frac{4\chi^6}{9}\left(\frac{m^2-1}{m^2+2}\right)^2 \right)$$
$$\cdot \left(\frac{j2\cos\varphi\sin\theta}{\rho^3}\hat{a}_r - \frac{j\cos\varphi\cos\theta}{\rho^3}\hat{a}_\theta + \frac{j\sin\varphi}{\rho^3}\hat{a}_\varphi \right)$$

$$= E_0 \frac{a^3}{r^3}\left(i\frac{m^2-1}{m^2+2} + \frac{i3k^2a^2}{5}\frac{(m^2-2)(m^2-1)}{(m^2+2)^2} - \frac{2k^3a^3}{3}\left(\frac{m^2-1}{m^2+2}\right)^2 \right)$$
$$\cdot \left(j2\cos\varphi\sin\theta\,\hat{a}_r - j\cos\varphi\cos\theta\,\hat{a}_\theta + j\sin\varphi\,\hat{a}_\varphi \right)$$

Notice the first term in a_1 corresponds to the quasi-static polarizability, the second term is a dynamic depolarization term, and the third term is a radiation damping term [34].

There are other author's who have done similar calculations as Bohren and Huffman, so it would be wise to cross reference results to confirm the derivation. Confirming Van de Holst's Approximation [35], it is given:

$$a_n = \frac{1}{2}\left(1 - e^{2i\alpha_n}\right)$$

given $n = 1$ $\alpha_1 = isx^3\left(1 + tx^2 - isx^3\right)$ $t = \frac{3}{5}\frac{m^2-2}{m^2+2}$ $u = \frac{1}{30}\left(m^2+2\right)$

$w = \frac{1}{10}\frac{m^2+2}{2m^2+3}$ $e^{2i\alpha_1} = \sum_{n=0}^{\infty}\frac{(i2\alpha_1)^n}{n!} = 1 + i2\alpha_1 + \frac{(i2\alpha_1)^2}{2} + \ldots$, and truncating to the

second term gives $e^{2i\alpha_1} = 1+i2\alpha_1$, so:

$$a_1 = \frac{1}{2}(1-1-i2\alpha_1) = i\alpha_1$$

This matches Van de Hulst's use of the angle α_1 and his stated relation of it to a_1 , confirming Bohren and Huffman's approach.

While the electrically small sphere approximation may be valid in some cases, it may be too imprecise in other cases. Additional Terms from the Mie Series may be used to generate a better approximation, without having to calculate the entire series.

If we do not assume the a_1 term is completely dominant, we may approximate other a_n and b_n terms using Taylor expansion in a similar manner. Doing so gives:

$$b_1 = -\frac{i\chi^5}{45}(m^2-1)+O(\chi^7)$$

$$a_2 = -\frac{i\chi^5}{15}\frac{m^2-1}{2m^2}+O(\chi^7)$$

$$b_2 = O(\chi^7)$$

So to the 5th order in χ all that is needed are three Mie series coefficients, a_1, a_2, b_1 .

The Spherical Harmonics for Three Dominant Mie Series Coefficients may be simplified. To do so, note that as previously mentioned, for the N_{e11} vector spherical harmonic we have $h_1^{(1)}(\rho) = j_n(\rho)+i\,y_n(\rho)$ and as $\rho \to 0$,

$\rho^{-n} j_n(\rho) \to \frac{1}{1\cdot 3\cdot 5\ldots(2n+1)}$, and $\rho^{n+1} y_n(\rho) \to -1\cdot 3\cdot 5\ldots(2n-1)$, so

$h_1^{(1)}(\rho) \to i\,y_1(\rho)\rho^{-2} \to -i\rho^{-2}$ for small ρ .

Then:

$$N_{e11} \rightarrow \frac{j}{\rho^3} 2\cos\varphi \sin\theta \hat{a}_r - \cos\varphi\cos\theta \frac{1}{\rho}\frac{d}{d\rho}\left[\rho\left(\frac{-j}{\rho^2}\right)\right]\hat{a}_\theta + \sin\varphi \frac{1}{\rho}\frac{d}{d\rho}\left[\rho\left(\frac{-j}{\rho^2}\right)\right]\hat{a}_\varphi$$

$$= \frac{j\,2\cos\varphi\sin\theta}{\rho^3}\hat{a}_r - \frac{j\cos\varphi\cos\theta}{\rho^3}\hat{a}_\theta + \frac{j\sin\varphi}{\rho^3}\hat{a}_\varphi$$

and in a similar manner, for N_{e12} :

$$N_{e12} = \frac{h_2^{(1)}(\rho)}{\rho}\cos\varphi\, 6\, P_2^1(\cos\theta)\hat{a}_r + \cos\varphi \frac{d}{d\theta}\left(P_2^1(\cos\theta)\right)\frac{1}{\rho}\frac{d}{d\rho}\left[\rho\, h_2^{(1)}(\rho)\right]\hat{a}_\theta$$
$$-\sin\varphi \frac{P_2^1(\cos\theta)}{\sin\theta}\frac{1}{\rho}\frac{d}{d\rho}\left[\rho\, h_2^{(1)}(\rho)\right]\hat{a}_\varphi$$

Recall $P_n^m(x) = (-1)^m(1-x^2)^{m/2}\frac{d^m}{dx^m}\left(P_n(x)\right)$ [33] so:

$$P_2^1(\cos\theta) = -(1-\cos^2\theta)^{1/2}\frac{d}{dx}\left(P_2(x)\right) = -(\sin^2\theta)^{1/2}\frac{d}{dx}\left(\frac{1}{2}\left(3x^2-1\right)\right)$$
$$= -\sin\theta(3\cos\theta) = -\frac{3}{2}\sin(2\theta)$$

and as $\rho \rightarrow 0$, $\rho^{-n} j_n(\rho) \rightarrow \frac{1}{1\cdot 3\cdot 5\ldots(2n+1)}$, and $\rho^{n+1} y_n(\rho) \rightarrow -1\cdot 3\cdot 5\ldots(2n-1)$,

so $h_2^{(1)}(\rho) \rightarrow i\, y_2(\rho)\rho^{-3} \rightarrow -i3\rho^{-3}$ for small ρ .

Then:

$$N_{e12} = \frac{-i3\rho^{-3}}{\rho}\cos\varphi\, 6\left(-\frac{3}{2}\sin(2\theta)\right)\hat{a}_r + \cos\varphi\frac{d}{d\theta}\left(-\frac{3}{2}\sin(2\theta)\right)\frac{1}{\rho}\frac{d}{d\rho}\left[\rho\left(-i3\rho^{-3}\right)\right]\hat{a}_\theta$$
$$-\sin\varphi\frac{\left(-\frac{3}{2}\sin(2\theta)\right)}{\sin\theta}\frac{1}{\rho}\frac{d}{d\rho}\left[\rho\left(-i3\rho^{-3}\right)\right]\hat{a}_\varphi$$

$$= \frac{i54}{\rho^4}\cos\varphi\sin\theta\cos\theta\,\hat{a}_r + i9\cos\varphi\cos(2\theta)\frac{1}{\rho}\frac{d}{d\rho}\left[\rho^{-2}\right]\hat{a}_\theta - i9\sin\varphi\frac{\sin\theta\cos\theta}{\sin\theta}\frac{1}{\rho}\frac{d}{d\rho}\left[\rho^{-2}\right]\hat{a}_\varphi$$

$$= \frac{i54}{\rho^4}\cos\varphi\sin\theta\cos\theta\,\hat{a}_r + i9\cos\varphi\cos(2\theta)\frac{1}{\rho}\left(-2\rho^{-3}\right)\hat{a}_\theta - i9\sin\varphi\cos\theta\frac{1}{\rho}\left(-2\rho^{-3}\right)\hat{a}_\varphi$$

$$= \frac{i18}{\rho^4}\left(3\cos\varphi\sin\theta\cos\theta\,\hat{a}_r - \cos\varphi\cos(2\theta)\hat{a}_\theta + \sin\varphi\cos\theta\,\hat{a}_\varphi\right)$$

and finally, for M_{o11} :

$$\vec{M}_{o11} = \frac{1}{\sin\theta}\cos\varphi P_1^1(\cos\theta)h_1^{(1)}(\rho)\hat{a}_\theta - \sin\varphi\frac{d}{d\theta}\left(P_1^1(\cos\theta)\right)h_1^{(1)}(\rho)\hat{a}_\varphi$$

again applying $P_1^1(\cos\theta) = -(1-\cos^2\theta)^{1/2}\frac{d}{dx}\left(P_1(x)\right) = -(\sin^2\theta)^{1/2}\frac{d}{dx}(x) = -\sin\theta$,

and $h_1^{(1)}(\rho) \rightarrow i\,y_1(\rho)\rho^{-2} \rightarrow -i\rho^{-2}$ for small ρ . We then have:

$$= \frac{1}{\sin\theta}\cos\varphi(-\sin\theta)\left(-i\rho^{-2}\right)\hat{a}_\theta - \sin\varphi\frac{d}{d\theta}(-\sin\theta)\left(-i\rho^{-2}\right)\hat{a}_\varphi$$

$$= i\frac{\cos\varphi}{\rho^2}\hat{a}_\theta - i\frac{\sin\varphi\cos\theta}{\rho^2}\hat{a}_\varphi$$

We now a variety of interpretations based on Mie theory, usable in each of their realms of validity.

APPENDIX D

POLARIZABILITY OF Z DIRECTED AND X DIRECTED SPHERES

First, consider the polarizability of a sphere stimulated by a *z* directed field. No free charge, so Laplace's equation for isolated dielectric sphere $\nabla^2 V = 0$. We're interested in the electrostatic approximation, so $-\nabla V = E$. In spherical coordinates, and for spherical boundary conditions, we know the Laplacian has Legendre polynomial solutions. Since there is no φ dependence, we will have normal Legendre polynomials:

$$V(r,\theta) = \sum_{n=0}^{\infty} \left(A_n r^n + \frac{B_n}{r^{n+1}} \right) P_n(\cos\theta)$$

Boundary conditions include $V(r \to \infty, \theta) = 0$, $V(r \to 0, \theta) < \pm\infty$ (finite at origin), $-\nabla V(r \to \infty, \theta = 0) = E_0$ (E at infinity is just the applied field, sphere effect dies down to nothing), $V(r = a^+, \theta) = V(r = a^-, \theta)$ (potential is continuous at sphere boundary – required if we are to have $E_{\|}$ continuous), and $D_{\perp}(r = a^+, \theta) = D_{\perp}(r = a^-, \theta)$.

Since $-\nabla V(r \to \infty, \theta = 0) = E_0$, and assuming we orient the x-axis along the direction of the applied E-field, then $V(r \to \infty, \theta) = -E_0 x = -E_0 r \sin\theta \cos\varphi$.

$P_1^1(\cos\theta) = \sin\theta$ so to match BCs at infinity:

$$V(r,\theta) = \sum_{m=n}^{\infty} \sum_{n=0}^{\infty} \left(A_{nm} r^n + \frac{B_{nm}}{r^{n+1}} \right) P_n^m(\cos\theta) \cos m\varphi = \left(A_{11} r + \frac{B_{11}}{r^2} \right) \sin\theta \cos\varphi$$

Then consider interior and exterior of dielectric sphere:

$$V_1 = \left(A_1 r + \frac{B_1}{r^2} \right) \sin\theta \cos\varphi \quad r \le a$$

$$V_2 = \left(A_2 r + \frac{B_2}{r^2} \right) \sin\theta \cos\varphi \quad r > a$$

Then applying BC $V(r\to\infty,\theta)=-E_0x=-E_0r\sin\theta\cos\varphi$ shows $A_2=-E_0$. At the origin the potential must remain finite, hence $B_1=0$. So:

$$V_1=A_1r\sin\theta\cos\varphi \quad r\le a$$

$$V_2=\left(-E_0r+\frac{B_2}{r^2}\right)\sin\theta\cos\varphi \quad r>a$$

At the boundary between the interior and exterior of the sphere $V_1(a,\theta)=V_2(a,\theta)$, so :

$$A_1a=-E_0a+\frac{B_2}{a^2}\Rightarrow A_1=-E_0+\frac{B_2}{a^3}$$

BC $D_\perp(r=a^+,\theta)=D_\perp(r=a^-,\theta)$ means $\epsilon_1E_{r1}(r=a)=\epsilon_2E_{r2}(r=a)$. Since

$E=-\nabla V=-\frac{\partial V}{\partial r}\hat{a}_r-\frac{1}{r}\frac{\partial V}{\partial\theta}\hat{a}_\theta-\frac{1}{r\sin\theta}\frac{\partial V}{\partial\varphi}\hat{a}_\varphi$ then $E_r=-\frac{\partial V}{\partial r}$ and

$$\epsilon_1\left.\frac{\partial V_1}{\partial r}\right|_{r=a}=\epsilon_2\left.\frac{\partial V_2}{\partial r}\right|_{r=a}\Rightarrow A_1\epsilon_1\sin\theta\cos\varphi=\epsilon_2\left(-E_0-\frac{2B_2}{a^3}\right)\sin\theta\cos\varphi \ ,$$

$$A_1\epsilon_1=-\epsilon_2\left(E_0+\frac{2B_2}{a^3}\right) \ .$$

Then substitution gives:

$$-\epsilon_1\left(E_0-\frac{B_2}{a^3}\right)=-\epsilon_2\left(E_0+\frac{2B_2}{a^3}\right)\Rightarrow \epsilon_1a^3E_0-\epsilon_1B_2=\epsilon_2a^3E_0+2\epsilon_2B_2$$

$$\Rightarrow B_2(2\epsilon_2+\epsilon_1)=(\epsilon_1-\epsilon_2)E_0a^3$$

So:

$$B_2=\frac{\epsilon_1-\epsilon_2}{\epsilon_1+2\epsilon_2}E_0a^3$$

And: $V_1 = \frac{-3\epsilon_2 E_0}{\epsilon_1 + 2\epsilon_2} r \sin\theta\cos\varphi \;\; r \le a \qquad V_2 = \left(-E_0 r + \frac{\epsilon_1 - \epsilon_2}{\epsilon_1 + 2\epsilon_2}\frac{E_0 a^3}{r^2}\right)\sin\theta\cos\varphi \;\; r > a$,

so the electric fields are:

$$\vec{E}_1 = -\nabla V_1 = \frac{3\epsilon_2 E_0}{\epsilon_1 + 2\epsilon_2}\left(\sin\theta\cos\varphi\,\hat{a}_r + \cos\theta\cos\varphi\,\hat{a}_\theta - \sin\varphi\,\hat{a}_\varphi\right) \quad r \le a$$

$$\vec{E}_2 = -\nabla V_2 = \left(E_0 + \frac{\epsilon_1 - \epsilon_2}{\epsilon_1 + 2\epsilon_2}\frac{2E_0 a^3}{r^3}\right)\left(\sin\theta\cos\varphi\,\hat{a}_r + \cos\theta\cos\varphi\,\hat{a}_\theta - \sin\varphi\,\hat{a}_\theta\right) \quad r > a$$

Note that if the sphere is just suspended in free space $\epsilon_2 = \epsilon_0$, then we have the more familiar:

$$\vec{E}_1 = -\nabla V_1 = \frac{3E_0}{\epsilon_{r1} + 2}\left(\sin\theta\cos\varphi\,\hat{a}_r + \cos\theta\cos\varphi\,\hat{a}_\theta - \sin\varphi\,\hat{a}_\varphi\right) \quad r \le a$$

$$\vec{E}_2 = -\nabla V_2 = \left(E_0 + \frac{\epsilon_{r1} - 1}{\epsilon_{r1} + 2}\frac{2E_0 a^3}{r^3}\right)\left(\sin\theta\cos\varphi\,\hat{a}_r + \cos\theta\cos\varphi\,\hat{a}_\theta - \sin\varphi\,\hat{a}_\theta\right) \quad r > a$$

where ϵ_{r1} is the relative permittivity inside sphere, IE $\epsilon_1 = \epsilon_{r1}\epsilon_0$.

This is the electric field of the Laplace equation solution for the isolated sphere. Note for inside the sphere it might be easier to observe that $x = r\sin\theta\cos\varphi$, so in

Cartesian, $V_1 = \frac{-3\epsilon_2 E_0}{\epsilon_1 + 2\epsilon_2} x \;\; r \le a$,and:

$$\vec{E}_1 = -\nabla V_1 = -\frac{\partial V_1}{\partial x}\hat{a}_z = \frac{3\epsilon_2 E_0}{\epsilon_1 + 2\epsilon_2}\hat{a}_x$$

a constant x directed field. For outside the sphere, recall the fields for an electrostatic dipole with dipole moment *p*. For the electrostatic case:

$$V_{dip}(\vec{r}) = \frac{1}{4\pi\epsilon}\frac{\hat{r}\cdot\vec{p}}{r^2} = \frac{p\sin\theta\cos\varphi}{4\pi\epsilon r^2} \quad \text{where} \quad p = |\vec{p}|$$

$$E = -\nabla V = -\frac{\partial V}{\partial r}\hat{a}_r - \frac{1}{r}\frac{\partial V}{\partial \theta}\hat{a}_\theta - \frac{1}{r\sin\theta}\frac{\partial V}{\partial \varphi}\hat{a}_\varphi$$

$$= \frac{2p\sin\theta\cos\varphi}{4\pi\epsilon r^3}\hat{a}_r - \frac{p\cos\theta\cos\varphi}{4\pi\epsilon r^3}\hat{a}_\theta + \frac{p\sin\varphi}{4\pi\epsilon r^3}\hat{a}_\varphi$$

So for the case of the sphere where:

$$\vec{E}_2 = -\nabla V_2 = \left(E_0 + \frac{\epsilon_{rl}-1}{\epsilon_{rl}+2}\frac{2E_0a^3}{r^3}\right)\sin\theta\cos\varphi\,\hat{a}_r + \left(E_0 - \frac{\epsilon_{rl}-1}{\epsilon_{rl}+2}\frac{E_0a^3}{r^3}\right)\cos\theta\cos\varphi\,\hat{a}_\theta$$
$$-\left(E_0 - \frac{\epsilon_{rl}-1}{\epsilon_{rl}+2}\frac{E_0a^3}{r^3}\right)\sin\varphi\,\hat{a}_\theta \qquad r>a$$

Then quite clearly outside the sphere, the field is equal to the applied field E_0 plus that of a dipole centered on the origin along the z axis with dipole moment *p* given by:

$$p = 4\pi\epsilon_2\left(\frac{\epsilon_1-\epsilon_2}{\epsilon_2+2\epsilon_2}\right)a^3E_0$$

Now consider the polarizability of a sphere stimulated by an x-directed field. There is no free charge so $\nabla^2 V = 0$ and we're considering the electrostatic case, so $-\nabla V = E$. In spherical coordinates, for spherical boundary conditions, we know the Laplacian has Legendre polynomial solutions:

$$V(r,\theta) = \sum_{n=0}^{\infty}\left(A_n r^n + \frac{B_n}{r^{n+1}}\right)P_n^m(\cos\theta)$$

Boundary conditions include $V(r\to\infty,\theta) = 0$, $V(r\to 0,\theta) < \pm\infty$ (finite at origin), $-\nabla V(r\to\infty,\theta=0) = E_0$ (E at infinity is just the applied field, sphere effect dies down to nothing), $V(r=a^+,\theta) = V(r=a^-,\theta)$ (potential is continuous at sphere boundary –

required if we are to have $E_{\|}$ continuous), and $D_{\perp}(r=a^{+},\theta)=D_{\perp}(r=a^{-},\theta)$. Since $-\nabla V(r\to\infty,\theta=0)=E_0$, and assuming we orient the x-axis along the direction of the applied E-field, then $V(r\to\infty,\theta)=-E_0x=-E_0r\sin\theta\cos\varphi$.

It must be the case that $P_1^1(\cos\theta)=\sin\theta$ to match BCs at infinity, so:

$$V(r,\theta)=\sum_{m=n}^{\infty}\sum_{n=0}^{\infty}\left(A_{nm}r^n+\frac{B_{nm}}{r^{n+1}}\right)P_n^m(\cos\theta)\cos m\varphi=\left(A_{11}r+\frac{B_{11}}{r^2}\right)\sin\theta\cos\varphi$$

Then consider interior and exterior of dielectric sphere:

$$V_1=\left(A_1r+\frac{B_1}{r^2}\right)\sin\theta\cos\varphi\quad r\le a$$

$$V_2=\left(A_2r+\frac{B_2}{r^2}\right)\sin\theta\cos\varphi\quad r>a$$

Then applying BC $V(r\to\infty,\theta)=-E_0x=-E_0r\sin\theta\cos\varphi$ shows $A_2=-E_0$. At the origin the potential must remain finite, hence $B_1=0$, and:

$$V_1=A_1r\sin\theta\cos\varphi\quad r\le a$$

$$V_2=\left(-E_0r+\frac{B_2}{r^2}\right)\sin\theta\cos\varphi\quad r>a$$

At the boundary between the interior and exterior of the sphere $V_1(a,\theta)=V_2(a,\theta)$, and:

$$A_1a=-E_0a+\frac{B_2}{a^2}\Rightarrow A_1=-E_0+\frac{B_2}{a^3}$$

BC $D_{\perp}(r=a^{+},\theta)=D_{\perp}(r=a^{-},\theta)$ means $\epsilon_1E_{r1}(r=a)=\epsilon_2E_{r2}(r=a)$. Since

$$E = -\nabla V = -\frac{\partial V}{\partial r}\hat{a}_r - \frac{1}{r}\frac{\partial V}{\partial \theta}\hat{a}_\theta - \frac{1}{r\sin\theta}\frac{\partial V}{\partial \varphi}\hat{a}_\varphi \quad \text{then} \quad E_r = -\frac{\partial V}{\partial r} \quad \text{and:}$$

$$\epsilon_1 \frac{\partial V_1}{\partial r}\bigg|_{r=a} = \epsilon_2 \frac{\partial V_2}{\partial r}\bigg|_{r=a} \Rightarrow A_1\epsilon_1 \sin\theta\cos\varphi = \epsilon_2\left(-E_0 - \frac{2B_2}{a^3}\right)\sin\theta\cos\varphi$$

$$A_1\epsilon_1 = -\epsilon_2\left(E_0 + \frac{2B_2}{a^3}\right)$$

Then substitution gives:

$$-\epsilon_1\left(E_0 - \frac{B_2}{a^3}\right) = -\epsilon_2\left(E_0 + \frac{2B_2}{a^3}\right) \Rightarrow \epsilon_1 a^3 E_0 - \epsilon_1 B_2 = \epsilon_2 a^3 E_0 + 2\epsilon_2 B_2$$

$$\Rightarrow B_2(2\epsilon_2 + \epsilon_1) = (\epsilon_1 - \epsilon_2)E_0 a^3$$

So:

$$B_2 = \frac{\epsilon_1 - \epsilon_2}{\epsilon_1 + 2\epsilon_2}E_0 a^3$$

And:

$$V_1 = \frac{-3\epsilon_2 E_0}{\epsilon_1 + 2\epsilon_2} r\sin\theta\cos\varphi \quad r \le a$$

$$V_2 = \left(-E_0 r + \frac{\epsilon_1 - \epsilon_2}{\epsilon_1 + 2\epsilon_2}\frac{E_0 a^3}{r^2}\right)\sin\theta\cos\varphi \quad r > a$$

So the electric fields are:

$$\vec{E}_1 = -\nabla V_1 = \frac{3\epsilon_2 E_0}{\epsilon_1 + 2\epsilon_2}\left(\sin\theta\cos\varphi\,\hat{a}_r + \cos\theta\cos\varphi\,\hat{a}_\theta - \sin\varphi\,\hat{a}_\varphi\right) \quad r \le a$$

$$\vec{E}_2 = -\nabla V_2 = \left(E_0 + \frac{\epsilon_1 - \epsilon_2}{\epsilon_1 + 2\epsilon_2}\frac{2E_0 a^3}{r^3}\right)\left(\sin\theta\cos\varphi\,\hat{a}_r + \cos\theta\cos\varphi\,\hat{a}_\theta - \sin\varphi\,\hat{a}_\theta\right) \quad r > a$$

Note that if the sphere is just suspended in free space $\epsilon_2 = \epsilon_0$, then we have the more

familiar:

$$\vec{E}_1 = -\nabla V_1 = \frac{3E_0}{\epsilon_{r1}+2}\left(\sin\theta\cos\varphi\,\hat{a}_r + \cos\theta\cos\varphi\,\hat{a}_\theta - \sin\varphi\,\hat{a}_\varphi\right) \quad r \le a$$

$$\vec{E}_2 = -\nabla V_2 = \left(E_0 + \frac{\epsilon_{r1}-1}{\epsilon_{r1}+2}\frac{2E_0 a^3}{r^3}\right)\left(\sin\theta\cos\varphi\,\hat{a}_r + \cos\theta\cos\varphi\,\hat{a}_\theta - \sin\varphi\,\hat{a}_\theta\right) \quad r > a$$

where ϵ_{r1} is the relative permittivity inside sphere, IE $\epsilon_1 = \epsilon_{r1}\epsilon_0$. This is the electric field of the Laplace equation solution for the isolated sphere. Note for inside the sphere it might be easier to observe that $x = r\sin\theta\cos\varphi$ so in Cartesian:

$$V_1 = \frac{-3\epsilon_2 E_0}{\epsilon_1 + 2\epsilon_2} x \quad r \le a$$

and:

$$\vec{E}_1 = -\nabla V_1 = -\frac{\partial V_1}{\partial x}\hat{a}_z = \frac{3\epsilon_2 E_0}{\epsilon_1+2\epsilon_2}\hat{a}_x$$

a constant x directed field. While for outside the sphere, recall the fields for an electrostatic dipole with dipole moment *p:*

$$V_{dip}(\vec{r}) = \frac{1}{4\pi\epsilon}\frac{\hat{r}\cdot\vec{p}}{r^2} = \frac{p\sin\theta\cos\varphi}{4\pi\epsilon r^2} \quad \text{where} \quad p = |\vec{p}|$$

$$E = -\nabla V = -\frac{\partial V}{\partial r}\hat{a}_r - \frac{1}{r}\frac{\partial V}{\partial\theta}\hat{a}_\theta - \frac{1}{r\sin\theta}\frac{\partial V}{\partial\varphi}\hat{a}_\varphi$$

$$= \frac{2p\sin\theta\cos\varphi}{4\pi\epsilon r^3}\hat{a}_r - \frac{p\cos\theta\cos\varphi}{4\pi\epsilon r^3}\hat{a}_\theta + \frac{p\sin\varphi}{4\pi\epsilon r^3}\hat{a}_\varphi$$

So for the case of the sphere where:

$$\vec{E}_2 = -\nabla V_2 = \left(E_0 + \frac{\epsilon_{r1}-1}{\epsilon_{r1}+2}\frac{2E_0 a^3}{r^3}\right)\left(\sin\theta\cos\varphi\,\hat{a}_r + \cos\theta\cos\varphi\,\hat{a}_\theta - \sin\varphi\,\hat{a}_\theta\right) \quad r > a$$

Then quite clearly outside the sphere, the field is equal to the applied field E_0 plus that of a dipole centered on the origin along the z axis with dipole moment *p* given by:

$$p = 4\pi\epsilon_2\left(\frac{\epsilon_1-\epsilon_2}{\epsilon_1+2\epsilon_2}\right)a^3 E_0$$

That is the dipole moment of the sphere is proportional to the applied electric field by a polarizability constant α :

$$p = \alpha E_0 \qquad \alpha = 4\pi\epsilon_2\left(\frac{\epsilon_1-\epsilon_2}{\epsilon_1+2\epsilon_2}\right)a^3$$

APPENDIX E

GREEN FUNCTION SOLUTION DERIVATION

In the typical fashion, the supported modes of a dielectric waveguide may be determined by solving Helmholtz wave equation and applying appropriate boundary conditions. Given the frequency of interest, it is safe to assume that the structure constructed to behave as the effective media will be lossy, hence it is appropriate to solve for the modes of a lossy dielectric rod. As mentioned, this blurs our evaluation of what exactly can be considered a mode onset, and cutoff, as instead of a completely real propagation constant β, we will have a complex constant $k = -j\gamma = \beta - j\alpha$, with significantly large attenuation constant α. This means the resulting Bessel functions of the system describing the behavior of radially dependent fields will be the sum of evanescent and propagating waves, making the distinction between "guided" and "radiating" modes blurred.

To evaluate a lossy dielectric rod, and for later comparison to heterogeneous structures, an atypical approach at determining the fields of such a structure is beneficial [9]. Assume a negligibly permeable lossy dielectric rod ($\mu_r \approx 1$ $\epsilon_r = \epsilon' - j\epsilon''$ where $\epsilon' = \Re\left(\frac{\epsilon}{\epsilon_0}\right)$ and $\epsilon'' = \Im\left(\frac{\epsilon}{\epsilon_0}\right)$), oriented along the z-axis, of radius *a*, which is electrically thin outside the rod ($k_0 a \ll 1$) but may be operated at frequencies which may result in electrically large waves *inside* the rod ($k_m a \approx 1$).

For stimulating modes in the rod, assume a small band of circulating current around the rod is used, either electric or magnetic depending on the stimulation desired. For TEz only modes, we would consider the case in which the cylinder is excited by a uniform (φ independent), φ directed, current band encircling it at the z=0 plane.

This only excites TE modes since the φ independent current I_{φ} can only create φ directed vector potential A_{φ} and only φ directed E-fields (by $B = \nabla \times A$ there can be no H_{φ})

For TMz only modes, we would only consider the case in which the cylinder is excited by a uniform (φ independent), φ directed *magnetic* current band encircling the rod at the z=0 plane.

For hybrid modes, we would consider a *non*-uniform (φ dependent) φ directed current band at the z=0 plane. If the current band is electric, HEz modes would be stimulated, and if magnetic, EHz modes.

From the typical application of vector potentials and separating the problem into TEz and TMz components, we have the following [22]:

TEz	TMz
$E_z = 0$	$E_z = -jB_{mn}\frac{k_\rho^2}{\omega\mu\epsilon}J_m(k_\rho\rho)\begin{bmatrix}D\cos m\varphi\\ C\sin m\varphi\end{bmatrix}$
$E_\rho = -A_{mn}\frac{m}{\epsilon\rho}J_m(k_\rho\rho)\begin{bmatrix}-C\sin m\varphi\\ D\cos m\varphi\end{bmatrix}$	$E_\rho = -B_{mn}\frac{k_\rho k_z}{\omega\mu\epsilon}J_m'(k_\rho\rho)\begin{bmatrix}D\cos m\varphi\\ +C\sin m\varphi\end{bmatrix}$
$E_\varphi = A_{mn}\frac{k_\rho}{\epsilon}J_m'(k_\rho\rho)\begin{bmatrix}C\cos m\varphi\\ D\sin m\varphi\end{bmatrix}$	$E_\varphi = -B_{mn}\frac{mk_z}{\omega\mu\epsilon}\frac{1}{\rho}J_m(k_\rho\rho)\begin{bmatrix}-D\sin m\varphi\\ +C\cos m\varphi\end{bmatrix}$
$H_z = -jA_{mn}\frac{k_\rho^2}{\omega\mu\epsilon}J_m(k_\rho\rho)\begin{bmatrix}C\cos m\varphi\\ D\sin m\varphi\end{bmatrix}$	$H_z = 0$
$H_\rho = -A_{mn}\frac{k_\rho k_z}{\omega\mu\epsilon}J_m'(k_\rho\rho)\begin{bmatrix}C\cos m\varphi\\ D\sin m\varphi\end{bmatrix}$	$H_\rho = B_{mn}\frac{m}{\mu\rho}J_m(k_\rho\rho)\begin{bmatrix}-D\sin m\varphi\\ +C\cos m\varphi\end{bmatrix}$
$H_\varphi = -A_{mn}\frac{mk_z}{\omega\mu\epsilon}\frac{1}{\rho}J_m(k_\rho\rho)\begin{bmatrix}-C\sin m\varphi\\ D\cos m\varphi\end{bmatrix}$	$H_\varphi = -B_{mn}\frac{k_\rho}{\mu}J_m'(k_\rho\rho)\begin{bmatrix}D\cos m\varphi\\ +C\sin m\varphi\end{bmatrix}$

Where J_m is a placeholder standing for the appropriate Bessel function depending on boundary conditions (1st kind, 2nd, Hankel, etc.), and prime on the Bessel function implies derivative with respect to the argument of the function.

Observe that if there is no φ dependence, $m = 0$, and either $C = 0$ or $D = 0$, depending on whether the boundary/initial conditions are such that either a TE_z or TM_z wave is excited. So for instance, if an exciting magnetic current source is φ independent and φ directed, then a TM_z mode will be excited, and $C, m = 0$.

If a φ - directed, φ independent, magnetic current band $C_m = C_0 \hat{a}_\varphi$ Volts/m is assumed, in a band between $z=-s/2$ and $z=s/2$ at radius $\rho = a$. Then the current in the band is $I_0 = C_0 s$. The surface current may be decomposed using the Fourier integral pair:

$$K_\varphi(k_z)=\frac{1}{2\pi}\int_{-\infty}^{+\infty}\left\{C_0\left(\frac{-s}{2}\quad\frac{+s}{2}\right)\right\}e^{jk_z z}dz$$

$$C_0\left(\frac{-s}{2}\quad\frac{+s}{2}\right)=\int_{-\infty}^{+\infty}K_\varphi(k_z)e^{-jk_z z}dk_z$$

This is an infinite sum (integral) of magnetic current waves, each carrying $K_\varphi(k_z)dk_z$ V/m traveling along the z-axis with propagation constant k_z . Its spectrum is a sinc function in k_z :

$$K_\varphi(k_z)=\frac{1}{2\pi}\int_{\frac{-s}{2}}^{\frac{+s}{2}}C_0 e^{jk_z z}dz=\frac{C_0 s}{2\pi}\left[\frac{\sin\left(k_z\frac{s}{2}\right)}{\left(k_z\frac{s}{2}\right)}\right]$$

The fields may be expanded inside and outside the rod in cylindrical harmonic solutions of the wave equation, then the boundary conditions and source conditions may be satisfied with:

$k_{\rho 0}^2+k_z^2=k_0^2=\omega^2\mu_0\varepsilon_0$ inside the medium outside the cylinder, IE $\rho>a$

$k_{\rho 1}^2+k_z^2=k_1^2=\omega^2\mu_1\varepsilon_1$ inside the medium inside the cylinder, IE $\rho<a$

Then for $\rho<a$:

$$E_z = -jA_{0n}\frac{k_{\rho 1}^2}{\omega\mu_1\epsilon_1}J_0(k_{\rho 1}\rho)e^{-jk_z z}$$

$$E_\rho = -A_{0n}\frac{k_{\rho 1}k_z}{\omega\mu_1\epsilon_1}J_1(k_{\rho 1}\rho)e^{-jk_z z}$$

$$E_\varphi = 0$$

$$H_z = 0$$

$$H_\rho = 0$$

$$H_\varphi = -A_{0n}\frac{k_{\rho 1}}{\mu_1}J_1(k_{\rho 1}\rho)e^{-jk_z z}$$

and for $\rho>a$:

$$E_z = -jB_{0n}\frac{k_{\rho 0}^2}{\omega\mu_0\epsilon_0}H_0^{(2)}(k_{\rho 0}\rho)e^{-jk_z z}$$

$$E_\rho = -B_{0n}\frac{k_{\rho 0}k_z}{\omega\mu_0\epsilon_0}H_1^{(2)}(k_{\rho 0}\rho)e^{-jk_z z}$$

$$E_\varphi = 0$$

$$H_z = 0$$

$$H_\rho = 0$$

$$H_\varphi = -B_{0n}\frac{k_{\rho 0}}{\mu_0}H_1^{(2)}(k_{\rho 0}\rho)e^{-jk_z z}$$

Applying boundary conditions gives:

$$A_{0n} = \frac{\frac{k_{\rho 0}\mu_1 H_1^{(2)}(k_{\rho 0}a)}{k_{\rho 1}\mu_0 J_1(k_{\rho 1}a)} j K_\varphi(k_z) e^{jk_z z}}{\frac{k_{\rho 0}^2}{\omega\mu_0\epsilon_0} H_0^{(2)}(k_{\rho 0}a)\left(1 - \frac{k_{\rho 1}\epsilon_0}{k_{\rho 0}\epsilon_1}\frac{H_1^{(2)}(k_{\rho 0}a)}{H_0^{(2)}(k_{\rho 0}a)}\frac{J_0(k_{\rho 1}a)}{J_1(k_{\rho 1}a)}\right)}$$

$$B_{0n} = \frac{j K_\varphi(k_z) e^{jk_z z}}{\frac{k_{\rho 0}^2}{\omega\mu_0\epsilon_0} H_0^{(2)}(k_{\rho 0}a)\left(1 - \frac{k_{\rho 1}\epsilon_0}{k_{\rho 0}\epsilon_1}\frac{H_1^{(2)}(k_{\rho 0}a)}{H_0^{(2)}(k_{\rho 0}a)}\frac{J_0(k_{\rho 1}a)}{J_1(k_{\rho 1}a)}\right)}$$

Now examine the role of surface wave poles:

For $\rho < a$:

$$E_z = \frac{k_{\rho 1}}{k_{\rho 0}\epsilon_r}\frac{J_0(k_{\rho 1}\rho)}{J_1(k_{\rho 1}a)}\frac{\frac{H_1^{(2)}(k_{\rho 0}a)}{H_0^{(2)}(k_{\rho 0}a)}K_\varphi(k_z)}{\left(1 - \frac{k_{\rho 1}}{k_{\rho 0}\epsilon_r}\frac{H_1^{(2)}(k_{\rho 0}a)}{H_0^{(2)}(k_{\rho 0}a)}\frac{J_0(k_{\rho 1}a)}{J_1(k_{\rho 1}a)}\right)}$$

$$H_\varphi = j\frac{\omega\epsilon_0}{k_{\rho 0}}\frac{J_1(k_{\rho 1}\rho)}{J_1(k_{\rho 1}a)}\frac{\frac{H_1^{(2)}(k_{\rho 0}a)}{H_0^{(2)}(k_{\rho 0}a)}K_\varphi(k_z)}{\left(1 - \frac{k_{\rho 1}}{k_{\rho 0}\epsilon_r}\frac{H_1^{(2)}(k_{\rho 0}a)J_0(k_{\rho 1}a)}{H_0^{(2)}(k_{\rho 0}a)J_1(k_{\rho 1}a)}\right)}$$

$$E_\rho = \frac{k_z}{\omega\epsilon_1} H_\varphi$$

and for $\rho > a$:

$$E_z = \frac{H_0^{(2)}(k_{\rho 0}\rho)}{H_0^{(2)}(k_{\rho 0}a)} \frac{K_\varphi(k_z)}{\left(1 - \frac{k_{\rho 1}}{k_{\rho 0}\epsilon_r} \frac{H_1^{(2)}(k_{\rho 0}a)}{H_0^{(2)}(k_{\rho 0}a)} \frac{J_0(k_{\rho 1}a)}{J_1(k_{\rho 1}a)}\right)}$$

$$H_\varphi = j\frac{\omega \epsilon_0}{k_{\rho 0}} \frac{H_1^{(2)}(k_{\rho 1}\rho)}{H_0^{(2)}(k_{\rho 0}a)} \frac{K_\varphi(k_z)}{\left(1 - \frac{k_{\rho 1}}{k_{\rho 0}\epsilon_r} \frac{H_1^{(2)}(k_{\rho 0}a)J_0(k_{\rho 1}a)}{H_0^{(2)}(k_{\rho 0}a)J_1(k_{\rho 1}a)}\right)}$$

$$E_\rho = \frac{k_z}{\omega \epsilon_0} H_\varphi$$

Where, $K_\varphi(k_z) = \frac{I_0}{2\pi}\left[\frac{\sin\left(k_z \frac{s}{2}\right)}{\left(k_z \frac{s}{2}\right)}\right]$ v/m.

All terms have the following pole:

$$\left(1 - \frac{k_{\rho 1}}{k_{\rho 0}\epsilon_r} \frac{H_1^{(2)}(k_{\rho 0}a)J_0(k_{\rho 1}a)}{H_0^{(2)}(k_{\rho 0}a)J_1(k_{\rho 1}a)}\right)$$

When setting equal to 0 for the pole condition, and rearranging terms, we see the transcendental equation for the propagation constant of the TM01 mode in the dielectric rod as has been seen before in the literature and textbooks [25]:

$$k_{\rho 0}\epsilon_r H_0^{(2)}(k_{\rho 0}a)J_1(k_{\rho 1}a) = k_{\rho 1} H_1^{(2)}(k_{\rho 0}a)J_0(k_{\rho 1}a)$$

Temporarily assuming completely real k , we see these poles may only arise in the range $k_0 < k_z < k_1$, because in this range $k_{\rho 0} = \sqrt{k_0^2 - k_z^2} = -jk_0\sqrt{k_z^2 - k_0^2}$; $k_{\rho 0}a$ is a negative imaginary number while $k_{\rho 1} = \sqrt{k_1^2 - k_z^2}$ is a positive number. Since

$K_0(\chi) = -j\frac{\pi}{2}H_0^{(2)}(-j\chi)$ $K_1(\chi) = -\frac{\pi}{2}H_1^{(2)}(-j\chi)$ the quantity

$\frac{H_1^{(2)}(-j\chi)}{H_0^{(2)}(-j\chi)} = -j\frac{K_1(\chi)}{K_0(\chi)}$ is known as the logarithmic derivative of $K_0(\chi)$ and is well behaved. The quantity $\frac{1}{(-j\chi)}\frac{H_1^{(2)}(-j\chi)}{H_0^{(2)}(-j\chi)}$ is purely real and negative, while in the same range $\frac{(k_{\rho 1}a)J_0(k_{\rho 1}a)}{J_1(k_{\rho 1}a)}$ is purely real. So only in this range can the denominator vanish, giving us a pole.

What this shows is that the guided waves travel slower than free space, but no slower than the rod medium. Hence it is only in this range between k_0 and k_1 that the k_z spectrum waves can match in speed the slow wave modes, and it is then that they can strongly couple to them.

However, that is assuming completely real *k,* lossy material removes this distinction between "guidance" and "non-guidance", and requires a different method of evaluation which will be considered shortly.

The fields in the spatial domain may be expressed by applying the inverse Fourier transform. For $\rho<a$:

$$E_z = \int_{-\infty}^{\infty} \frac{k_{\rho 1}}{k_{\rho 0}\epsilon_r}\frac{J_0(k_{\rho 1}\rho)}{J_1(k_{\rho 1}a)}\frac{\frac{H_1^{(2)}(k_{\rho 0}a)}{H_0^{(2)}(k_{\rho 0}a)}K_\varphi(k_z)e^{-jk_z z}\,dk_z}{\left(1-\frac{k_{\rho 1}}{k_{\rho 0}\epsilon_r}\frac{H_1^{(2)}(k_{\rho 0}a)}{H_0^{(2)}(k_{\rho 0}a)}\frac{J_0(k_{\rho 1}a)}{J_1(k_{\rho 1}a)}\right)}$$

$$H_\varphi = \int_{-\infty}^{\infty} j\frac{\omega\epsilon_0}{k_{\rho 0}}\frac{J_1(k_{\rho 1}\rho)}{J_1(k_{\rho 1}a)}\frac{\dfrac{H_1^{(2)}(k_{\rho 0}a)}{H_0^{(2)}(k_{\rho 0}a)}K_\varphi(k_z)e^{-jk_z z}dk_z}{\left(1-\dfrac{k_{\rho 1}}{k_{\rho 0}\epsilon_r}\dfrac{H_1^{(2)}(k_{\rho 0}a)J_0(k_{\rho 1}a)}{H_0^{(2)}(k_{\rho 0}a)J_1(k_{\rho 1}a)}\right)}$$

$$E_\rho = \int_{-\infty}^{\infty} j\frac{k_z}{\epsilon_r k_{\rho 0}}\frac{J_1(k_{\rho 1}\rho)}{J_1(k_{\rho 1}a)}\frac{\dfrac{H_1^{(2)}(k_{\rho 0}a)}{H_0^{(2)}(k_{\rho 0}a)}K_\varphi(k_z)e^{-jk_z z}dk_z}{\left(1-\dfrac{k_{\rho 1}}{k_{\rho 0}\epsilon_r}\dfrac{H_1^{(2)}(k_{\rho 0}a)J_0(k_{\rho 1}a)}{H_0^{(2)}(k_{\rho 0}a)J_1(k_{\rho 1}a)}\right)}$$

for $\rho > a$:

$$E_z = \int_{-\infty}^{\infty} \frac{H_0^{(2)}(k_{\rho 0}\rho)}{H_0^{(2)}(k_{\rho 0}a)}\frac{K_\varphi(k_z)e^{-jk_z z}dk_z}{\left(1-\dfrac{k_{\rho 1}}{k_{\rho 0}\epsilon_r}\dfrac{H_1^{(2)}(k_{\rho 0}a)}{H_0^{(2)}(k_{\rho 0}a)}\dfrac{J_0(k_{\rho 1}a)}{J_1(k_{\rho 1}a)}\right)}$$

$$H_\varphi = \int_{-\infty}^{\infty} j\frac{\omega\epsilon_0}{k_{\rho 0}}\frac{H_1^{(2)}(k_{\rho 0}\rho)}{H_0^{(2)}(k_{\rho 0}a)}\frac{K_\varphi(k_z)e^{-jk_z z}dk_z}{\left(1-\dfrac{k_{\rho 1}}{k_{\rho 0}\epsilon_r}\dfrac{H_1^{(2)}(k_{\rho 0}a)J_0(k_{\rho 1}a)}{H_0^{(2)}(k_{\rho 0}a)J_1(k_{\rho 1}a)}\right)}$$

$$E_\rho = \int_{-\infty}^{\infty} j\frac{k_z}{k_{\rho 0}}\frac{H_1^{(2)}(k_{\rho 0}\rho)}{H_0^{(2)}(k_{\rho 0}a)}\frac{K_\varphi(k_z)e^{-jk_z z}dk_z}{\left(1-\dfrac{k_{\rho 1}}{k_{\rho 0}\epsilon_r}\dfrac{H_1^{(2)}(k_{\rho 0}a)J_0(k_{\rho 1}a)}{H_0^{(2)}(k_{\rho 0}a)J_1(k_{\rho 1}a)}\right)}$$

Observe the poles common to each term:

$$Pole(k_z) = \frac{1}{\left(1-\dfrac{k_{\rho 1}}{k_{\rho 0}\epsilon_r}\dfrac{H_1^{(2)}(k_{\rho 0}a)J_0(k_{\rho 1}a)}{H_0^{(2)}(k_{\rho 0}a)J_1(k_{\rho 1}a)}\right)}$$

And for simplification later, we may also define a common factor function of k_z term in each each expression:

$$\frac{1}{k_{\rho 0}a}\frac{H_1^{(2)}(k_{\rho 0}a)}{H_0^{(2)}(k_{\rho 0}a)}$$

so the total common expression in each term is:

$$Common(k_z)=\frac{k_{\rho 0}a}{\frac{1}{J_1(k_{\rho 1}a)}\left(J_1(k_{\rho 1}a)-\frac{k_{\rho 1}}{k_{\rho 0}\epsilon_r}\frac{H_1^{(2)}(k_{\rho 0}a)J_0(k_{\rho 1}a)}{H_0^{(2)}(k_{\rho 0}a)}\right)}\left(\frac{1}{k_{\rho 0}a}\frac{H_1^{(2)}(k_{\rho 0}a)}{H_0^{(2)}(k_{\rho 0}a)}\right)$$

and also recall in the spectrum of the current band:

$K_\varphi(k_z)=\frac{I_0}{2\pi}\frac{\sin(k_z\frac{s}{2})}{k_z\frac{s}{2}}$, where I_0 is the *magnetic* current source in Volts exciting

the rod. Also recall:

$$k_{\rho 0}^2+k_z^2=k_0^2=\omega^2\mu_0\epsilon_0$$

$$k_{\rho 1}^2+k_z^2=k_1^2=\omega^2\mu_1\epsilon_1$$

Then the total fields for $\rho<a$

$$E_z(\rho,z)=\frac{1}{\epsilon_r}\frac{I_0}{2\pi}\int_{-\infty}^{\infty}Common(k_z)(k_{\rho 1}a)J_0(k_{\rho 1}\rho)\left(\frac{\sin(k_z\frac{s}{2})}{k_z\frac{s}{2}}\right)e^{-jk_z z}dk_z$$

$$H_\varphi=j\omega\epsilon_0 a\frac{I_0}{2\pi}\int_{-\infty}^{\infty}Common(k_z)J_1(k_{\rho 1}\rho)\left(\frac{\sin(k_z\frac{s}{2})}{k_z\frac{s}{2}}\right)e^{-jk_z z}dk_z$$

$$E_\rho = \frac{j}{\epsilon_r}\frac{I_0}{2\pi}\int_{-\infty}^{\infty} Common(k_z)(k_z a)J_1(k_{\rho 1}\rho)\left(\frac{\sin(k_z\frac{s}{2})}{k_z\frac{s}{2}}\right)e^{-jk_z z}dk_z$$

For electrically small current source, IE a delta function source, $s \to 0$ and:

$$\left(\frac{\sin(k_z\frac{s}{2})}{k_z\frac{s}{2}}\right)\to 1$$

then for $\rho < a$

$$E_z(\rho, z) = \frac{1}{\epsilon_r}\frac{I_0}{2\pi}\int_{-\infty}^{\infty} Common(k_z)(k_{\rho 1}a)J_0(k_{\rho 1}\rho)e^{-jk_z z}dk_z$$

$$H_\varphi = j\omega\epsilon_0 a\frac{I_0}{2\pi}\int_{-\infty}^{\infty} Common(k_z)J_1(k_{\rho 1}\rho)e^{-jk_z z}dk_z$$

$$E_\rho = \frac{j}{\epsilon_r}\frac{I_0}{2\pi}\int_{-\infty}^{\infty} Common(k_z)(k_z a)J_1(k_{\rho 1}\rho)e^{-jk_z z}dk_z$$

similarly, for $\rho > a$

$$E_z(\rho, z) = \frac{I_0}{2\pi}\int_{-\infty}^{\infty} Common(k_z)(k_{\rho 0}a)\frac{H_0^{(2)}(k_{\rho 0}\rho)}{H_1^{(2)}(k_{\rho 0}a)}J_1(k_{\rho 1}a)e^{-jk_z z}dk_z$$

$$H_\varphi = j\omega\epsilon_0 a\frac{I_0}{2\pi}\int_{-\infty}^{\infty} Common(k_z)\frac{H_1^{(2)}(k_{\rho 0}\rho)}{H_1^{(2)}(k_{\rho 0}a)}J_1(k_{\rho 1}a)e^{-jk_z z}dk_z$$

$$E_\rho = \frac{jI_0}{2\pi}\int_{-\infty}^{\infty} Common(k_z)(k_z a)\frac{H_1^{(2)}(k_{\rho 0}\rho)}{H_1^{(2)}(k_{\rho 0}a)}J_1(k_{\rho 1}a)e^{-jk_z z}dk_z$$

The first quantity of interest is the current wave carried by the rod. *If* the current was electric current, we could integrate dB_z/dt inside the rod over the cross sectional

area from $\rho = 0$ to $\rho = a$ and call that the total magnetic current. Conversely, for our case, where we have a magnetic current source, we can integrate $-dD_z/dt$ across the same cross sectional area and call that the total electric current. Or we could think of it from the point of view of an outside observer unaware of the electrical thickness of the rod. Since $k_{r0}a$ is small the observer would assume the circulating H-field at the surface obeys Ampere's Law. Both methods give the same answer:

$$\oint \vec{H}\cdot\vec{dl} = \int \frac{\partial \vec{D}}{\partial t}\cdot d\vec{S} = I_e$$

The first integral requires the magnetic field be known at the surface of the rod, something we determined earlier. The second integral requires the electric flux density through the cross section of the rod , information not available to us. Hence using the first integral,

$$I_e(z) = \oint \vec{H}\cdot\vec{dl} = \int_0^{2\pi}\left(j\omega\epsilon_0 a \frac{I_0}{2\pi}\int_{-\infty}^{\infty} Common(k_z)\frac{H_1^{(2)}(k_{\rho 0}\rho)}{H_1^{(2)}(k_{\rho 0}a)}J_1(k_{\rho 1}a)e^{-jk_z z}dk_z\right)d\varphi$$

and since there is no φ dependence in the expression we can integrate immediately to see:

$$I_e(z) = j\omega\epsilon_0 a I_0\int_{-\infty}^{\infty} Common(k_z)\frac{H_1^{(2)}(k_{\rho 0}\rho)}{H_1^{(2)}(k_{\rho 0}a)}J_1(k_{\rho 1}a)e^{-jk_z z}dk_z$$

This is the electric current along the rod in amperes. Recall the k_z integral will give a result with the units m^{-1} . Actual determination of the integral may be achieved numerically, with the application of residue theory.

The TMz modes of the dielectric rod will be comparable to the longitudinal modes of the chain of spheres. One might assume TEz modes may be equally important, however, TEz modes of the rod are not analogous to the transverse modes of the chain of spheres, as one may at first assume. Due to the angular dependence of the transverse polarization of the sphere of chains supporting a transverse mode, the appropriate analog are HEz modes of the rod. Future considerations may make the TEz modes relevant, in which cause the previously derived TMz expressions may be readily used by a slight alteration using duality to determine the TEz components of such a structure (i.e. replace the stimulating magnetic current with an electric, swap μ and ϵ, and care for signs appropriately, etc.) Then these terms from the TEz modes may be coupled with the TMz terms to determine the HEz hybrid modes.

We have derived the TMz modes completely, and will simulate them shortly. For the HEz modes we will now derive the closed form expression, but due to their current unimportance in our efforts, they will not be simulated unless needed at a later date.

HEz modes of a lossy dielectric cylinder should be analogous to the transverse modes of a chain of spheres. To analyze such modes, assume φ - directed, φ *dependent, electric* current band $C_e = C_0 \cos\varphi \hat{a}_\varphi$ Amps/m, in a band between $z=-s/2$ and $z=s/2$ at radius $\rho = a$. The current in the band is $I_e = C_0 \cos\varphi s$. Decompose the surface current using the Fourier integral pair:

$$K_\varphi(k_z,\varphi)=\frac{1}{2\pi}\int_{-\infty}^{+\infty}\left\{C_0\cos\varphi\left(\frac{-s}{2}\quad\frac{+s}{2}\right)\right\}e^{jk_z z}dz$$

$$C_0 \cos\varphi \left(\frac{-s}{2} \quad \frac{+s}{2} \right) = \int_{-\infty}^{+\infty} K_\varphi(k_z) \cos\varphi \, e^{-jk_z z} \, dk_z$$

The band has been decomposed into an infinite sum (integral) of electric current waves, each carrying $K_\varphi(k_z)\,dk_z$ A/m traveling along the z-axis with propagation constant k_z . The spectrum is a sinc function in k_z , with an amplitude dependence of $\cos\varphi$ with respect to φ :

$$K_\varphi(k_z, \varphi) = \frac{1}{2\pi} \int_{\frac{-s}{2}}^{\frac{+s}{2}} C_0 \cos\varphi \, e^{jk_z z} dz = \frac{C_0 \cos\varphi \, s}{2\pi} \left[\frac{\sin\left(k_z \frac{s}{2}\right)}{\left(k_z \frac{s}{2}\right)} \right]$$

Expanding the fields inside and outside the rod in cylindrical harmonic solutions of the wave equation, we then satisfy the boundary conditions and source conditions with:

$k_{\rho 0}^2 + k_z^2 = k_0^2 = \omega^2 \mu_0 \varepsilon_0$ inside the medium outside the cylinder, IE $\rho > a$

$k_{\rho 1}^2 + k_z^2 = k_1^2 = \omega^2 \mu_1 \varepsilon_1$ inside the medium inside the cylinder, IE $\rho < a$

From the expressions of the fields of an HEz mode, for $\rho < a$, we have a $D_2 = 0$, $m = 1$ dependence, resulting in an HE_{11} modes. Note that some of the Bessel functions for the expressions of the fields are derivatives of Bessel functions of the first kind. That is to say, before for the TMz_{0n} modes in the previous section we applied $J_0(z) = -J_1'(z)$, for $J_1'(z)$, we need the more general expression:

$$\left(\frac{1}{z} \frac{d}{dz} \right)^k \left(z^v J_v(z) \right) = z^{v-k} J_{v-k}(z)$$

or:

$$\left(\frac{1}{z}\frac{d}{dz}\right)\left(zJ_1(z)\right) = J_0(z)$$

$$J_1(z)+z\frac{d}{dz}J_1(z) = zJ_0(z)$$

$$\frac{d}{dz}J_1(z) = J_0(z)-\frac{J_1(z)}{z}$$

Applying the recurrence relation:

$$J_{v-1}(z)+J_{v+1}(z) = \frac{2v}{z}J_v(z)$$

we see

$$J_0(z)+J_2(z) = \frac{2}{z}J_1(z) \quad \text{or} \quad \frac{J_1(z)}{z} = \frac{1}{2}\left(J_0(z)+J_2(z)\right)$$

then:

$$\frac{d}{dz}J_1(z) = J_0(z)-\frac{J_1(z)}{z} = \frac{J_0(z)-J_2(z)}{2}$$

so for any $J_1'(z)$ or $H_1^{(2)'}(z)$ for the HE modes, replace it with $\frac{J_0(z)-J_2(z)}{2}$ or

$\frac{H_0^{(2)}(z)-H_2^{(2)}(z)}{2}$ respectively. Then for $\rho<a$:

$$E_z = -jB_{1n}\frac{k_{\rho 1}^2}{\omega\mu_1\epsilon_1}J_1(k_{\rho 1}\rho)\cos\varphi\, e^{-jk_z z}$$

$$E_\rho = \left(-A_{1n}\frac{1}{\epsilon_1\rho}J_1(k_{\rho 1}\rho)-B_{1n}\frac{k_{\rho 1}k_z}{\omega\mu_1\epsilon_1}J_1'(k_{\rho 1}\rho)\right)\cos\varphi\, e^{-jk_z z}$$

$$E_\varphi = \left(A_{1n}\frac{k_{\rho 1}}{\epsilon_1}J_1'(k_{\rho 1}\rho)+B_{1n}\frac{k_z}{\omega\epsilon_1\mu_1\rho}J_1(k_{\rho 1}\rho)\right)\sin\varphi\, e^{-jk_z z}$$

$$H_z = -j\,A_{1n}\frac{{k_{\rho 1}}^2}{\omega\epsilon_1\mu_1}J_1(k_{\rho 1}\rho)\sin\varphi\,e^{-jk_z z}$$

$$H_\rho = \left(-A_{1n}\frac{k_{\rho 1}k_z}{\omega\epsilon_1\mu_1}J_1'(k_{\rho 1}\rho) - B_{1n}\frac{1}{\mu_1\rho}J_1(k_{\rho 1}\rho)\right)\sin\varphi\,e^{-jk_z z}$$

$$H_\varphi = \left(-A_{1n}\frac{k_z}{\omega\epsilon_1\mu_1\rho}J_1(k_{\rho 1}\rho) - B_{1n}\frac{k_{\rho 1}}{\mu_1}J_1'(k_{\rho 1}\rho)\right)\cos\varphi\,e^{-jk_z z}$$

and for $\rho > a$:

$$E_z = -j\,D_{1n}\frac{k_{\rho 0}^2}{\omega\mu_0\epsilon_0}H_1^{(2)}(k_{\rho 0}\rho)\cos\varphi\,e^{-jk_z z}$$

$$E_\rho = \left(-C_{1n}\frac{1}{\epsilon_0\rho}H_1^{(2)}(k_{\rho 0}\rho) - D_{1n}\frac{k_{\rho 0}k_z}{\omega\mu_0\epsilon_0}H_1^{(2)\prime}(k_{\rho 0}\rho)\right)\cos\varphi\,e^{-jk_z z}$$

$$E_\varphi = \left(C_{1n}\frac{k_{\rho 0}}{\epsilon_0}H_1^{(2)\prime}(k_{\rho 0}\rho) + D_{1n}\frac{k_z}{\omega\epsilon_0\mu_0\rho}H_1^{(2)}(k_{\rho 0}\rho)\right)\sin\varphi\,e^{-jk_z z}$$

$$H_z = -j\,C_{1n}\frac{{k_{\rho 0}}^2}{\omega\epsilon_0\mu_0}H_1^{(2)}(k_{\rho 0}\rho)\sin\varphi\,e^{-jk_z z}$$

$$H_\rho = \left(-C_{1n}\frac{k_{\rho 0}k_z}{\omega\epsilon_0\mu_0}H_1^{(2)\prime}(k_{\rho 0}\rho) - D_{1n}\frac{1}{\mu_0\rho}H_1^{(2)}(k_{\rho 0}\rho)\right)\sin\varphi\,e^{-jk_z z}$$

$$H_\varphi = \left(-C_{1n}\frac{k_z}{\omega\epsilon_0\mu_0\rho}H_1^{(2)}(k_{\rho 0}\rho) - D_{1n}\frac{k_{\rho 0}}{\mu_0}H_1^{(2)\prime}(k_{\rho 0}\rho)\right)\cos\varphi\,e^{-jk_z z}$$

Since the stimulating current source is completely electric, *E* tangential to the surface of the rod is continuous, so $E_z^{II}(\rho=a) = E_z^{I}(\rho=a)$ shows:

$$-j\,B_{1n}\frac{k_{\rho 1}^2}{\omega\mu_1\epsilon_1}J_1(k_{\rho 1}a)\cos\varphi\,e^{-jk_z z} + j\,D_{1n}\frac{k_{\rho 0}^2}{\omega\mu_0\epsilon_0}H_1^{(2)}(k_{\rho 0}a)\cos\varphi\,e^{-jk_z z} = 0$$

and $E_\varphi^{II}(\rho=a) = E_\varphi^{I}(\rho=a)$ shows:

$$-A_{1n}\frac{k_{\rho 1}}{\epsilon_1}J_1'(k_{\rho 1}a)-B_{1n}\frac{k_z}{\omega\epsilon_1\mu_1 a}J_1(k_{\rho 1}a)+C_{1n}\frac{k_{\rho 0}}{\epsilon_0}H_1^{(2)\prime}(k_{\rho 0}a)$$
$$+D_{1n}\frac{k_z}{\omega\epsilon_0\mu_0 a}H_1^{(2)}(k_{\rho 0}a)=0$$

Since $\vec{K}=K_\varphi\hat{a}_\varphi$, $\vec{A}$ must be completely $\hat{a}_\varphi$ directed, which means

$H_\varphi^{II}(a)=H_\varphi^{I}(a)$, which shows:

$$-A_{1n}\frac{k_z}{\omega\epsilon_1\mu_1 a}J_1(k_{\rho 1}a)-B_{1n}\frac{k_{\rho 1}}{\mu_1}J_1'(k_{\rho 1}a)+C_{1n}\frac{k_z}{\omega\epsilon_0\mu_0 a}H_1^{(2)}(k_{\rho 0}a)$$
$$+D_{1n}\frac{k_{\rho 0}}{\mu_0}H_1^{(2)\prime}(k_{\rho 0}a)=0$$

apply $H_z^{II}(\rho=a)-H_z^{I}(\rho=a)=K_\varphi$ to see:

$$-jA_{1n}\frac{k_{\rho 1}^{\ 2}}{\omega\epsilon_1\mu_1}J_1(k_{\rho 1}a)+jC_{1n}\frac{k_{\rho 0}^{\ 2}}{\omega\epsilon_0\mu_0}H_1^{(2)}(k_{\rho 0}a)=\frac{K_\varphi}{\cos\varphi}e^{+jk_z z}=\frac{C_0}{2\pi}\left[\frac{\sin\left(k_z\frac{s}{2}\right)}{\left(k_z\frac{s}{2}\right)}\right]e^{+jk_z z}$$

So we have four equations in four unknowns:

$$-jB_{1n}\frac{k_{\rho 1}^2}{\omega\mu_1\epsilon_1}J_1(k_{\rho 1}a)+jD_{1n}\frac{k_{\rho 0}^2}{\omega\mu_0\epsilon_0}H_1^{(2)}(k_{\rho 0}a)=0$$

$$-A_{1n}\frac{k_{\rho 1}}{\epsilon_1}J_1'(k_{\rho 1}a)-B_{1n}\frac{k_z}{\omega\epsilon_1\mu_1 a}J_1(k_{\rho 1}a)+C_{1n}\frac{k_{\rho 0}}{\epsilon_0}H_1^{(2)\prime}(k_{\rho 0}a)+D_{1n}\frac{k_z}{\omega\epsilon_0\mu_0 a}H_1^{(2)}(k_{\rho 0}a)=0$$

$$-A_{1n}\frac{k_z}{\omega\epsilon_1\mu_1 a}J_1(k_{\rho 1}a)-B_{1n}\frac{k_{\rho 1}}{\mu_1}J_1'(k_{\rho 1}a)+C_{1n}\frac{k_z}{\omega\epsilon_0\mu_0 a}H_1^{(2)}(k_{\rho 0}a)+D_{1n}\frac{k_{\rho 0}}{\mu_0}H_1^{(2)\prime}(k_{\rho 0}a)=0$$

$$-jA_{1n}\frac{k_{\rho 1}^{\ 2}}{\omega\epsilon_1\mu_1}J_1(k_{\rho 1}a)+jC_{1n}\frac{k_{\rho 0}^{\ 2}}{\omega\epsilon_0\mu_0}H_1^{(2)}(k_{\rho 0}a)=\frac{K_\varphi}{\cos\varphi}e^{+jk_z z}$$

which can be put into matrix form:

$$\begin{bmatrix} a_{11} & a_{12} & a_{13} & a_{14} \\ a_{21} & a_{22} & a_{23} & a_{24} \\ a_{31} & a_{32} & a_{33} & a_{34} \\ a_{41} & a_{42} & a_{43} & a_{44} \end{bmatrix} \cdot \begin{bmatrix} A_{1n} \\ B_{1n} \\ C_{1n} \\ D_{1n} \end{bmatrix} = \begin{bmatrix} 0 \\ 0 \\ 0 \\ K_{soln} \end{bmatrix}$$

where

$$a_{11} = 0 \quad a_{12} = -j\frac{k_{\rho 1}^2}{\omega \mu_1 \epsilon_1} J_1(k_{\rho 1} a) \quad a_{13} = 0 \quad a_{14} = j\frac{k_{\rho 0}^2}{\omega \mu_0 \epsilon_0} H_1^{(2)}(k_{\rho 0} a)$$

$$a_{21} = -\frac{k_{\rho 1}}{\epsilon_1} J_1'(k_{\rho 1} a) \quad a_{22} = -\frac{k_z}{\omega \epsilon_1 \mu_1 a} J_1(k_{\rho 1} a) \quad a_{23} = \frac{k_{\rho 0}}{\epsilon_0} H_1^{(2)\prime}(k_{\rho 0} a)$$

$$a_{24} = \frac{k_z}{\omega \epsilon_0 \mu_0 a} H_1^{(2)}(k_{\rho 0} a) \quad a_{31} = -\frac{k_z}{\omega \epsilon_1 \mu_1 a} J_1(k_{\rho 1} a) \quad a_{32} = -\frac{k_{\rho 1}}{\mu_1} J_1'(k_{\rho 1} a)$$

$$a_{33} = \frac{k_z}{\omega \epsilon_0 \mu_0 a} H_1^{(2)}(k_{\rho 0} a) \quad a_{34} = \frac{k_{\rho 0}}{\mu_0} H_1^{(2)\prime}(k_{\rho 0} a) \quad a_{41} = -j\frac{k_{\rho 1}{}^2}{\omega \epsilon_1 \mu_1} J_1(k_{\rho 1} \rho)$$

$$a_{42} = 0 \quad a_{43} = j\frac{k_{\rho 0}{}^2}{\omega \epsilon_0 \mu_0} H_1^{(2)}(k_{\rho 0} \rho) \quad a_{44} = 0$$

and:

$$K_{soln} = \frac{K_\varphi}{\cos\varphi} e^{+jk_z z}$$

Notice $a_{12} = a_{41} \quad a_{14} = a_{43} \quad a_{22} = a_{31} \quad a_{24} = a_{33}$, and let $\eta_1^2 = \frac{\mu_1}{\epsilon_1} \quad \eta_0^2 = \frac{\mu_0}{\epsilon_0}$

then $a_{23} = \eta_0^2 a_{34} \quad a_{21} = \eta_1^2 a_{32}$. Putting the zeros back into the matrix, and substituting like terms to help with simplification:

$$\begin{bmatrix} 0 & a_{12} & 0 & a_{14} \\ \eta_1^2 a_{32} & a_{22} & \eta_0^2 a_{34} & a_{24} \\ a_{22} & a_{32} & a_{24} & a_{34} \\ a_{12} & 0 & a_{14} & 0 \end{bmatrix} \cdot \begin{bmatrix} A_{1n} \\ B_{1n} \\ C_{1n} \\ D_{1n} \end{bmatrix} = \begin{bmatrix} 0 \\ 0 \\ 0 \\ K_{soln} \end{bmatrix}$$

so we have form $\left[M_{4x4}\right] \cdot \vec{V}_1 = \vec{K}_1$

so $\vec{V}_1 = \left[M_{4x4}\right]^{-1} \cdot \vec{K}_1$

$$\left[M_{4x4}\right]^{-1} = \frac{1}{Det\left(M_{4x4}\right)} \begin{bmatrix} b_{11} & b_{12} & b_{13} & b_{14} \\ b_{21} & b_{22} & b_{23} & b_{24} \\ b_{31} & b_{32} & b_{33} & b_{34} \\ b_{41} & b_{42} & b_{43} & b_{44} \end{bmatrix}$$

Where the "b" terms in the new matrix are related to the "a" terms in the usual linear algebra fashion when calculating matrix inverses. However the key point is we have a closed form expression that can be used to numerically solve for the coefficients of the HEz modes. Also notice we again have a constant pole term when the determinate is 0. This is as before for the TMz case, except the previous derivation wasn't in terms of linear algebra, hiding this identity of the pole.

Whatever our numeric expression for the fields are in the spectral domain, we may numerically find the spatial fields by inverse Fourier transform:

$$E_z = \int_{-\infty}^{\infty} \boldsymbol{E}_z e^{-jk_z z} dk$$

$$E_\rho = \int_{-\infty}^{\infty} \boldsymbol{E}_\rho e^{-jk_z z} dk$$

$$E_\varphi = \int_{-\infty}^{\infty} \boldsymbol{E}_\varphi e^{-jk_z z} dk$$

$$H_z = \int_{-\infty}^{\infty} \boldsymbol{H_z} e^{-jk_z z}\, dk$$

$$H_\rho = \int_{-\infty}^{\infty} \boldsymbol{H_\rho} e^{-jk_z z}\, dk$$

$$H_\varphi = \int_{-\infty}^{\infty} \boldsymbol{H_\varphi} e^{-jk_z z}\, dk$$

Then:

$$K_\varphi(k_z) = \frac{I_0 \cos\varphi}{2\pi}\left[\frac{\sin\left(k_z \frac{s}{2}\right)}{\left(k_z \frac{s}{2}\right)}\right]$$

Where $I_0 = C_0 s$ is the *electric* current source in Amps exciting the rod, and the spectral fields are functions of:

$$K_{soln} = \frac{K_\varphi}{\cos}\varphi = \frac{I_0}{2\pi}\left[\frac{\sin\left(k_z \frac{s}{2}\right)}{\left(k_z \frac{s}{2}\right)}\right]$$

also recall:

$$k_{\rho 0}^2 + k_z^2 = k_0^2 = \omega^2 \mu_0 \epsilon_0$$

$$k_{\rho 1}^2 + k_z^2 = k_1^2 = \omega^2 \mu_1 \epsilon_1$$

For electrically small current source, IE a delta function source, $s \to 0$ and

$$\left(\frac{\sin\left(k_z \frac{s}{2}\right)}{k_z \frac{s}{2}}\right) \to 1$$

Again, we are concerned with the current wave carried by the rod. The current was

electric current, so for this case we can integrate dB_z/dt inside the rod over the cross sectional area from $\rho = 0$ to $\rho = a$ and call that the total magnetic current. Or we could think of it from the point of view of an outside observer unaware of the electrical thickness of the road. Since $k_{r0}a$ is small the observer would assume the circulating Efield at the surface obeys Faraday's Law. The fact is that both methods give the same answer:

$$\oint \vec{E}\cdot\vec{dl} = \int \frac{-\partial \vec{B}}{\partial t}\cdot d\vec{S} = I_m$$

The first integral requires the electric field be known at the surface of the rod, something we may determine with the derived expressions for the electric field. The second integral requires the magnetic flux density through the cross section of the rod to be known, information which we do not have. Hence:

$$I_m(z) = \oint \vec{E}\cdot\vec{dl}$$

This expression may be used to determine the amplitude and phase of the supported current wave of the structure, which in turn shows us when the structure guides, and the parameters of its guidance (attenuation and propagation constant through the current wave intensity and phase).